# INTELLIGENT CONTROL TECHNIQUE OF SOLAR PANEL USING NANOFLUID AND POROUS MEDIA

**2023**
**MASTER THESIS**
**MECHANICAL ENGINEERING**

**Alyaa Jaafar Abdulhasan AL-DAAEWE**

**Thesis Advisors**
**Prof. Dr. Kamil ARSLAN**
**Assist. Prof. Dr. Mohammed J. MOHAMMED**

# INTELLIGENT CONTROL TECHNIQUE OF SOLAR PANEL USING NANOFLUID AND POROUS MEDIA

**Alyaa Jaafar Abdulhasan AL-DAAEWE**

**Thesis Advisors**
**Prof. Dr. Kamil ARSLAN**
**Assist. Prof. Dr. Mohammed J. MOHAMMED**

**T.C.**
**Karabuk University**
**Institute of Graduate Programs**
**Department of Mechanıcal Engıneerıng**
**Prepared as**
**Master Thesis**

**KARABUK**
**August 2023**

I certify that in my opinion the thesis submitted by Alyaa Jaafar Abdulhasan AL-DAAEWE titled "INTELLIGENT CONTROL TECHNIQUE OF SOLAR PANEL USING NANOFLUID AND POROUS MEDIA" is fully adequate in scope and in quality as a thesis for the degree of Master of Science.

Prof. Dr. Kamil ARSLAN ..........................
Thesis Advisor, Department of Mechanical Engineering

Assist. Prof. Dr. Mohammed J. MOHAMMED ..........................
Thesis Advisor, Department of Mechanical Engineering

This thesis is accepted by the examining committee with a unanimous vote in the Department of Mechanical Engineering as a Master of Science thesis. 28/08/2023

Examining Committee Members (Institutions) Signature

Chairman : Assist. Prof. Dr. Ali CAN (KBU) ..........................

Member : Prof. Dr. Kamil ARSLAN (KBU) ..........................

Member : Assist. Prof. Dr. Mohammed J. MOHAMMED (UT) ..........................

Member : Assist. Prof. Dr. Abdülrezzak AKROOT (KBU) ..........................

Member : Assist. Prof. Dr. Ali Abdulwahab ISMAEEL (UT) ..........................

The degree of Master of Science by the thesis submitted is approved by the Administrative Board of the Institute of Graduate Programs, Karabuk University.

Assoc. Prof. Dr. Zeynep ÖZCAN ..........................
Director of the Institute of Graduate Programs

Alyaa Jaafar Abdulhasan AL-DAAEWE

# ABSTRACT

## M. Sc. Thesis

## INTELLIGENT CONTROL TECHNIQUE OF SOLAR PANEL USING NANOFLUID AND POROUS MEDIA

**Alyaa Jaafar Abdulhasan AL-DAAEWE**

**Karabük University**
**Institute of Graduate Programs**
**Department of Mechanical Engineering**

Thesis Advisors:
**Prof. Dr. Kamil ARSLAN**
**Assist. Prof. Dr. Mohammed J. MOHAMMED**
**Augst 2023, 97 pages**

The operating temperature of the cells influences the electrical parameters of the photovoltaic modules due to the properties of the crystalline silicon used in photovoltaic panels. The aim of this thesis is to design and experimentally build a photovoltaic panel and to collect data. *PV* temperature was experimentally checked with and without nanofluid. Experimental works were performed to collect the parameters (ambient temperature, irradiance, humidity, wind speed, and the temperature of the *PV* module). In addition, the collected input and output data were used to develop a neural network time series with three models, *NAR*, *NARX* and nonlinear. The data obtained from the network time series were compared with the parameters of the fuzzy *PID* controller.

The porosity magnitude of the system was used as 0.965. The results showed that *NARX* with *MSE* is the best modelling method with 0.2255, while the worst nonlinear *I/O* with *MSE* is 2.57. Also, the results manifested that MSE is the best way to control this system with the values of *KP*, *KI*, and *KD* as 80, 88.05, and 11.1, respectively. A cooling system was connected to the *PV* module, which consists mainly of a jacket (water container) mounted on the back of the *PV* panel. $Al_2O_3$ nano particles were added to the water with a size *20 nm* to create nanofluid with concentration of 2 *wt*.%. The reduction in temperature with using nanofluid as coolant was seen as *23 ℃* when compared to non-cooling case. It was concluded that the overall efficiency of the panel increases to 111% with using nanofluid, compared to without cooling case (40%).

In the last part of the thesis study, the usage of the controller in the system with the panel temperature set point was carried out. The temperature was set to 40℃ and it was determined that the control system successfully reaches the set temperature.

# ÖZET

**Yüksek Lisans Tezi**

**NANO AKIŞKAN VE GÖZENEKLİ ORTAM KULLANILAN GÜNEŞ PANELİNİN AKILLI KONTROL TEKNİĞİ**

**Alyaa Jaafar Albdulhasan AL-DAAEWE**

**Karabük Üniversitesi**
**Lisansüstü Eğitim Enstitüsü**
**Makine Mühendisliği Bölümü**

**Tez Danışmanları:**
**Prof. Dr. Kamil ARSLAN**
**Dr. Öğr. Üyesi Mohammed J. MOHAMMED**
**Ağustos 2023, 97 sayfa**

Hücrelerin çalışma sıcaklığı, fotovoltaik panellerde kullanılan kristal silikonun özelliklerinden dolayı fotovoltaik modüllerin elektriksel parametrelerini etkilemektedir. Bu tezin amacı bir fotovoltaik panel tasarlamak, deneysel olarak oluşturmak ve veri toplamaktır. *PV* sıcaklığı nanoakışkan kullanılan ve kullanılmayan durumlar için deneysel olarak kontrol edilmiştir. Parametreleri (ortam sıcaklığı, ışınım, nem, rüzgar hızı ve *PV* modülün sıcaklığı) toplamak için deneysel çalışmalar gerçekleştirilmiştir. Ayrıca, toplanan giriş ve çıkış verileri, *NAR, NARX* ve doğrusal olmayan üç modele sahip bir sinir ağı zaman serisi geliştirmek için kullanılmıştır. Ağ zaman serisinden elde edilen veriler bulanık *PID* denetleyicinin parametreleriyle karşılaştırılmıştır.

Sistemin gözeneklilik değeri 0,965 olarak kullanılmıştır. Sonuçlar, *MSE*'li *NARX*'ın 0,2255 ile en iyi modelleme yöntemi olduğunu, MSE ile en kötü doğrusal olmayan *I/O*'nun ise 2,57 olduğunu göstermiştir. Ayrıca sonuçlar, sırasıyla 80, 88.05 ve 11.1 olan *KP, KI* ve *KD* değerleriyle *MSE*'nin bu sistemi kontrol etmenin en iyi yolu olduğunu ortaya koymuştur. Esas olarak *PV* panelinin arkasına monte edilen bir ceketten (su kabı) oluşan *PV* modülüne bir soğutma sistemi bağlanmıştır. Ağırlıkça %2 konsantrasyonda nanoakışkan oluşturmak için suya *20 nm* boyutunda $Al_2O_3$ nano parçacıklar eklenmiştir. Soğutucu olarak nanoakışkan kullanılmasıyla sıcaklıktaki azalma, soğutulmayan duruma göre 23 ℃ olduğu görülmüştür. Nanoakışkan kullanıldığında panelin genel verimliliğinin soğutmasız duruma (%40) kıyasla %111'e çıktığı sonucuna varılmıştır.

Tez çalışmasının son kısmında ise panel sıcaklık ayar noktası ile kontrolörün sistemde kullanılması gerçekleştirilmiştir. Sıcaklık 40 ℃ olarak ayarlanmış ve kontrol sisteminin ayarlanan sıcaklığa başarıyla ulaştığı saptanmıştır.

**Anahtar Kelimeler :** Akıllı Kontrol Tekniği, Nanoakışkan, Güneş Paneli
**Bilim Kodu** : 91408

# ACKNOWLEDGMENT

First and foremost, "All the praises and thanks be to Allah, The Beneficent, The Merciful", "praise be to Him who has taught by the pen, who taught man that which he knew not". I would like to express my deepest thanks and gratitude to my supervisors Prof. Dr. Kamil Arslan the leader who give me the science and information needed to make this research done successfully, and Assist. Prof. Dr. Mohammed J. Mohammed who has given much of his time in this search.

Deep thanks and appreciation to my first family my husband, my children, my mother, and my sisters and brothers, friends, loved ones and everyone who supported me. Finally, I would like to express my thanks and appreciation to everyone who helped in one way or another to implement this thesis.

# CONTENTS

# LIST OF FIGURES

# LIST OF TABLES

# SYMBOLS AND ABBREVITIONS INDEX

## SYMBOLS

$A_c$     : PV panel module area

$C_p$     : Fluid heat capacity

$d$     : The past values of the predicted and external series

$F$     : The nonlinear function

$G$     : Solar radiation

$I_{sc}$     : Short circuit current $I$

$KV$     : Voltage temperature coefficient

$KI$     : Current temperature coefficient

$K_P$     : Proportional gain

$K_I$     : Integral gain

$K_D$     : Derivative gain

$L$     : Length

$\dot{m}$     : Mass flow rate

$mp$     : Peak current

$N$     : Number of data

$N_n$     : Number of hidden neurons

$N_d$     : Number of delays

$Np$     : Number of parallel cells

$Ns$     : Number of series cell

$P_{mp}$     : Maximum power

$Q$     : The rate of heat transfer

$T_a$     : Ambient Temperature

$Th$     : Thickness

$T_i$     : Fluid inlet temperature

$T_o$     : Fluid outlet temperature

$T_m$     : Panel surface temperature

$x t$    : External series

$y t$    : The predicted series

$y(t)$  : Actual output

$\hat{y}(t)$  : Predicted output

$V_p$   : Porous media volume

$V_{oc}$  : Open circuit voltage

$V_{pm}$ : Peak voltage

$V t$   : Sink total volume

$W$   : Width

$u(t)$  : The controller output

$\sigma$    : Standard deviation

$\rho$    : Density of fluid

$\eta_e$   : Electrical efficiency

$\eta_{th}$  : Thermal efficiency

$\eta_0$   : Overall efficiency

## ABBREVITIONS

*ALCA*  *:* Average Linkage Cluster Analysis

*AI*     *:* Artificial Intelligence

*cov*    : covariance

*MSE*   : Mean Square Error

*MPPT*  : Maximum Power Point Tracking

*NARX*  :Nonlinear Autoregressive with External Input

*NAR*   : Non-linear Autoregressive

*PID*    : Proportional Integral Derivative

*P*      : Photovoltaic

*PSO*   : Particle Swarm Optimization

*log*    : logarithmic

*var*    : variance

# PART 1

## INTRODUCTION

### 1.1. OVERVIEW

The renewable energy sources include the sun's rays, the wind, and even the heat generated by the earth's geothermal activity. Because non-sustainable power sources, such as oil, fuel, and oil products are not permitted, it is critical to have access to a source of energy that does not deplete natural resources. In the past few years, solar energy has been increasingly popular in a lot of countries because of the rising prices of fuel and the restricted traditional supplies [1]. Sustainable power sources expand by 2.6% annually on average, while nuclear, gaseous petrol, and coal each increase by 2.3%, 1.9%, and 0.9%, respectively, given in Figure 1.1. This indicates that there will be an increment in the consumption of energy on a global scale of up to 48% between the years 2012 and 2040. In this light, it can be observed that both the significance of a renewable power source and the propensity of nations all over the world must adopt.
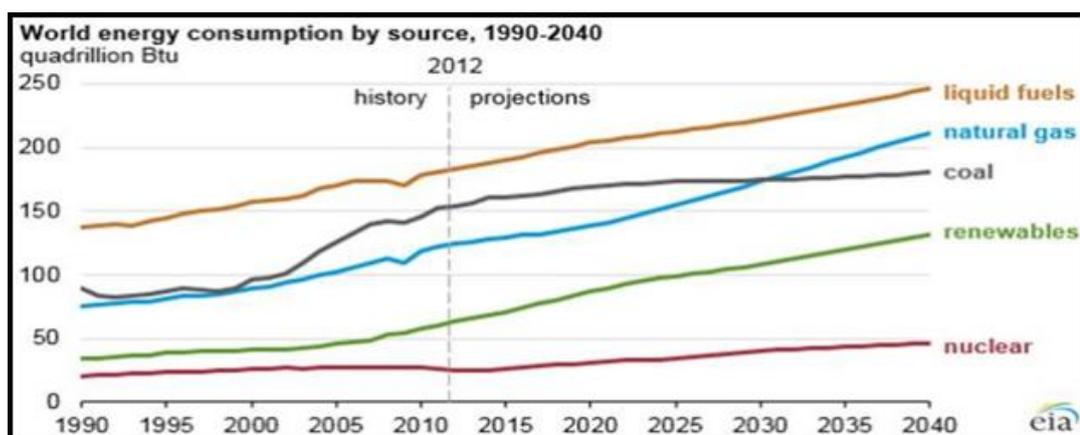


Figure 1.1. Global Energy Development from 1990 to 2040 [2].

Solar power is the most exciting and promising option there is to meet the ever-increasing demand for electricity. This technology has an extremely wide range of

potential applications, some of which include the building of integrated systems, solar-powered homes and spacecraft, as well as pumps and irrigation systems.

*PV* cells are able to convert more than 80% of the radiation that they are exposed to into thermal energy or reflected cooling, which allows them to function well in environments that are both hot and highly irradiated. The temperature of the *PV* system has a considerable impact on the functioning of the *PV* system, particularly in hot regions like the summers in Iraq. When the temperature of the photovoltaic array approaches *80 ℃*, there is a significant drop in the efficiency of the *PV* system. Therefore, finding a solution to this problem and bringing the temperature of the panel down are the key issues [2].

Variety of techniques, such as air and water coolers, liquid immersion cooling, and thermoelectric cooling can be utilized in order to bring the temperature of the *PV* panel down. Monitoring and controlling the temperature of solar panels necessitate the use of a design or model method for determining the temperature of the solar panels. The subject of soft computing makes extensive use of artificial intelligence (*AI*) techniques, with many of the most essential ones being included into intelligent modeling methodologies for optimization.

In order to simulate and anticipate the performance of complex energy systems, Artificial Intelligence (*AI*) methods, such as Artificial Neural Networks (*ANNs*), Fuzzy Logic (*FL*), and Adaptive Neuro-Fuzzy Inference Systems (*ANFIS*) can be utilized. In this thesis, the temperature of the PV panel is predicted using Neural network time series which is Nonlinear Autoregressive with external input (*NARX*), Non-Linear Autoregressive NAR and Nonlinear Input-Output representing the System Identification. The results of this prediction will be used later by traditional and intelligent simulation *PID*-heuristic and *PID-PSO* controllers to control the temperature of the *PV* panel for obtaining higher efficiencies [3].

## 1.2. SOLAR COLLECTORS BASED ON NANO-FLUIDS

Nano-fluids have a rapid and efficient heat transfer ratio, which makes them ideal for use in solar collectors based on nano-fluids. This category of apparatus is also known as volumetric absorption systems in some circles. They are utilized in solar thermal energy-based nano-fluids applications, such as the gasification of biomass and the cooling of microchips, amongst other things. Nano-fluids, in contrast to liquids such as water, ethylene glycol, and other similar substances, have the ability to both absorb and scatter the solar light, which makes them valuable for applications involving solar power. Excellent absorption can be found in a wide variety of pure materials; however, some of these materials are inaccessible to the sun wavelengths.

In systems known as Direct Absorption Solar Collectors (*DASC*), nano-fluids are used to facilitate the passage of solar energy from its source to the working fluid. Figure 1.2 depicts the surface absorption systems in which high absorber coatings have been replaced with a glass coating to enable the interaction between nano-fluids and solar irradiation. The working fluid is able to directly absorb the sun's rays thanks to the design of this system, which helps reduce the heat transfer losses that are produced by radiation and conduction [4].
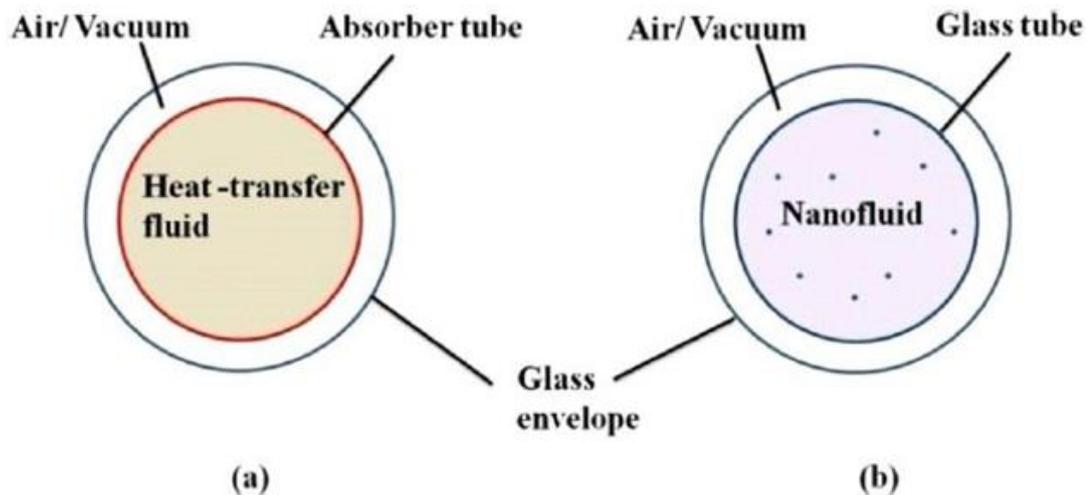
Figure 1.2. (a) Heat transfer fluid, (b) Nanofluid [4].

Because they have a low absorption ratio, ordinary fluids, like water and molten salt, as well as others, appear transparent. In solar systems that use direct absorption, the solar

absorber fluid must have a high viscosity. It is recommended that the working fluid be seeded with nanoparticles, such as silicon carbide and silicon dioxide since the nano-fluid has a high capacity for absorption. Nanoparticles, in general, are prone to instability and dispersion, both of which result in the suspension equilibrium being disrupted and altered. At the nanoscale scale, the Brownian and gravitational forces are the two most relevant forces. When the Brownian motion that occurs at very small scales is taken into account, the gravitational forces are changed, and the viscosity effect helps stabilize the system.

## 1.3. COOLING METHODS AND TECHNIQUES

Most of the heat produced by photovoltaic cells comes from the absorption of solar light that does not result in the generation of electricity. Without taking into consideration the cooling of photovoltaic panels, the design and functioning of solar cells would be incomplete [5]. Throughout the process of cooling, there should be as little variation in the temperature of the cell as possible [6]. A wide number of applications have been found for water- and air-cooling systems. Active cooling and passive cooling are the two distinct types of cooling strategies that can be implemented in cooling systems. The term "passive cooling systems" refers to the technologies that do not require any additional power consumption to remove the heat from the *PV* panel and decrease the amount of heat that it absorbs [7]. A component of the process is the transmission of heat from the location where it is created to the surrounding atmosphere. Simplified forms of passive cooling include the use of metal solids with high thermal conductivities, such as copper and aluminum, or a set of fins or other extruded surfaces that allow for easier heat passage to the atmosphere. Complex systems not only make use of heat pipes, which are able to successfully convey heat through a boiling condensation cycle, but also make use of phase-change materials (*PCMs*) and diverse natural circulation systems. Active cooling systems, on the other hand, remove the heat from the panels by utilizing heat removal equipment, such as water pumps and air ventilators. In these types of systems, the two modes of heat transfer that are utilized most frequently are conduction and convection [8]. Although active systems have a power consumption, they are frequently used when the efficiency of the panels is higher than the amount of energy required to power the device. These kinds of devices can also be put to use for additional reasons,

such as the recovery of waste heat for the purpose of heating domestic water. Both active and passive cooling systems typically make extensive use of water and nano-fluid as their primary cooling media. Utilizing either natural or induced air movement makes the process of removing the heat from solar modules straightforward and budget friendly [9, 10]. The use of nano-fluid to cool photovoltaic modules is a frequent practice that can result in significant benefits for the modules. Because of its thermal properties, using water as a refrigerant is not as effective as using other substances. It is not possible to extract the thermal energy contained in the photovoltaic absorber by chilling the air in hot climes. On the other hand, cooling via nano-fluid can function at temperatures that are noticeably higher, and it is more effective than other methods at recycling previously used heat. Because of this, water cooling is an alternative that is less desirable in a lot of different situations [11].

## 1.4. MOTIVATION

- The price of fossil fuels continues to rise, and supplies could run out, whereas the supply of solar energy does not cost anything and will not run out.
- Power plants that run on fossil fuels are responsible for the emission of pollutants into the atmosphere, whereas the solar photovoltaic power plants are not.
- Solar photovoltaics (*PVs*) mitigate the effects of climate change, while the power production systems that rely on fossil fuels exacerbate the problem.
- In contrast to energy-generating technologies that rely on non-renewable resources, it has an abundant supply of photovoltaic energy that is derived from the sun.
- As a direct consequence of this, solar *PV* systems have lower costs of operation and maintenance.

## 1.5. PROBLEM STATEMENT

The main problem of the *PV* panels is overheating, due to high ambient temperture and extreme solar radiation. This happens because further than *80 ºC* of solar irradiation reaches the *PV* cells convert in thermal energy and during power

generation, cells temperature increases causing a darmatic reduce of the *PV* panel effectiveness.

In the blistering atomosphere summer season countries similar as Iraq, the temperture of the *PV* panels exceeds and the *PV* panel temperture must be reduced. To promote *PV* panels performance andites effectiveness there are numerous cooling mechanisms similar as water cooling, thermoelectric cooling, liquid absorption cooling, air cooling, adding fins, etc.

## 1.6. GOALS OF THE THESIS

The followings are the key goals of this thesis:

- It's necessary to design and develop a *PV* panel experimentally and collecting the input data (ambient temperature, wind speed and solar radiation) and output data (panel temperature).
- To model the *PV* system using non-parametric system identification based on Neural Network techniques (*NARX*, *NAR*, and *NU*).
- To contrail the panel temperature using *PIO-PSO* controller for simulating part.
- To design the actuator using porous media.
- To control the *PV* temperature experimentiy with and without nano-fluid.

## 1.7. LAYOUT OF THE THESIS

The chapters of this research are organized as follows:

- Chapter One: The introduction, background, research challenge, and research goals are all discussed in this chapter.
- Chapter Two: It focuses on the *PV* panel theory and fundamentals, in addition to conventional and intelligent tuning approaches and their contributions. This chapter also describes the use of predictive strategies to manage increases in *PV* temperature.

- Chapter Three: To forecast the temperature of a photovoltaic (*PV*) module, nonlinear SI techniques and a *MATLAB* application are discussed in this chapter. Neural network time series and (*NARX*) are also illustrated. A procedure known as *MSE* validation was used to validate both models. In addition, intelligent controllers, such as *PID*-heuristic and PSO tuning method approaches, which may be utilized to regulate the tempeture of the PV module and achieve high efficiency, are debated in this chapter.

- Chapter Four: This chapter is divided into two parts; The first part is testing the thermal output of *PV* modules with without cooling systems and then without cooling systems as second part, is also considered. These tests are the starting step. *NARX* methodology was used to estimate the module's temperature values, which were compared to the actual observed temperature. There are a variety of controllers in this subject. Heuristics were used to fine-tune the initial controller (*PID*). The *PID* controller's parameters, particle swarm optimization (*PSO*) was used to fine-tune.

- Chapter Five: It summarizes the outcomes of the study and provides suggestions for future research.

# PART 2

# LITERATURE REVIEW

## 2.1. INTRODUCTION

The degree of the module temperature variation has a considerable impact on the effectiveness of these systems, making it a key characteristic for solar energy systems. There are many different cooling control systems that can each give an accurate reading of the solar panel's temperature. This aids in reducing the amount of extra heat that results in energy loss. There have been a sizable number of research papers in this field of study that involve both experimental and theoretical inquiries. It is crucial to have a thorough awareness of the diverse scientific viewpoints on various kinds of cooling techniques.

Some studies have attempted to implement this idea experimentally. Irwan et al. [12] discussed improving the indoor photovoltaic (*PV*) panel energy efficiency. Temperature and sunlight affect on the PV panel performance. PV panel efficiency decreases with temperature. Steel-framed sun simulators lift all halogen lamps. Halogen lights resemble sunlight. Solar model test surfaces average *413, 620, 821*, and *1016 W/m²*. *DC* water pumps function better because water flows over the *PV* screen. Water cools *PV* panels. The *PV* screen system cools and increases the solar power. Solar panels lose heat when watered.

According to the research of Nouri [13], the effectiveness of photovoltaic panels can be improved by combining a sun tracking system with a cooling system. In a near loop cooling system, the front side of the photovoltaic module panel was cooled by employing a technology known as water flow double glazing (*WFDG*). This technique flows water via an underground heat exchanger to achieve the desired cooling effect. In this work, the water mass flow rate as well as the thickness were enhanced through

the utilization of an optimization approach known as the Taguchi method. The increase in electrical production was significantly increased as a result of the (35 %) drop in temperature (16 %).

Schiro et al. [14] came up with a method to cool a model of the photovoltaic system by spraying water on it. The effectiveness of the photovoltaic system as a cooler was investigated using both a steady-state and a dynamic model. The wind speed, the sun's radiation, and the temperature that is currently present in the environment are all factors that are taken into consideration while calculating the temperature module of this model. A transient model was used in order to simulate the thermal mass of a *PV* module and its thermal reaction time to the conditions of its surrounding environment. At an angle of ninety degrees to the air, flow rates of 0.02 liters per second per square meter were applied to the top edge of the *PV* module. Temperatures in the cooled steady state were between 8 and 24 degrees Celsius higher than those in the uncooled steady state.

Ahmed [15] conducted a research and experiments with a variety of cooling methods in order to improve the performance of the *PV* module. It was suggested that a heat sink, a humid pad, and a moist pad made of wood wool could work together as a cooling system. Gains in both thermal and electrical performance can be accomplished by employing a damp wood wool cooling system either on its own or in conjunction with a heat sink. When the *PV* panel was placed inside of a cooling chamber, the panel's ability to generate electricity increased by 9.1 %, 13.04 %, and 14.20 %, respectively (back, front, or both).

Yazdani et al. [16] devloped an intelligent system for estimating the production of solar panels was developed with the help of *MATLAB's* radial-based approach by default. The Radial Based Neural Network (*RBFNN*) model was employed in this process. The proposed model made use of it as an input training data category, while the real output energy was put to use as a training controller. This method was used to get estimates of the amount of energy required for manufacturing over the course of a month and an entire year. In order to get an accurate estimate of solar energy, a power

output equation that was predicated on the solar irradiance and ambient temperature was established.

Hamrouni et al. [17] In order to study the system's performance and dynamic response, a schematic control that utilized traditional controller methods. The goal of this control was to optimize the amount of power and current that the solar *PV* systems contributed to the grid. *MATLAB* and Simulink were used to design and simulate the photovoltaic (*PV*) system with a rated power of 3 *kW*. The voltage and current controller loops were constructed so that the total harmonic distortion (*THD*) in the current could be removed, and the unity power factor could be modified. *P&O* were used to monitor the maximum power, and it was based on the *MPPT*s. The correct amount of power was given despite demonstrating outstanding stability and dynamic response, even if the weather conditions were variable (solar radiation and temperature). This was accomplished while maintaining unity power factor and low harmonic distortion.

Mosaad Ali et al. [18] studied and compared the best *PID* and *NPID* controllers for use with two different combined wind solar *MPPT* controllers. The results of the simulation showed that adding nonlinearity to a standard *NPID* controller's *PID* features could improve the control performance.

Borni et al. [19] conducted a modeling and designing the *PV*/wind hybrid network that is connected to the grid is done with the help of a *PSO* Fuzzy algorithm. The inverter compared the *PI* technique with the *Fuzzy-PI* technique in order to better regulate the current that was injected into the grid. Matlab and Simulink were utilized in order to carry out the simulation investigation. The recommended controller was put through its paces in a series of experiments, and the results indicated that the *PI* controller provides a time response and visuals that are inferior to those generated by the Fuzzy-*PI* controller.

Pannase et al. [20] investigated nano-fluid substances *SiO$_2$-water-EG* nano-fluids are measured by *SiO2, EG*, water, and oil. Nanoparticles and fluids with *SiO2* improve their thermal characteristics. *Al-water* and *Al/H$_2$O-EGl* nano-fluids were investigated for a laminar heat exchange and pressure penalty in circular tubes. Nanoparticles

thickened and warmed the base fluids. The authors measured $SiO_2/H2O$ nano-fluid heat flow coefficient. Thermal characteristics and heat transfer coefficient reached 10.3% and *14.2% at 0.02 vol.%. Re=1860.* Water transports heat 12% better with 2% nanocomposites EG thermal conductivity increased by 12.5% with the same nano particles (*25 °C).*

Hammed [21] experimentally tested the thermal performance of the coating counter low tube heat exchanger; the investigation of two cases. The first case involved smooth tubes and the other with a porous media of 7.0 mm diameter alumina beads placed in tubes. The cold liquid mass flow rate on the shell side was 0.32 kg/s, while the hot water mass flow rate was 0.32% *Kg/s*, this bitrate was variable between 0.15 and 0.30 *kg/sec*. The results of the experiment showed 36% wt efficiency and number of heat exchanger unites increased by 40% due to porous media.

Daradji et al. [22] theoretically studied the temperature distribution equation for porous spiral fin the temperture rise increased the temperature of the fin conductivity which improves the performance of the fins.

Rydalina et al. [23] studied the intensity of heat exchange in the jacket and tube heat exchanger with porous metal supports. comparison of theoretical calculations with the experimental data was carried out. The result depicted that the efficiency of heat exchanger increased when the porous metal was introduced into the construction of shell and tube heat exchangers.

Boussaada et al. [24] fowsed on a horizontal surface of the photovoltaic module in direct sunlight using nonlinear autoregressive *ANN* (*NARX*). The best prediction performance was obtained when the neural network training phase was performed regularly.

Hasan et al. [25] predicted panel temperature using *NARX* and *ANFIS* on the *MSE*. The best prediction method was *ANFIS* with the lowest *MSE*.

Lafta et al. [26] controlled the temperature of the photovoltaic module using the *PID-PSO* technique. The controller had positively regulated the panel temperature to the set point of *30°C*.

Samara and Natsheh [27] introduced a new efficient, compact and easy-to-implement error detection algorithm based on a non-linear autoregressive neural network using exogenous artificial intelligence (*NARX*) and Sugeno's fuzzy reasoning to separate and identify errors in the *PV* scheme, the algorithm was used fuzzy reasoning requires the actually measured power of the *PV* system, the expected power of the *PV* system and the measured environmental conditions. The estimated efficiency of the *PV* device was calculated using the *NARX* artificial intelligence neural network. With the help of the sensors, the actual performance of the *PV* device and the environmental conditions could be determined in real time. It was shown that the algorithm can be implemented on an inexpensive microcontroller. The results revraled that the fault diagnosis algorithm is able to identify a variety of faults, including opens and shorts, erroneous maximum power point tracking (*MPPT*), and partial shade (*PS*) situations, that can affect a photovoltaic device. In addition, the proposed algorithm captures the irradiance and temperature as well as other non-linear trend correlations between predictors to determine the correct maximum power point for a *PV* device.

Lee et al. [28] improved the efficiency of flat photovoltaic (*PVT*) systems. with water and nano liquid separately as coolant. A reliability study was carried out with different water flow rates as the working medium. The flow affecting the efficiency of the *PVT* method was found to be more effective at *3 L/min* than at *1.2* and *4 L/min*. The influence of nano liquids (*CuO/water*, *Al$_2$O$_3$/water*) and water as operating liquids on the performance of the *PVT* device was also examined. The thermal and electrical performance of *PVT* with *CuO/Water* as the nano-fluid improved by 21.30 percent or *0.07* percent compared to a water-based system. The thermal efficiency of the *PVT* device using *Al$_2$O$_3$/water* as the nano-fluid increased by *15.14%,* but there was no difference in electrical efficiency between the water and *Al$_2$O$_3$/water* systems.

Ahmed et al. [29] presented an overview of the latest applications of nanotechnology in solar thermal photovoltaic systems. They examined different forms of nanoparticles and nanoliquids already used in the literature and specified the methods for their production. Both *PV/T* and *CPV/T* systems were studied, and the relevant results were collected to summarize the potential benefits of using nano-fluids. They often illustrate the critical parameters that can improve the performance of nano-fluids.

Connor et al. [30] produced high-efficiency green energy systems as the electricity demand rises. Solar *PV-T* co-generation systems cool the cells, improving the performance. A nano-fluid reverse flow channel improved the solar *PV-T* co-generation cells in this study. *Zn-H₂O* nanofluid cools. *MATLAB*/Simulink simulated the *PV* panel models to improve the efficiency. *PV* and *MPPT* systems were examined. A back-channel PV panel system was compared to the proposed system. The current panels were *1.5%* less efficient than projected panels. *PV-T* energy system. The panel performance determined the *PV-T* cogeneration energy efficiency. The lower panel temperatures improve system performance. This evinced that the nano-fluid back flow cogeneration systems were more efficient than air or water ones. The *MPPT PV* panels have *13.14%* efficiency and power, while the air flow channel systems have *12.5%* and *12.8%.* Analyzing the proposed system indicates its efficacy. Nano-fluids technology improves the large *PV-T* co-generation systems.

The retrofit rooftop *PV* system that Mah et al. [31] installed featured water-film cooling on the front surface of the solar panels at the location that was located in a tropical environment. It was found that the quality has improved by *15%.*

Diwania et al. [32] demonstrated various electrical and thermal aspects photovoltaic and heating systems as well as research in the field of constructive, productive and application-related adaptation of absorbers. Based on previous analytical work, it was found that the thermal energy emitted by the *PV* module can be used in various ways to increase the efficiency. In addition, various forms of photovoltaic-thermal systems, such as air collectors, water collectors and combined systems, as well as their evaporation with heat pumps and use in the home are discussed. This Rule also addressed the design issues, such as flow channel modifications with ribs, thin metal blocks, roll bond

absorber and porous support, and the impact of these changes on the performance of the hybrid system. In addition, the use of advanced technologies such as Nano-fluids, thermoelectric generators and phase change materials improves the overall performance of the device. addition, flexible calculation methods were investigated to predict the influence of different parameters on a photovoltaic-thermal device. The systems that use water and nano liquids as cooling methods improve the efficiency of electrical and thermal *PV/T* modules.

Rajput et al. [33] implemented a passive method of cooling the photovoltaic module at high temperatures and discussed the concept of using a finned cylindrical heat sink with a water-cooling system to cool the panel and improve its warmth. The results elucidated that after the proposed change, the backside temperature droped from *88.81°C* to approximately *58.45°C*.

Table 2.1 displays the summarized studies in related area.

Table 2.1. Literature review.

| Author | Metholdogy of coolling system and Identification type | Results |
|---|---|---|
| Irwan et al. [12] | Cooling methods have been developed that include a heat sink, moist wood wool pads, and a moist pad and heat sink. | Cooling chambers improve the electrical efficiency of *PV* panels by 9.1%, 13.04%, and 14.20%, respectively. |
| Nouri [13] | Water Flow Dual Glazed (*WFDG*) | About 16% of the increase in electrical efficiency was due to this. |
| Schiro et al. [14] | Spray apparatus for cooling | Power output was highest if the cooling plate was used as soon as the PV panel's temperature above 45 Celsius. Each solar panel produced 0.354 watts of power per degree of angle. The difference in temperature between both the cooled and uncooled steady states is between 8 and 24 ° Celsius. A 15% increase in efficiency. |
| Ahmed [15] | a heat sink, a humid pad, and a moist pad made of wood wool could work together as a cooling system. | the PV panel is placed inside of a cooling chamber, the panel's ability to generate electricity increases by *9.1 %, 13.04 %,* and *14.20 %,* respectively (back, front, or both). |

| | | |
|---|---|---|
| Yazdani et al. [16] | The Radial Based Neural Network (*RBFNN*) model was employed in this process. | The model showed great results with minor root- mean-square mistakes |
| Hamrouni et al. [17] | *MATLAB* and Simulink were used to design and simulate the photovoltaic (*PV*) system and P&Oas controller | high stability and dynamic response under weather change |
| Borni et al. [19] | Modeling and designing the *PV*/wind hybrid network that is connected to the grid is done with the help of a *PSO* Fuzzy algorithm | *PI* performance better than fuzzy-*PI* |
| Mosaad Ali et al. [18] | compared the best *PID* and *NPID* controllers for use with two different combined wind solar *MPPT* controllers | adding nonlinearity to a standard *NPID* controller's *PID* features could improve the control performance. |
| Pannase et al. [20] | *Al-water* and *Al/H$_2$O-EGl* nano-fluids were investigated for a laminar heat exchange and pressure penalty in circular tubes | Thermal characteristics and heat transfer coefficient reached *10.3%* and *14.2%* at *0.02 vol.%. Re=1860* nano-fluids.<br>Water transports heat 12% better with *2%* nanocomposites *EG* thermal conductivity increased by *12.5%* with the same nano particle *(25$^\circ$C)* |
| Hammed [21] | experimentally tested the thermal performance of the coating counter flow tube heat exchanger: This involved smooth tubes with a porous media of *7.0 mm* diameter alumina beads placed in tubes | The results of the experiment showed *36%* wt efficiency and number of heat exchanger unites increased by *40%* due to porous media. |
| Daradji et al. [22] | theoretically studied the temperature distribution equation for porous spiral fin | The rise of the temperature of the fin conductivity that improve the performance of the fins. |
| Rydalina et al. [23] | the intensity of heat exchange in the jacket and tube heat exchanger with porous metal supports | The resultdepicted that the efficiency of heat exchanger increased when the porous metal was introduced into the construction of shell and tube heat exchangers. |
| Boussaada et al. [24] | İts used the module in direct sunlight using nonlinear autoregressive *ANN* (*NARX*). | The best prediction performance was obtained when the neural network training phase was performed regularly. |
| Hasan et al. [25] | predicted panel temperature using *NARX* and *ANFIS* on the *MSE*. | The best prediction method was *ANFIS* with the lowest *MSE*. |

| Lafta et al. [26] | controlled the temperature of the photovoltaic module using the *PID-PSO* technique. | The controller had positively regulated the panel temperature to the set point of *30°C*. |
|---|---|---|
| Samara et al. [27] | the algorithm was used fuzzy reasoning requires the actually measured power of the *PV* system, | The results revraled that the fault diagnosis algorithm is able to captures the irradiance and temperature as well as other non-linear trend correlations between predictors to determine the correct maximum power point for a *PV* device. |
| Lee et al. [28] | İts used the water and nano-fluid separately as coolant | The thermal efficiency of the *PVT* device using $Al_2O_3$/water as the nano-fluid increased by *15.14%,* but there was no difference in electrical efficiency between the water and $Al_2O_3$/water systems. |
| Ahmed et al. [29] | The different forms of nanoparticles and nanoliquids is examined | They were used in the literature and specified the methods for their production. |
| Connor et al. [30] | Nano-fluid (*Zn-H₂O*) was used to cool the solar *PV-T*. *MATLAB*/Simulink simulated the *PV* panel models | Nano-fluids technology improves the large *PV-T* co-generation systems |
| Mah et al. [31] | installed featured water-film cooling on the front surface of the solar panels at the location | It was found that the quality has improved by *15%.* |
| Diwania et al. [32] | the use of advanced technologies such as nano-fluids, thermoelectric generators and phase change materials improves the overall performance of the device. addition, flexible calculation methods were investigated to predict the influence of different parameters on a photovoltaic-thermal device | The systems that use water and nano liquids as cooling methods improve the efficiency of electrical and thermal *PV/T* modules |
| Rajput et al . [33] | Afinned cylindrical heat sink with a water was used to cool the panel and improve its warmth | The results elucidated that after the proposed change, the backside temperature droped from *88.81°C* to approximately *58.45°C.* |

## 2.2. CONTRIBUTIONS TO LITERATURE

As can be seen from the list below, these are the most significant contributions:

- Simulation of *PV* panel devices, employing nonlinear system information techniques (*NARX* and *ANFIS*) to detect the photovoltaic temperatures and check the accuracy via means of squared error (*MSE*).
- Based on the Square error integration, a *PID-PSO* controller's performance can be evaluated (*ISE*).
- Controlling the temperature of a solar panel by using a nano- fluid cooling effect as an outer jacket is the goal of this experiment.

# PART 3

# THEORETICAL BACKGROUND

There are several approaches that can be used when conducting research; however, the strategy that is used the most frequently is to compile a list of references from pertinent technical papers or periodicals [34]. Step two consisted of constructing and putting into action an experimental setup in order to collect data on inputs and outputs. During the process of developing photovoltaic model and cooling system, in this work, a temperature recorder, a solar power meter, a wind speed meter, and a multimeter were used. A number of different water flow rates can be used as input data for a model that can predict the temperature of a *PV* panel. In the second part of the study, a nonlinear SI modeling approach was taken to simulate the *PV* panel system. In order to accurately anticipate the *PV* panel temperature's nonlinear dynamic behavior, nonparametric techniques, such as *NARX* were utilized [35]. The Mean Square Error (*MSE*) of all applicable methodologies has been compared in order to decide which model is the most accurate representation of reality. After doing some comparisons, it has been decided which model of *PV* panel is superior. In order to manage the temperature of the *PV* array and achieve a high level of efficiency, conventional and intelligent controls were employed and altered according to conventional and intelligent tuning strategies. In order to achieve a finer level of tuning for the *PID* controller, heuristic and *PSO* tuning methodologies were utilized. The inquiry into the *PV* model that included both comparative simulation and experimental validation has been drawn [36, 37]. The flow chart of research methodolgy is shown distinctly in Figure 3.1.
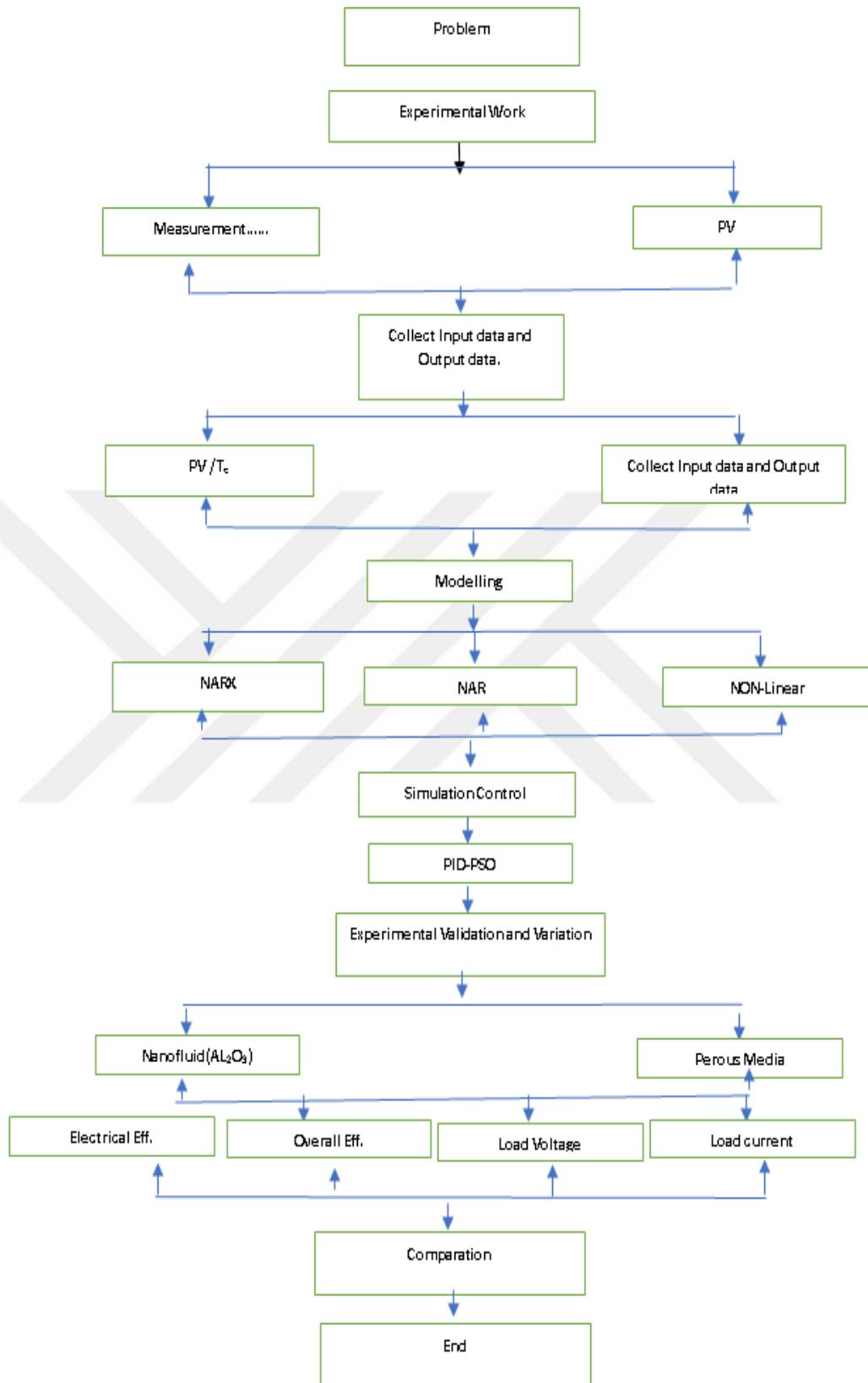
Figure 0.1. The flow chart of methodology research.

## 3.1. ELECTRICAL AND THERMAL EFFICIENCY OF PV PANEL

Electrical efficiency is an essential criterion to consider when evaluating the performance of a solar panel. Because it quantifies the module's capacity to convey heat, the degree of thermal efficiency is a critical metric. [38].

### 3.1.1.  *PV* Panel Electrical Efficiency

As demonstrated in Eq. (3.1), the electrical efficiency ($\eta_e$) of the *PV* panel is the ratio between the maximum electrical power of a photovoltaic unit to produce solar radiation and the unit area. [39].

$$\eta_e = \frac{P_w}{A_c G} \tag{0.1}$$

Where:

$P_w$ :  maximum electrical power output (*W*)

$\eta_e$: Effective use of electricity (*%*)

$P_m$: Highest possible electrical output (*W*)

$A_c$: PV module surface area (*$m^2$*)

$G$: Solar radiation (*$W/m^2$*)

### 3.1.2.  PV Panel Thermal Efficiency

The heat transmission equation is provided in Eq. (3.2) [40].

$$Q = \dot{m} \cdot c_p (T_o - T_i) \tag{0.2}$$

Where:

$Q$: The heat transfer rate (J/s)

$\dot{m}$: Rate of mass flow *(kg/s)*

$c_p$: Heat capacity of fluid *(J/kg. ℃)*

$T_i$ : Temperature at the fluid inflow *(℃)*

$T_o$: Temperature of the fluid outflow *(℃)*

The definition of the thermal efficiency *($\eta_{th}$)* is given in Eq. (3.3) [41].

$$\eta_{th} = Q A_C \cdot G \tag{0.3}$$

Where:

$\eta_{th}$: Thermal performance *(%)*

*Q:* The heat transferred rate *(J/s)*

$A_c$: PV module surface area *($m^2$)*

*G:* Solar electricity *($W/m^2$)*

### 3.1.3. *PV* Panel Overall Efficiency

The description of the overall efficiency is shown in eq. (3.4) [42]:

$$\eta_o = \eta_e + \eta_{th} \tag{0.4}$$

Where:

$\eta_o$ : *Overall efficiency (%)*

$\eta_e$: *Electrical efficiency (%)*

$\eta_{th}$: *Thermal efficiency (%)*

### 3.2. POROUS MEDIA POROSITY

Porosity is the percentage value of the ratio between void volume and total volume of the space that porous media inserted in [43]. It can be defined using Eqs. (3.5), (3.6) and (3.7) below.

$$Sink\ Total\ Volume\ \ (V_t)\ =\ L\ *\ W\ *\ Th \tag{0.5}$$

Where:

*L: Length (cm)*
*W: Width (cm)*
*Th: Thickness (cm)*

$$Porous\ media\ volume\ \ \ (V_p)\ =\ No.of\ parts\ *\ volume\ of\ one \tag{0.6}$$

$$Porosity\ =\ V_t - V_p\ V_t \tag{0.7}$$

## 3.3. INTELLIGENT MODELLING METHODS

The following subsections, Nonlinear Auto Regression with External Inputs (*NARX*), Nonlinear are presented.

It terminates the representation of Autoregressive (*NAR*) and Non-Linear Inputs and Outputs, respectively.

### 3.3.1. Auto Regressive Nonlinear with Outer Input (*NARX*)

*NARX* is a replicating neural network representation of nonlinear systems that predicts future values of time series based on previous outputs and external data. Equation (3.5) [44] can be used to define the *NARX*.

The dynamics of the *ANN* using *NARX* can be described by its input-output relationship:

$$\gamma(t)\ =\ \mathrm{F}(x)(t-1), x(t-2), \dots., x(t-d), y(t-1), y(t-2), \dots.(t-d)) \tag{0.8}$$

Where:

*f:* Nonlinear operation

*yt*: The predicated series

*xt*: Anthor series

*d*: The past values of *yt* and *xt.*

Figure 3.2 depicts the external as internal (delayed) inputs, Figure 3.3 reveals the block diagram prediction using the *NARX* approach, and Figure 3.4 illustrates the *NARX* methodology's flowchart.



Figure 0.2. The block diagram of (*NARX*).
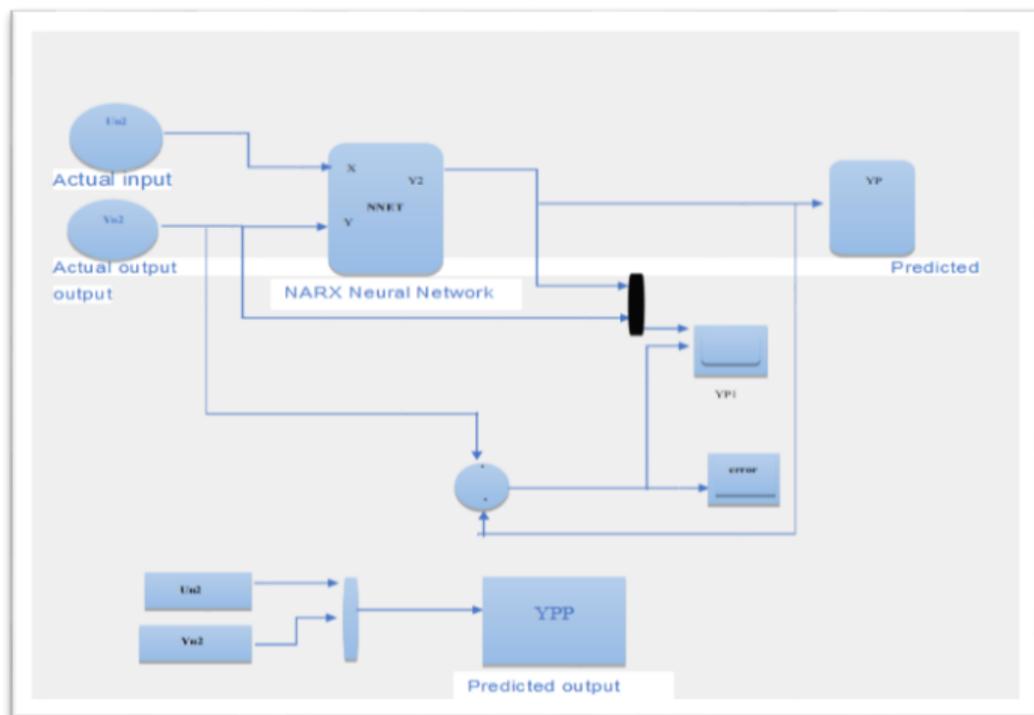
Figure 3.3. The block diagram of method prediction by (*NARX*).
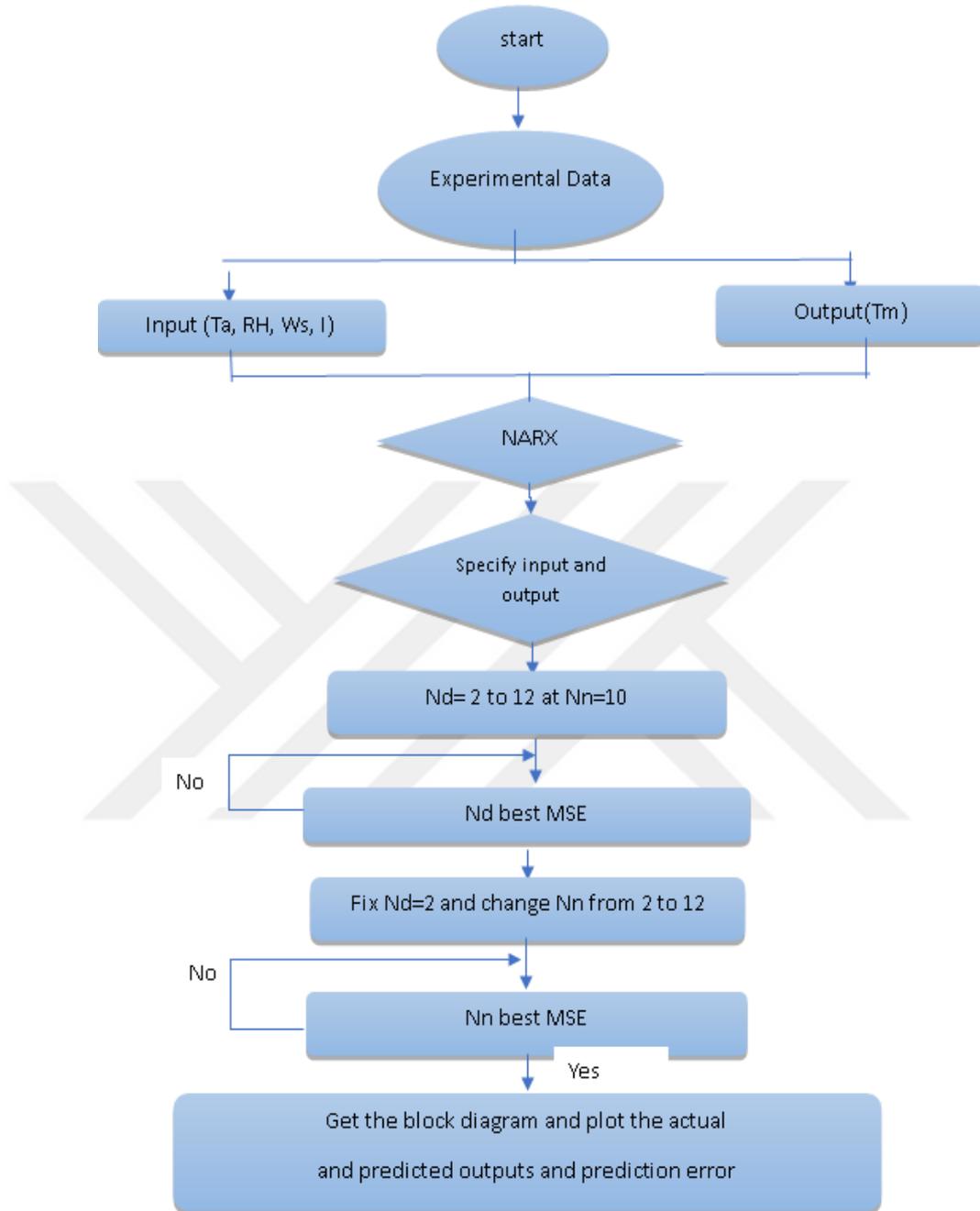


Figure 3.4. The flow chart methodology of (*NARX*).

### 3.3.2. Nonlinear Autoregressive (*NAR*)

The term "*ANN*" refers to intelligent nonlinear mapping systems, which are instruments for doing nonlinear regression analysis that may roughly approximate any kind of arbitrary function [45]. Because of their adaptability as function approximates, *ANNs* are trustworthy methods when dealing with time-series forecasting [46]. The

*NAR* network is a potent class of models that may represent any arbitrary nonlinear continuously changing mappings. It has favorable properties for simulating dynamical systems and forecasting nonlinear time series [47]. It is a technique for creating recurrent neural networks with embedded memory. The formula for the *NAR* model is:

$$\hat{y}(t) = f\left(y(t-1) + y(t-2) + \cdots + y(t-d)\right) \tag{0.9}$$

Where;

$f$: A non-linear function whose predicted values are independent of any
$d$: The output signal's earlier levels.
$Y_t$: The expected sequence

The closed loop network is utilized while employing a (*NAR*) network to make a multistep-ahead prediction. The closed-loop *NAR* network's output is represented as follows:

$$\hat{y}(t+p) = f\left(y(t-1) + y(t-2) + \cdots + y(t-d)\right) \tag{0.10}$$

Where:

$P$: Exemplifies the force

Figures (3.5), (3.6), and (3.7) manifest the *NAR* block diagram, the block design prediction by the *NAR* technique, and the flowchart of the *NAR* methodology stages in the future, respectively.
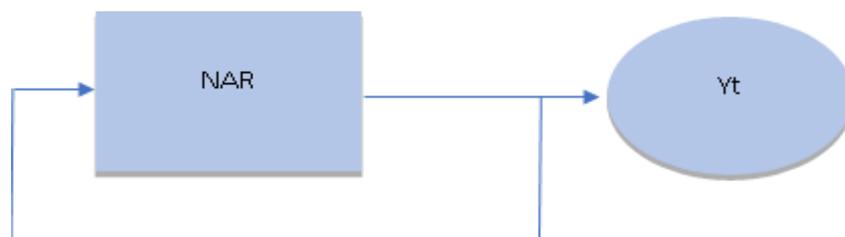


Figure 0.5. The block diagram of NAR.
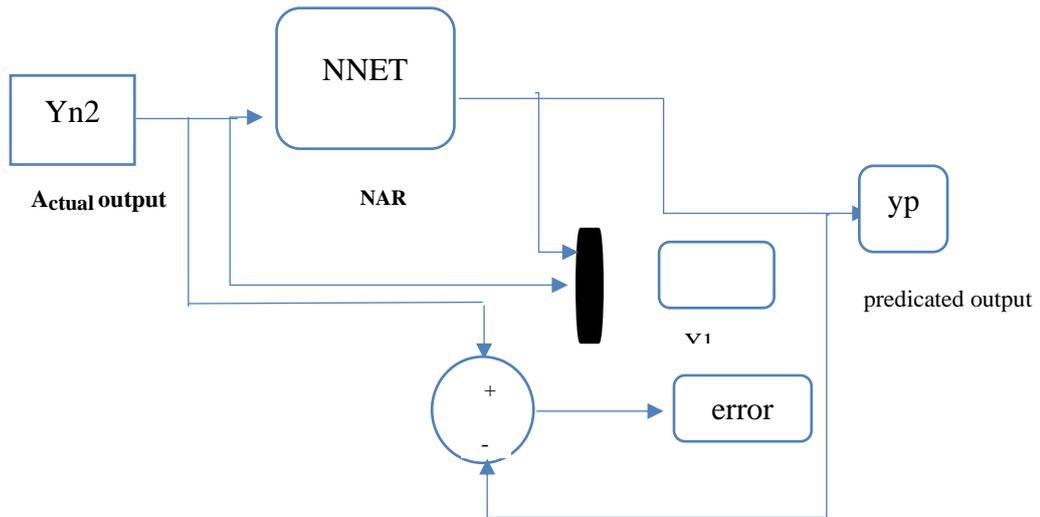
Figure 0.6. The block diagram of prediction method by *NAR*.
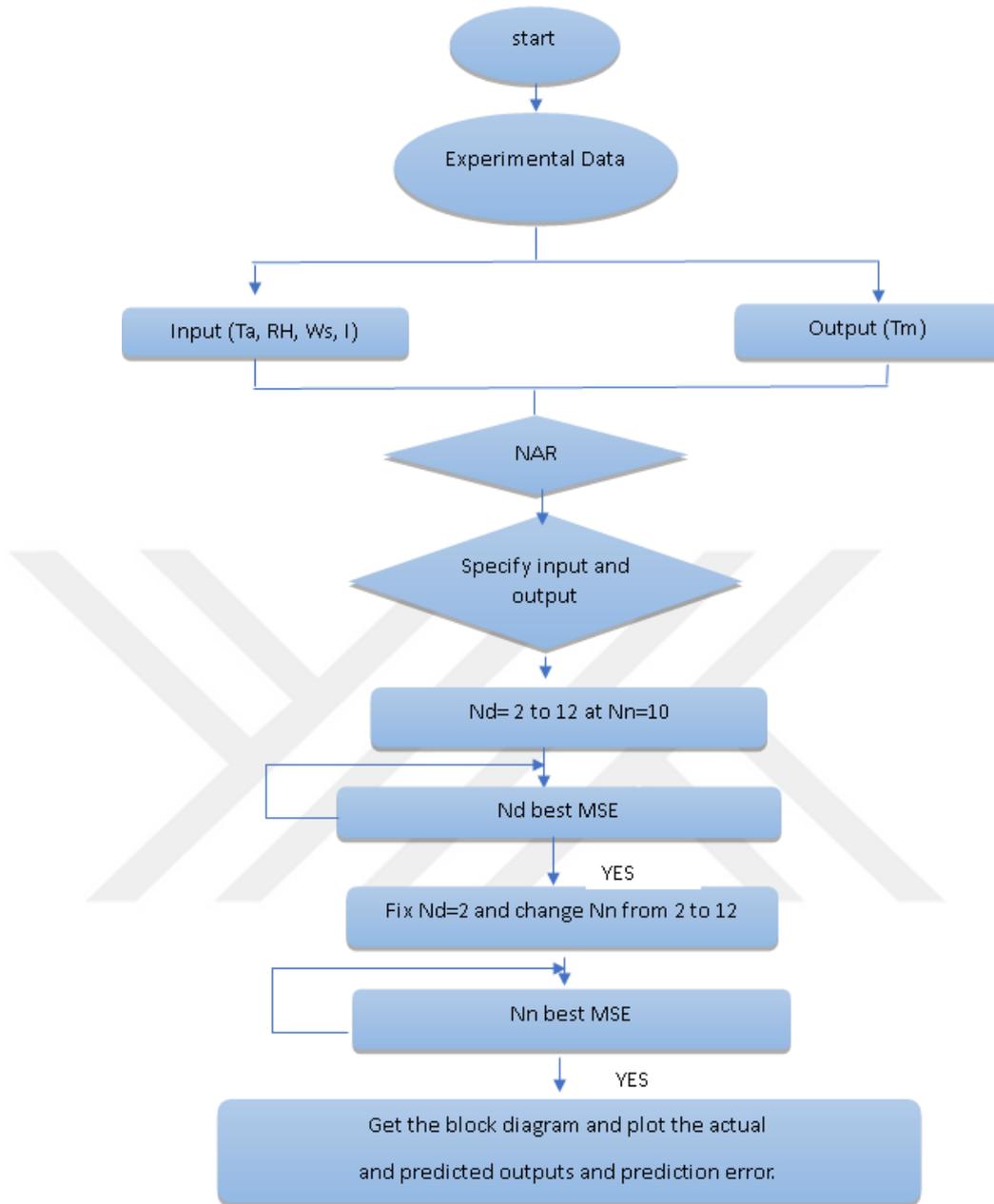
Figure 0.7. The flowchart of methodology *NAR*.

### 3.3.3. Input-Output Nonlinear

Since it has both input and output series as well as two time series without the knowledge of previous values, nonlinear input-output is comparable to the *NARX*. Eq. (3.11) [48] can be used to define it:

$$y(t) = f(x(t-1), x(t-2), \ldots, x(t-d))$$

(0.11)

Where:

*f*: Function of the nonlinear.

*yt*: Series predictions:

*xt*: The series of inputs.

*D:* xt's previous value.

Figure 3.7 elucidates the nonlinear input and output block diagram, figure 3.8 shows the nonlinear input and output block diagram prediction, and figure 3.9 details the nonlinear input-output method flowchart.
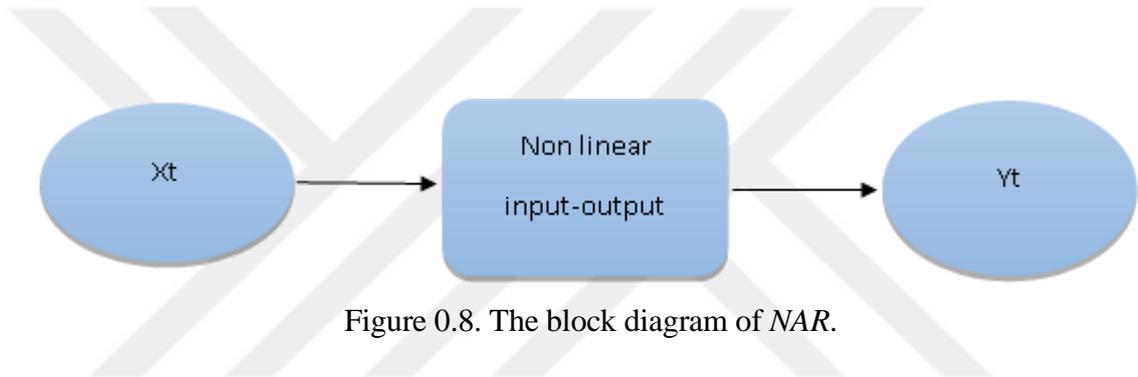


Figure 0.8. The block diagram of *NAR*.
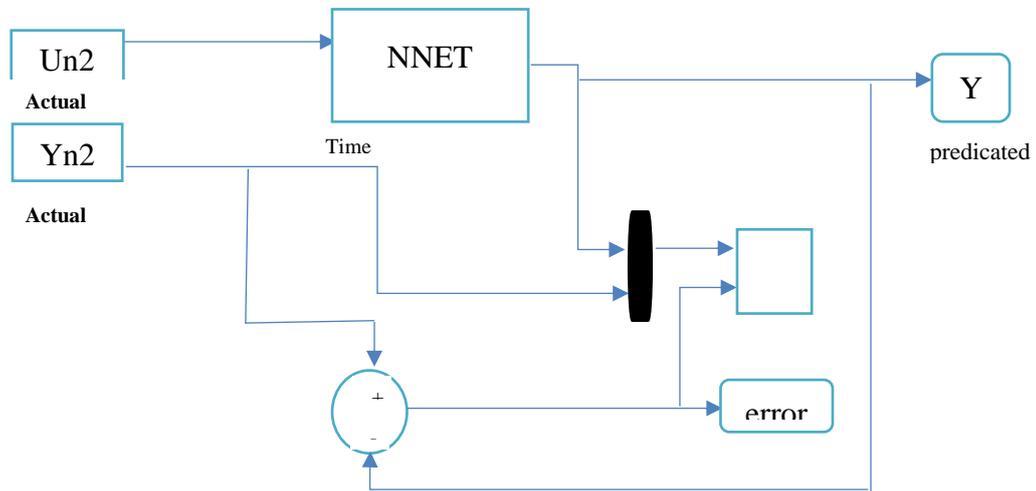


Figure 0.9. The block diagram of method prediction by nonlinear input-output.
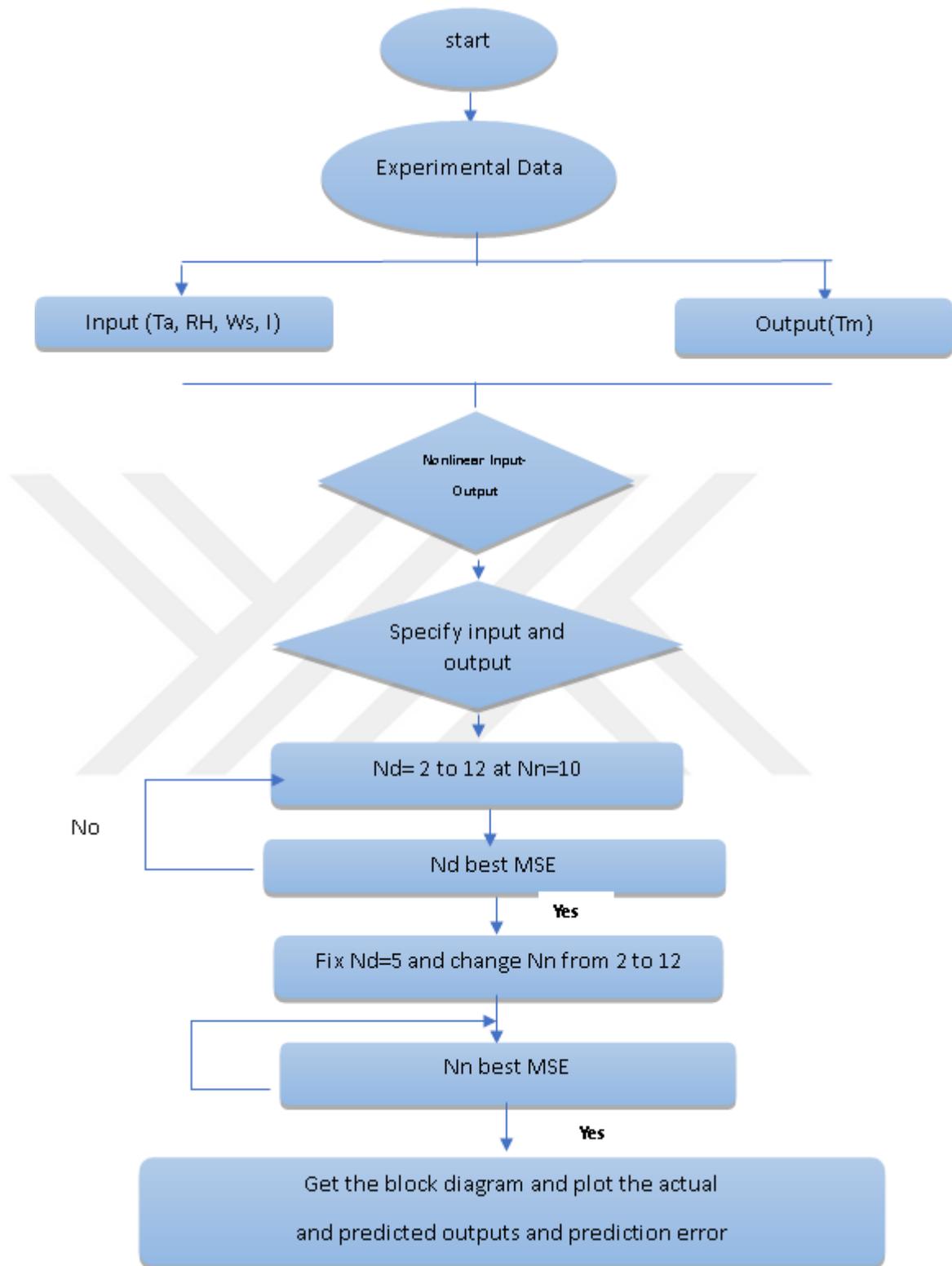
Figure 0.10. The flowchart of methodology nonlinear input-output.

## 3.4. NEURAL NETWORK MODEL VALIDATION

The performance of the various models is accessed by employing the criteria outlined below [5]:

The Mean Square Error (*MSE*) is calculated as:

$$\varepsilon(t) = 1 N \Sigma T = 1 N y(t) - \hat{y}(t)^2 \tag{0.12}$$

Where:

$\varepsilon(t)$: *MSE*.
 $N$: Amount of data.
$(t)$: Actual output
$\hat{y}(t)$: Predicted output

## 3.5. INTELLIGENT CONTROLLER

In this thesis, a proportional integral derivative controller tuned by *PSO*-Search Optimization Algorithm (*PID-PSO*) method will be used.

### 3.5.1. *PID* Controller

Because of its dependability, impact, and great performance when comparing actual values to anticipated values, the *PID* controller is frequently used in industrial control systems. The parameters of the controllers (*KP, KI*, and *KD*) are changed with the goal of attaining the best possible results. *KP, KI*, and *KD* are all related to the controller's name. If the proportional gain is greater than zero and none of the other controller parameters are, the controller is known as a *P* controller. If a controller's integral gain is positive, its proportional gain is positive, and its derivative gain is zero, it is known as a *PI* controller. The controller is referred to as a proportional-integral (*PD*) controller when the integral gain is zero, the derivative gain is non-zero, and both the proportional and derivative gains are not zero. When the integral gain is not zero, this

is the case. Last but not least, a *PID* controller has no parameters as zero. This is true for all *PID* controllers. The primary focus of this topic was the fundamental *PID* controller architecture, as seen in Figure 3.10. However, one of the most pressing difficulties is transforming the *PID* controller's traditional behavior into an intelligent one by utilizing inventive optimization algorithms to alter the *PID* settings [49]. A combination of heuristic and particle swarm optimization (*PSO*) methods was used to fine-tune the *PID* settings. When operating in continuous time, one alternative interpretation of the *PID* controller is as follows:

$$u(t) = kPe(t) + kI\int e(t)dt\, t\, 0 + k_D\, de(t)/dt \qquad (0.13)$$

The controller's output is denoted by *u(t)*, the expected error by *e(t)*, and the actual output by *e(t)*, where *KP*, *KI*, and *KD* are the proportional, integral, and derivative gains, respectively. The *PID* in block form can alternatively be modeled in the Laplace transformation domain as:

$$u(s) = (kP + kI/S + K_DS)\, e(S) \qquad (0.14)$$

In Eq. (3.15), the integral and derivative terms are converted into a discrete form of time:

$$\int_0^t e(t)dt \approx T\, \Sigma_{k=0}^n \qquad (0.15)$$

$$\frac{de(t)}{dt} \approx \frac{e(k)-e(k-1)}{T}\, or\, \frac{\Delta e(k)}{T} \qquad (0.16)$$

Where, *k* is a discrete phase at the time *t*, and where equation (3.17) is:

$$u(t) = KP\, e(k) + K_1\sum_{k=0}^n e(k) + K_D\Delta e(k) \qquad (0.17)$$

The PID controller can be represented in discrete time by Laplace transform:

$$G(z) = [KP + \frac{K1}{1-Z^{-1}} + KD(1 - Z^{-1})]\, e(z) \qquad (0.18)$$
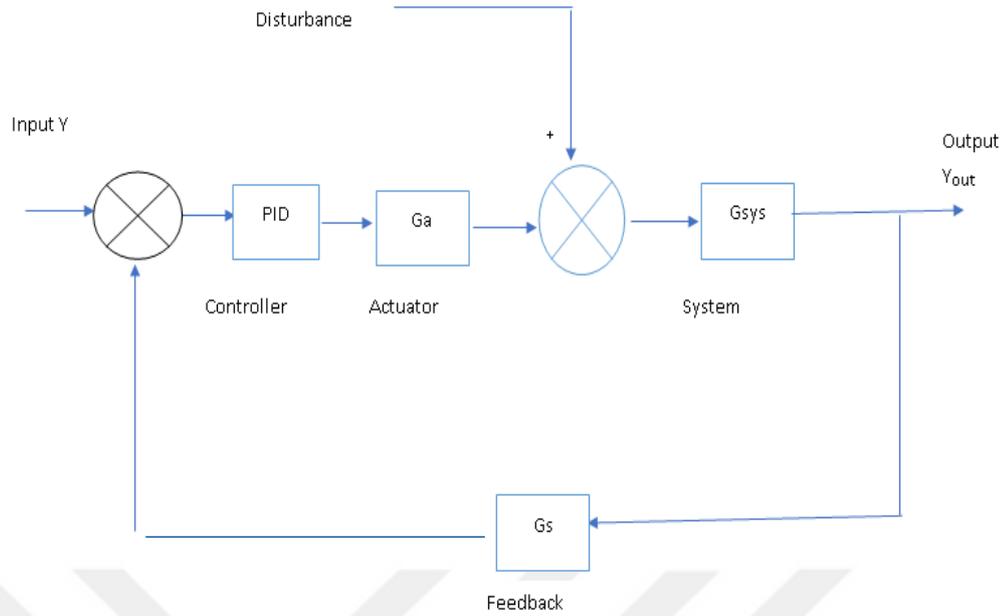
Figure 0.11. The design of basic *PID* controller.

### 3.5.2. *PSO* Tuning Method

Artificial intelligence (*AI*) and other heuristic techniques are used in engineering domains to tackle hard nonlinear problems in industrial applications based on the idea of indiscriminate optimization [50]. These techniques are inspired by the social behavior of fish, bees, and bird swarms. The primary tenet of this tactic is predicated on the notion that each bird presents in the quest area stands in for a distinct solution; this interpretation is contingent on the birds' movement and whereabouts. In the course of the generation, by working together and competing against one another, this is the meaning of the particle. Each particle increases its flying ability, but the amount of improvement is proportional to both their existing flying skills and the flying experience of their buddies. [51].

The $i^{th}$ particulate representation as $XI = xi1, xi2, \ldots \ldots$ while the best prior location for any particle giving the lowest value of fitness is represented as $PI = pi1, pi2, \ldots \ldots$ $pid$ and known pbest.

The symbol g represents the indicator for the strongest particle of all particles in the population and it is known as best. The speed of the particles (*i*) is represented as $VI = vi1, vi2, \ldots \ldots$ and its updating depends on the equations below [16]:

$$v_{id}^{n+1} = w.v_{id}^{n+1} + C_1.rand().(p_{id}^n - x_{id}^n) + C_2.rand().(p_{gd}^n - x_{id}^n) \quad (0.19)$$

$$x_{id}^{n+1} = x_{id}^n + v_{id}^{n+1} \quad (0.20)$$

Where, $c_1$ and $c_2$ are the same positive constants that are the same as 1.494, the iteration is *n*, the swarm size equivalent to 40 is *W*, and () is the function that is random equivalent to a value between 0 and 1 [15]. The equation (3.19), which measures the new particle speed in relation to the old speed and the distance between the current location and the best previous position as well as and the best experience for the group, is used to determine the new speed of the particles. After that, the particle accelerates its movement toward a new location. The square error integration (*ISE*) method was utilized for the purpose of performance evaluation of the *PID-PSO*. Figure (3.12) [17] provides an explanation of the method used to tune the *PSO*.

$$ISE = \int_0^\infty e^2(t)dt \quad (0.21)$$
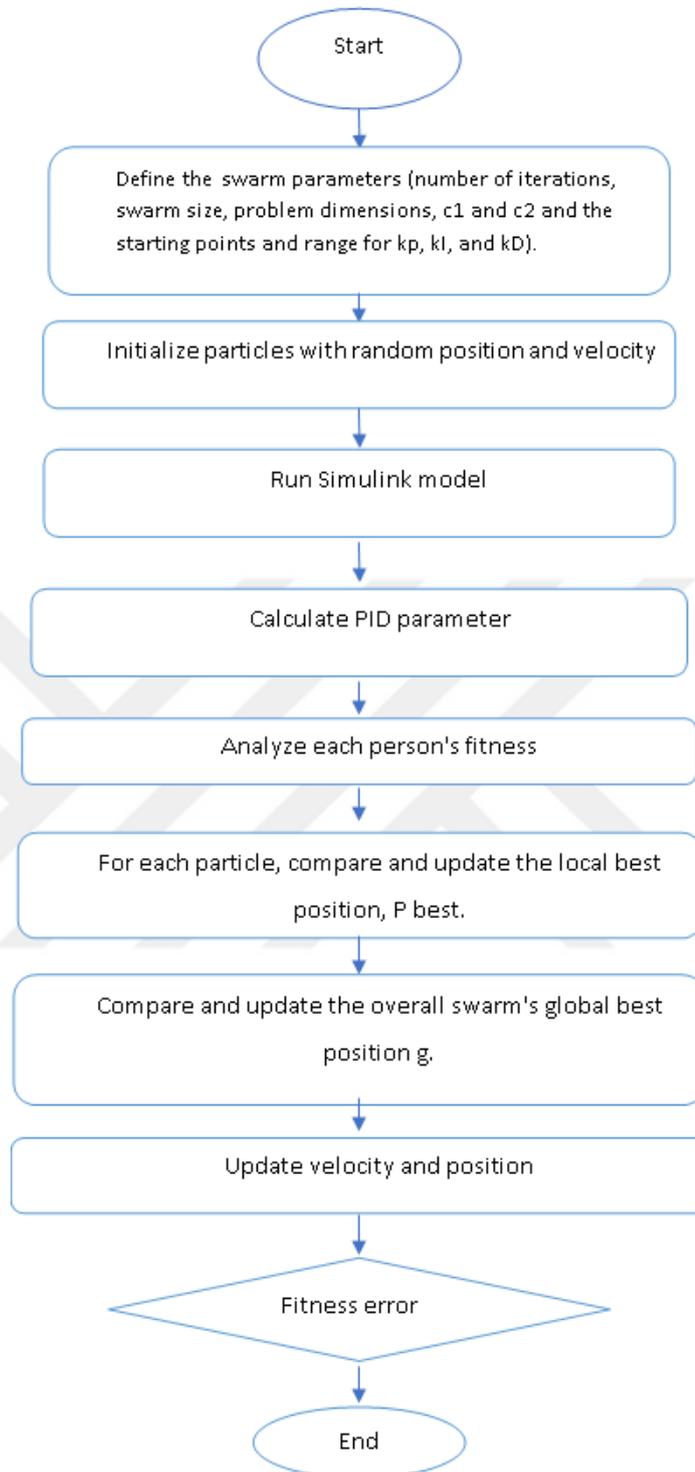
Figure 0.12. The flow chart of method *PSO* tuning.

## 3.6. UNCERTAINTY ANALYSIS

Any designed dimension  system  or  experimental program should be subject  to uncertainty  analysis,  which  is  an important part and  can be divided into  two parts:

Methodical uncertainty includes errors performing from measure equipment similar as estimation errors and data recording errors. Stochastic uncertainty is the uncertainty of the measured data due to change and scattering of the data stochastic query is the query of the measured data due to change and scattering of the data (75-76). The subscriber query $\omega\eta$ is calculated by the Eq. (3.22):

$$\omega_\eta = \left[\sqrt{(B_\eta)^2 + (P_\eta)^2}\right] \tag{3.22}$$

Where:

$B_\eta$ : represent the systematic

$P_\eta$: random uncertainty

The systematic uncertainty   is calculated in the equation below:

$$B_\eta = \left[\sqrt{(B_v)^2 + (B_t)^2 + (B_G)^2}\right] \tag{3.23}$$

where:

$B_v$ : the uncertainty of the measurement of velocity

$B_t$ : the uncertainty of the measurement of velocity

$B_G$: the uncertainty of the measurement of temperature

the random uncertainty $P_\eta$: can be calculated in Eq. (3.24)

$$P_\eta = \left[\frac{ts_\eta}{M^{1/2}}\right] \qquad \text{[KA1]} \tag{3.24}$$

where:

$t:$ the statistical amount of the student t-test at a 95% dependability level

$S_\eta$: the standard deviation

$M$: the number of repetitions for each case

# PART 4

## EXPERIMENT PROCDURE

### 4.1. INTRODUCTION

This section of the research defines the experimental investigations in detail. Al Mansour, a state-run enterprise in Baghdad, produced two PV panels for this purpose. These panels were installed in Baghdad at a southerly tilt of 31.2 degrees, at a longitude of 44.4803984 and a latitude of 33.3168805 [52].

### 4.2. EXPERIMENTAL SETUP

The experimental arrangement consists of two identical monocrystalline glass-glass *PV* panels, one being without cooling system, while the other has a cooling unit. The cooling unit has been developed by fixing a container of *8 mm* made of Perspex (Acrylic glass) on the backside of the panel to put the spiral aluminum porous media attached to *8 mm* thickness aluminum frame inside it and flowing nano-fluid through it. The experimental setup is presented in Figure 4.1.
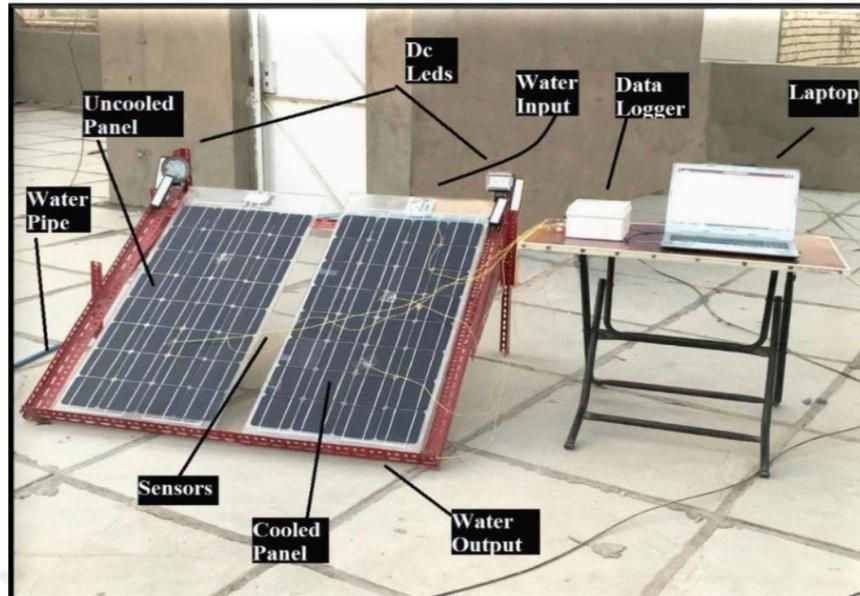
Figure 4.1. The experimental arrangement.

## 4.3. MANUFACTURING AND TESTING OF PV PANELS

Each photovoltaic panel has 32 monocrystalline solar cells that are wired in series and parallel, laminated for protection, and arranged in an array with a configuration of 4 coulombs by 8 rows.

## 4.4. MONITORING OF SOLAR CELLS

The photovoltaic (*PV*) panel modules have been put through their paces by a solar cell testing machine in order to get an idea of the panels' complete features and electrical attributes. Standard Testing Conditions (*STC*) measurements were carried out at a temperature of 25 degrees Celsius and 1000 watts per square meter, and the cell efficiency was found to be 16.1%. Table 4.1 gives details the design requirements.

Table 4.1. The design specifications of *PV* panel.

| *STC* Measurements | *1000 W/$m^2$, 25 ºC* |
|---|---|
| Open circuit voltage (*Voc*) | *21.05 V* |
| Peak voltage (*Vpm*) | *16.25 V* |
| Short circuit current (*Isc*) | *5.339 A* |
| Peak current (*Imp*) | *4.954 A* |
| Maximum power (*Pmp*) | *80.5 W* |
| Voltage temperature coefficient (*KV*) | *-2.10 mV/ cell/ ºC* |
| Current temperature coefficient (*KI*) | *15.00 µA/ cm 2 ºC* |
| Cell efficiency | *16.1%* |
| Module efficiency | *12.2 %* |
| Cell area | *156.25 $cm^2$* |
| Module area | *0.66 $m^2$* |
| Number of parallel cells ($N_p$) | *1* |
| Number of series cells ($N_s$) | *32* |

## 4.5. COOLING SYSTEM

For reducing the *PV* panel temperature and increasing the efficiency, a cooling system has been added to the one of the modules. The cooling system was divided into two parts, porous media and active nano-fluid cooling.

## 4.6. POROUS MEDIA COOLING

The porous media manufacturing process can be summarized by the following points:

I. Raw Materials: Porous media was produced using pure Aluminum shafts. There are many reasons for using aluminum. The reasons can be listed as, it is economical than other materials, the extraordinary thermal conductivity (*202.4 W/m.K*), it can be easily formed, and it's widely available in the market. Figure 4.2 shows the aluminum shaft used in the experiments.

Figure 4.2. Shaft of pure aluminum.

II. Fabrication Process: Porous media fabrication was done in the University of Technology /Training and Workshop Center/ Division of Lathing using a Star Chip *450 CNC* machine that is shown in Figure 4.3.



Figure 4.3.  The machine ofstar chip *450 CNC*.

III. Developed Porous Media: Porous media was produced in spiral shape, as presented in Figure 4.4. The porous media dimensions are *1 mm* thickness, *8 mm* diameter and *45 cm* length.

Figure 4.4.  The spiral shape porous media.

**IV.** Porous Media Arrangement: The spiral porous media were attached to an aluminum frame of (*98 cm × 45 cm × 8 mm*) dimensions. The porous media frame was inserted into a container made of Perspex (Acrylic glass) of 8 mm thickness, fixed on the backside of the cooled PV panel and perpendicular to the cooling nano-fluid flow direction. Figures 4.5 and 4.6 view the porous media plate and the Perspex container, while Figure 4.8 portrays the porous media plate inserted in the Perspex container.



Figure 4.5. The plate of porous media.

Figure 4.6. The perspex container.



Figure 4.7. The porous media plate inserted in the perspex container backside of the cooled photovoltaic panel.

## 4.7. PREPARING OF NANO-FLUID

A previous study found that ($AL_2O_3$) is the nanoparticle that is used most commonly in the cooling process due to its high thermal conductivity. Three distinct concentrations of nano-fluid s for the $Al_2O_3$ type were produced by weight : *1 wt% , 1.5wt%,* and *2wt%* [53]. The base fluid, pure water, was added to the nanoparticles right away after they were weighed using a digital electronic scale (Denver Instrument

*S-234*). One of the main goals of the study [54] being done on the role of nano-fluid stability and the synthesizing process is to demonstrate for the first time in a comparative experimental evaluation the effect of nano-fluid manufacturing method on the performance of *PV/T* systems. One of the main objectives of the research is this. The process of producing nano-fluid and its stability were found to have a significant impact on the performance of *PVTs* based on the results. Nano-fluid was produced using a one-step and a two-step procedure at one concentrations (2 *wt*%) where is the best concentration that gives. An *RSS* ultrasonic processor was utilized at the University of Technology to swirl the nanoparticles into the water for an hour. Almost immediately, the water-based base fluid was mixed with the nanoparticles while being rapidly swirled for an hour. Then, as described in Reference [55] and illustrated in Figure 3, nanoparticles were disseminated in distilled water for an hour using a strong probe ultrasonic processor (*UP400s* Ultrasonic Processor). 4 grams of polyethylene glycol as a surfactant were used per gram of material in the $Al_2O_3$ experiment. The nano-fluid turned white after the mixing process was completed.

### 4.7.1. Nanoparticles

$Al_2O_3$ nanoparticles were used with a particles size of *20 nm*, as shown in Figure 4.8.
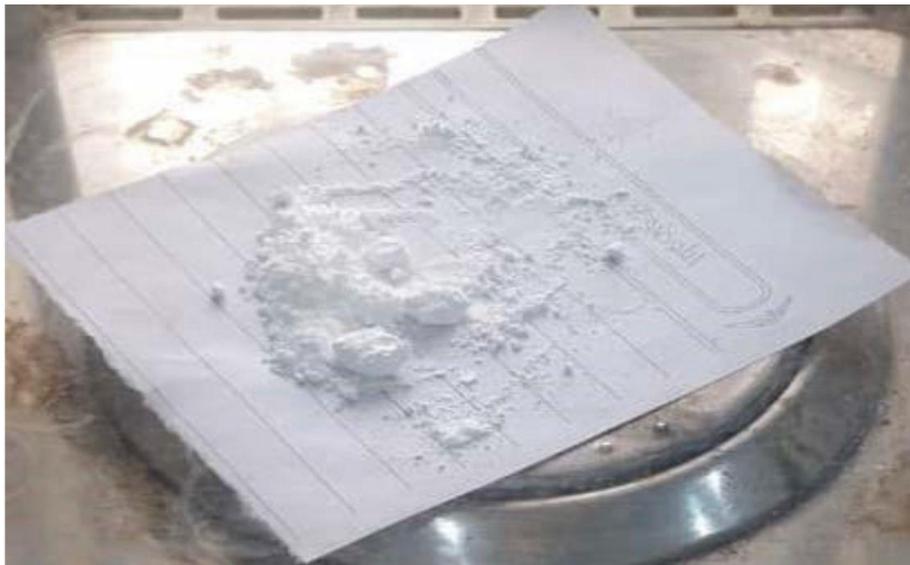


Figure 4.8. The nanoparticles of $Al_2O_3$.

### 4.7.2. Water Desalination

The pure water free of impurities and salts must be when preparing the nano-fluid because the salts and impurities affect the physical properties of nano-fluid.

### 4.7.3. Digital Balance

When preparing nano-fluid, a certain concentration must be carefully weighed for each quantity of water by using very sensible digital balance, as displayed in Figure 4.9.
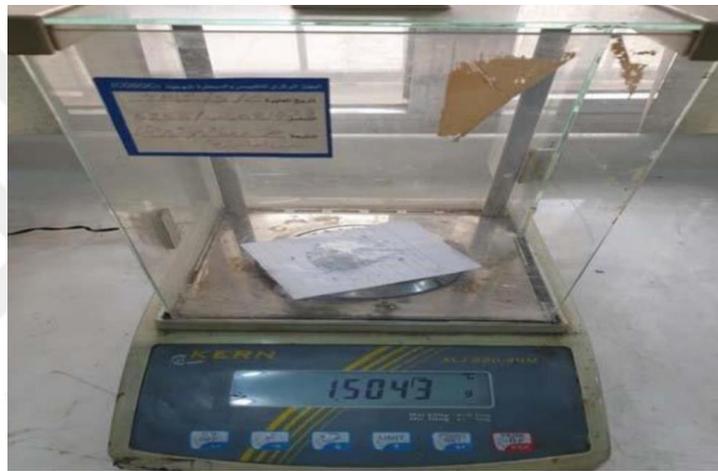


Figure 4.9. Digital balance.

### 4.7.4. Ultrasonic Homogenizer

Ultrasonic homogenizer type *UP200Ht* as shown in Figure 4.10 was used to get a mixture of constant properties.

Figure 4.10. Ultrasonic homogenizer.

## 4.8. DATA LOGGER

The measurement of different parameters that used to assist the solar penal performance was done by developed data logger, which consists of four sensors; k-type thermocouple to measure the temperature of the panel, voltage and current sensors to measure the panel electrical performance during operation time, and solar radiation sensor to measure the solar power received by the panel, finally an ambient

44

temperature and humidity sensors were used. The processor of the developed data logger is Arduino mega. Figure 4.11 presents the data logger schematic.
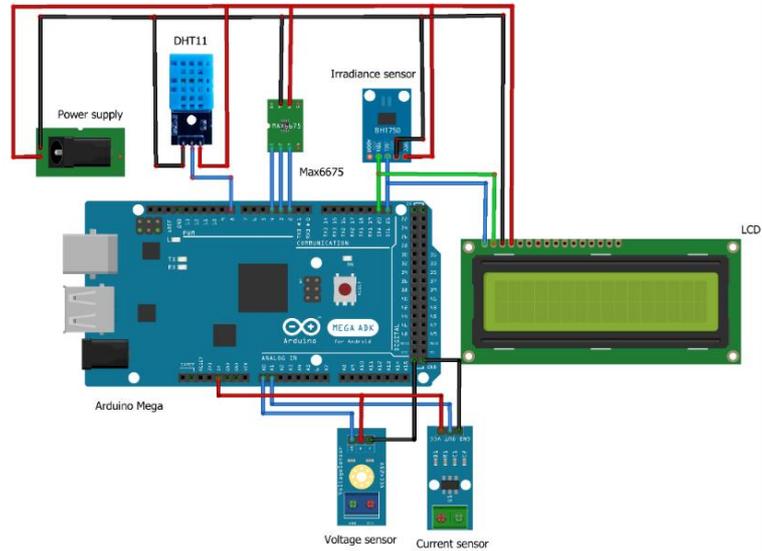


Figure 4.11. The schematic diagram of the data logger.

## 4.9. ARDUINO MEGA

The *Arduino Mega 2560* board is built upon the *AT* mega 2560 as its primary component. There are a total of 54 digital *I/O* pins, 16 analog *I/O* pins, and *14 PWM* signal *I/O* pins available on this board. The board incorporates all of the necessary components for the microcontroller into its design, its use a trademark of Arduino as part of a company name or logo [63]. Figure 4.12 exhibits the Arduino mega microcontroller board for your viewing pleasure.
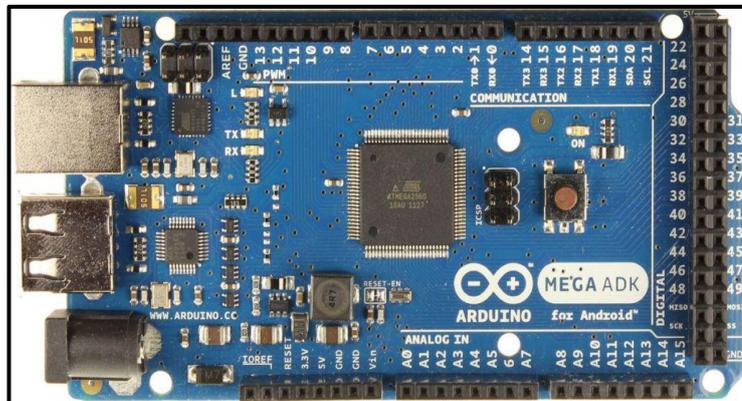


Figure 4.12. The mega board of Arduino.

The Arduino Mega could be fueled either by a connection to a USB port or an external power source, and the selection would be made automatically. The power for non-*USB* devices could come from either a battery or an adaptor. Arduino may function on voltages ranging from *6* to *20 volts*.

The power pins are as follows:

- *VIN*, Voltage of the Arduino's input while using an external power source.
- *5V*. The microcontroller is run by a regulated power supply.
- *3.3v*; The onboard regulator produces the power supply.
- *GND*, Ground pins.

The *Atmega 2560* memory *is 256 KB*.

Using procedures like pin Mode, digital Read, and digital Write, the 54 digital pins might be used as output or input. They operate on 5 volts. Each pin has a built-in pull-up resistor that allows it to deliver or receive a maximum of 40 *mA*.
Furthermore, some pins have dedicated purposes:

- Serial: utilized to receive (*RX*) and transmit (*TX*) serial data. Pins 0 and 1 are as well connected to corresponding pins USB to serial chip.
- External Interrupts: Those pins could be configured to trigger an interrupt on change in value, falling or rising edge, or low value.
- *PWM*: Provide 8 bit output with the function of "analogWrite".
- *SPI*: Those pins support SPI communication.
- *LED:* digital pin 13 has integral *LED.*
- *I2C*: communication using Wire library.

16 analog inputs are available on *Mega2560*, with resolution of 10 bits (i.e. 1024 different values).

- *AREF*, analog inputs reference voltage.
- Reset, bring the line *LOW* to reset microcontroller.

*Arduino Mega 2560* has several ways to communicate with another Arduino, *PC*, or other microcontrollers. Arduino has 4 *UARTs* to *TTL* sequential. An *Atmega8U2* on board channels is one of those over *USB* and gives virtual com port to programming by *PC*. Arduino programming incorporates a serial monitor which permits straightforward printed information to the *PC*. *RX* and *TX LEDs* on board will turn on/off once information is being communicated through the *Atmega8U2* chip and *USB* with the *PC*. It features *SPI* and *I2C*.

In this work, Arduino mega was selected due to fast processing power which ensures stability.

The signal from a *Type-K* thermocouple can be digitized using the *MAX6675*, and it can also conduct cold-junction compensation. The data is delivered in a format that is compatible with SPI and has a read-only resolution of 12 bits. This converter can take measurements as high as +1024 degrees Celsius and can resolve temperatures down to 0.25 degrees Celsius. Figure 4.13 provides a visual representation of the module's explanation. The *MAX6675* can detect and take into account differences in the temperature of its surroundings through the utilization of cold-junction compensation. The temperature data is converted into a voltage by the gadget, which makes use of a temperature-sensing diode. In order to calculate the actual temperature of the thermocouple, the *MAX6675* takes a reading of the voltage that is present between the thermocouple output and the detecting diode. The temperature of the thermocouple's hot junction is set by the internal circuitry of the device, which also passes the voltages of the diode (which detects the temperature of the surrounding environment) and the thermocouple (which senses the temperature of the remote location minus the temperature of the surrounding environment), its proudcted Maxim Integrated Products, Inc. [64].
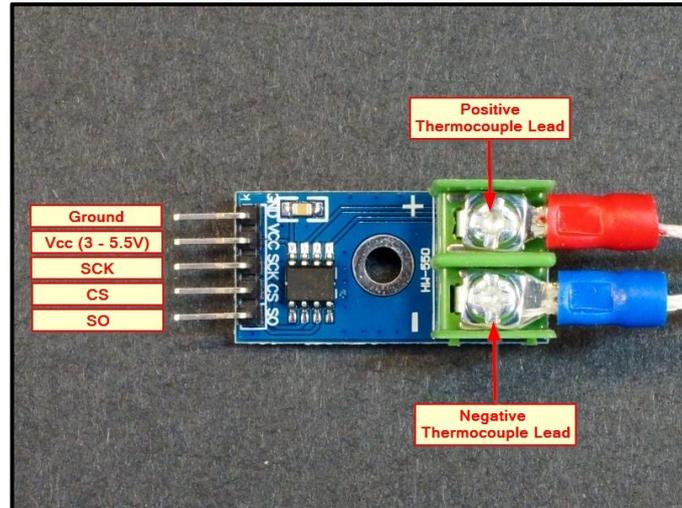
Figure 4.13. Module of *MAX6675*.

## 4.10. SENSORS

The *DHT11* sensor has been chosen because it provides a digital output that changes depending on the ambient temperature and humidity that is being measured. This made it possible to measure the humidity and temperature of the surrounding air accurately. This is accomplished using the sensor's resistive-type humidity detecting element and the negative temperature coefficient (*NTC*) thermistor. As the temperature being detected rises, the *NTC* thermistor's resistance decreases. The *DHT11* sensor was made using technology that guarantees a high level of dependability, excellent long-term stability, and an incredibly fast reaction time. The *DHT11* sensing device is meticulously calibrated before going on sale; the calibration coefficients are stored in the device's internal memory and are used by the embedded detecting/processing unit. This sensor is easy to integrate into digital systems since it utilizes a serial interface that only needs a single cable. The physical connectivity of the sensor is accomplished through a three-pin, 0.1-pitch connector. The sensor is powered by the power supply voltage and ground on the first two pins, while the digital serial output signal is connected to the third pin. Due to its extremely small physical dimensions (*26.7mm x 17.8mm*) and extremely low weight (*just 2.7g*), this board is a great choice for use in environmental monitoring systems. A single-wire data bus is used to facilitate synchronization and communication between the sensor and the Node MCU. The accuracy of the *DHT11* serial output, which has a resolution of 16 bits, is 3-5% for

humidity and 2% for temperature at 25 degrees Celsius, respectively. Temperature and humidity can be tracked with the *DHT11*. Consequently, the full serial digital data is made up of forty bits, which are divided as follows: A communication procedure takes about 4 milliseconds overall and includes 8 bits of integral humidity data, 8 bits of decimal humidity data, 8 bits of integral temperature data, 8 bits of decimal temperature data, and 8 bits of check-sum (which is the sum of the four bytes that came before it), its prouducted Mouser Electronics Co. [62]. The pinout for the *DHT* 11 is shown in Figure 4.14 below.
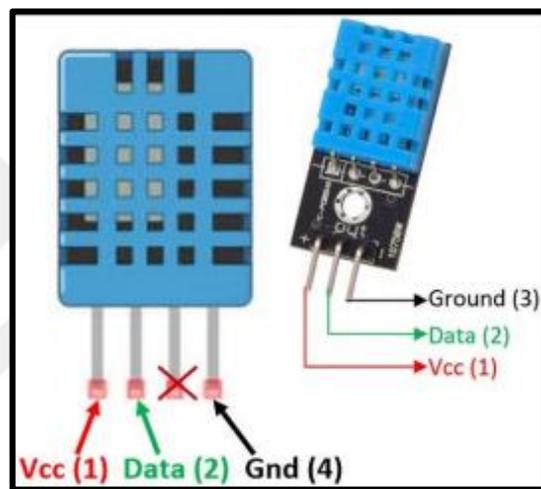


Figure 4.14. Pinout 11 of *DHT*

The Voltage Sensor is a straightforward module that works with Arduino (or any other microcontroller with a *5V* input tolerance) to measure external voltages that are higher than the microcontroller's maximum allowable value, which is 5 *V* in the case of Arduino. The Voltage Sensor is essentially a 5 to 1 voltage divider made up of two resistors with resistances of *30 KΩ* and 7.5 *KΩ*. As a result, for each input voltage, the output voltage is lowered by a factor of 5, its producted form Allegro Micro System Inc. [62]. Below, Figure 4.15, one can find the Voltage Sensor Module's internal circuit diagram.
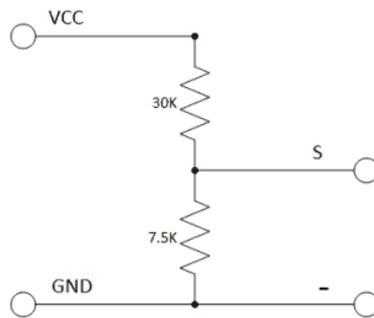
Figure 4.15. Diagram of the module of voltage sensor.

The *ACS*712 is a linear current sensor that is based on the Hall effect. This sensor is capable of measuring both direct current (*DC*) and alternating current (*AC*). *DC* stands for direct current. The integrated low-resistance current conductor and *2.1kVRMS* voltage isolation are two of its defining characteristics. Figure 4.17 illustrates the basic components of the sensor as well as the pinout of the sensor. To get an accurate reading of the current, this *IC* employs a low-offset Hall sensor. This sensor is positioned on the surface of the integrated circuit along a copper conductor route. Internally, it is equipped with a copper strip that serves to link to the *IP+* and **IP**- pins on the sensor. When enough current is passed through the copper conductor, a magnetic field is produced, which may be detected by the *Hall* Effect sensor. The hall effect sensor detects the presence of a magnetic field and then generates a voltage that is proportional to that field. This voltage can then be used to measure the current, its producted form Allegro Micro System Inc. [62].
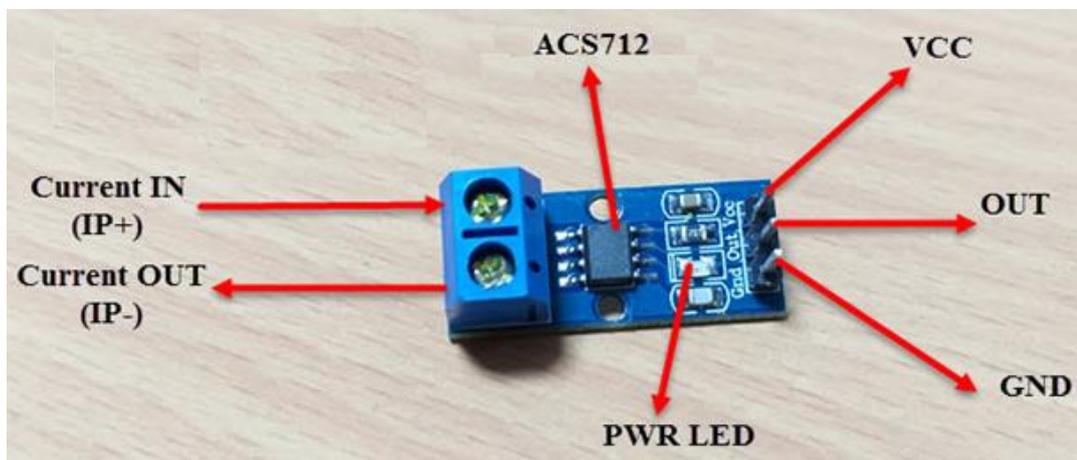


Figure 4.16.  The sensor of Current *ACS712*.

50

The *BH1750* is an *I2C*-compatible, 16-bit ambient light sensor. It produces readings of brightness in lux (the SI's illuminance unit). The range of measurable light intensity is from 1 lux up to 65535 lux. The light sensor schematic is revealed in Figure 4.17.
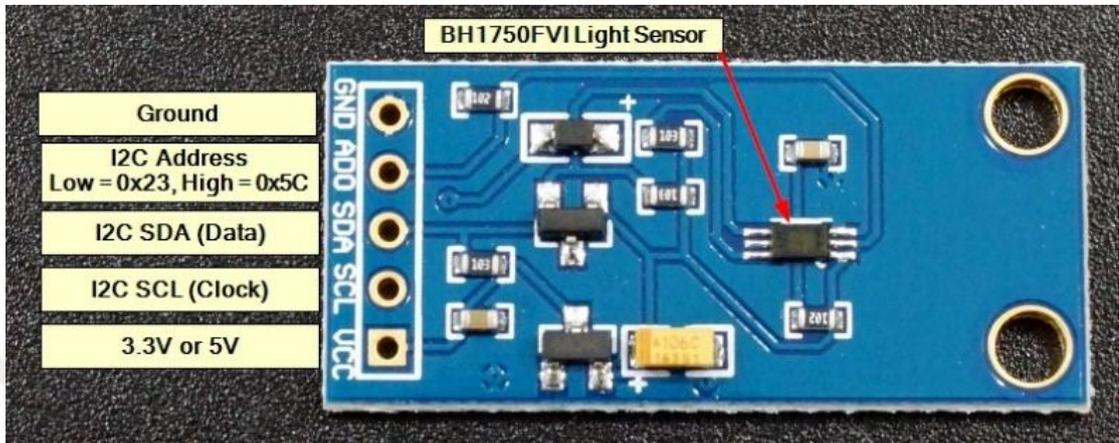


Figure 4.17. Module of sensor *BH1750*.

*LCD* screen 20x4 characters *LCD* was utilized to show the flow rate. The *LCD* is connected to Arduino via *I2 C* interface. *I2 C* communication interface. This means it only needs 4 pins for the *LCD* display: *VCC, GND, SDA,* and *SCL*. Figure (4.18) shows the *LCD* display module.



Figure 4.18. *LCD* (A2004).

As the Arduino board can provide a limited amount of power and to ensure each sensor is running smoothly, an external power supply is connected to the circuit that power the sensors (Figure 4.19).
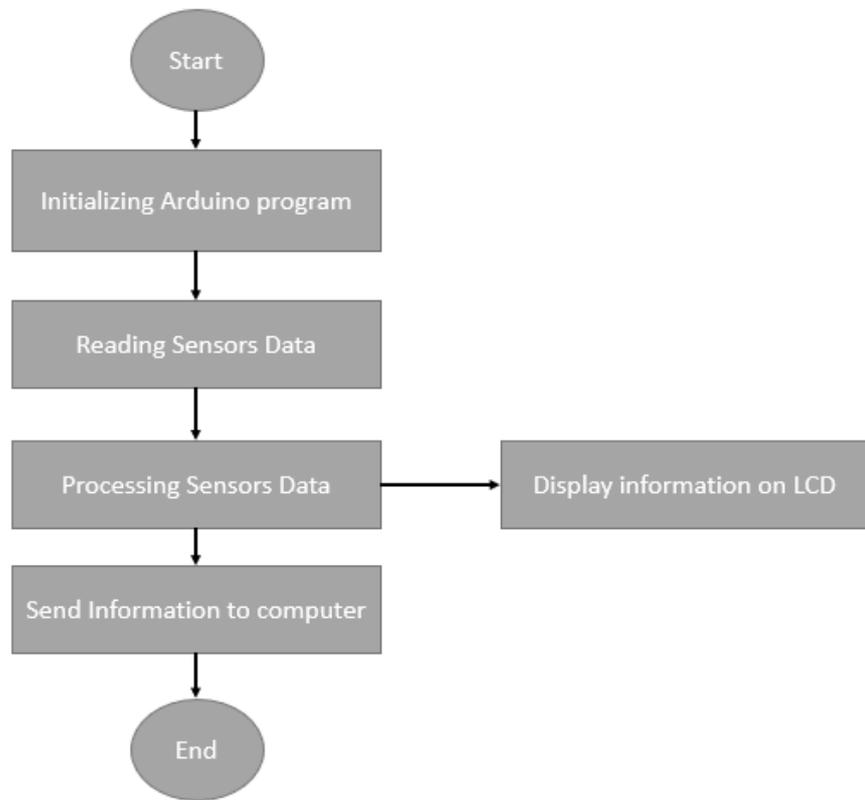
Figure 4.19. Flow chart of Arduino program.

## 4.11.    FLOW METER

To measure the cooling fluid flow rate an Arduino Based measurement device has been developed, as shown in Figure 4.20.
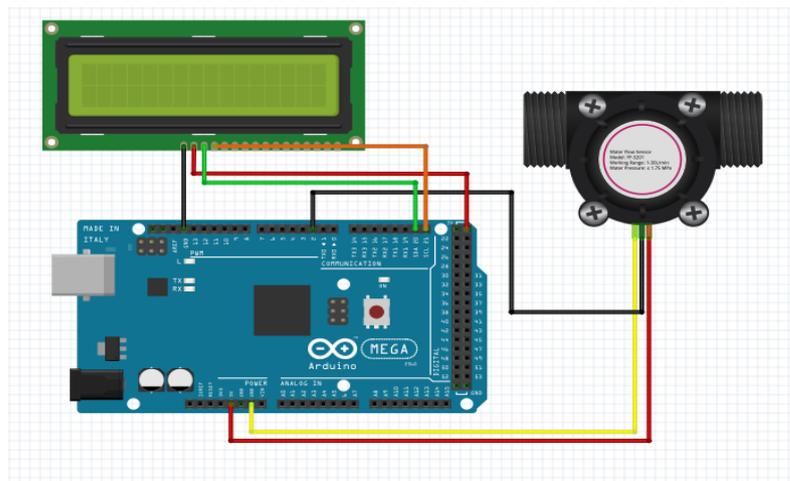


Figure 4.20. The Diagram of flow meter circuit.

Fluid stream sensor type (*YF-S201*) comprises a fluid rotor, a corridor impact sensor and a plastic valve body. The rotor rolls when fluid courses during the rotor, its velocity variations is at different paces of flow. The corridor impact sensor yields the relating beat signal, its use a trademark of Arduino as part of a company name or logo [63]. Figure 4.21 and 4.22 show the fluid flow sensor and flow chart of operation by flow meter, respectively.



Figure 4.21. Sensor of  fluid flow.
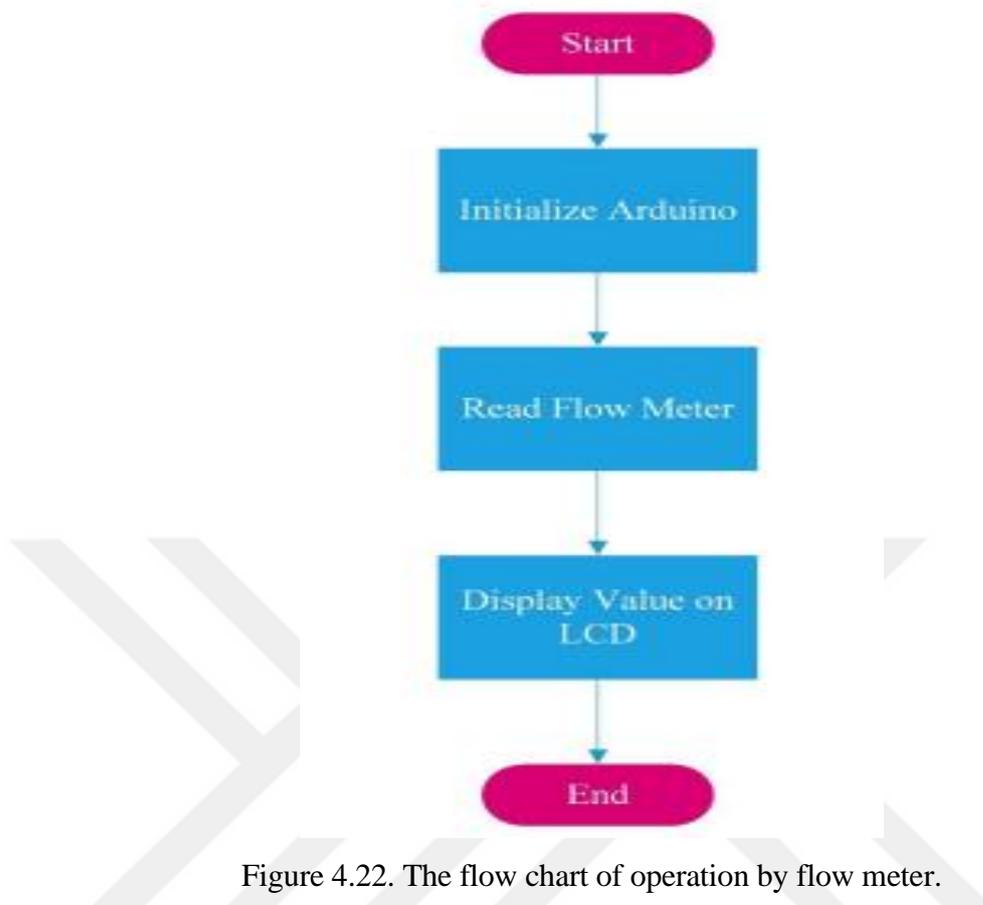
Figure 4.22. The flow chart of operation by flow meter.

## 4.12.    COOLING FLUID FLOW CONTROL

The working fluid flow rate was controlled via a developed device which measures the temperature of the enhanced *PV* panel cooling system at a specific location and adjusts the flow based on varying the supplied voltage to the pump (Figure 4.23). The control algorithm for the developed system based on *PID-PSO* algorithm was detailed earlier, where the parameters for the *PID* were *Kp=80, Ki=88.05,* and *Kd=11.1*.

The set point for system was 40 $^{o}C$, where the pump starts, and the flow sets to 3 *L/M* which will increase proportionally with the rise of *PV* panel temperature to reach a maximum of 5 *L/M*.
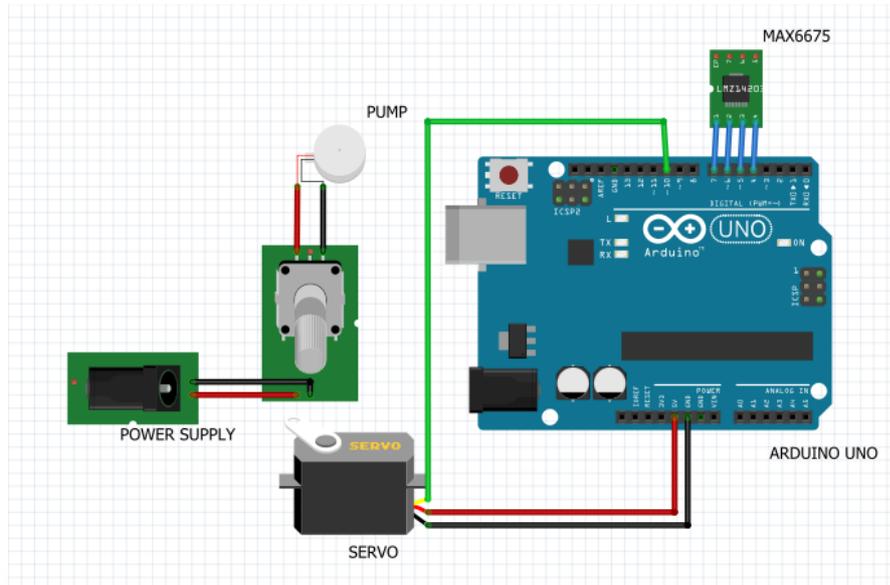
Figure 4.233. The system of working fluid control.

As the available option for the water pump was only a type of *DC* motor (brushless) which can't be controlled directly via Arduino *PWM* signal, a mechanism for controlling the pump speed was achieved by attaching servo motor to a potentiometer which changed the voltage of the supplied voltage to the motor via turning the nob of the potentiometer to the set position.

## 4.13. WATER PUMP MOTOR

The pump type shown in Figure 4.24 was used to pump the water to the cooling system from the storage tank with 6-12V *DC*, *18W*.



Figure 4.24. The water pump.

## 4.14.    SERVO MOTOR SG90

Servo Motor *SG90* is a tiny and lightweight server motor with a high output power. Servo can rotate approximately 180 degrees (90 in each direction) and works just like the standard kinds but smaller. One can use any servo code, hardware or library to control these servos. İt good for beginners who want to make stuff move without building a motor controller with feedback and gear box, especially since it will fit in small places, its produced from Desheng Intelligent Technology Co. [64]. Figure 4.25 presents the utilized servo motor.



Figure 4.25. Servo motor *SG90* [64].

# PART 5

## RESULTS AND DISCUSSION

Analytical modeling techniques and experimental findings are used to examine how the performance of the proposed cooling system affects the *PV* system's behavior. These experimental and analytical results are based on many main parameters, such as photovoltaic panel surface temperature, climate temperature, inlet and outlet Nano-fluid temperature, load voltage, and load current, note that the wind speed and humidity are not taken into account. Part five is divided into two parts presented below:

- The analytical modeling findings for three *ANN* nonlinear time series approaches—*NAR*, *NARX*, and Nonlinear input/output with the use of *MATLAB* operating system depending on *MSE*—are presented in the first section. These techniques were used for predicting the temperature regarding the *PV* panels with the use of data that was gathered in September.

- In the second section, the theoretical results of the *PSO* intelligent controller are introduced. This controller regulates the temperature regarding the *PV* panels depending on data from the previous part's best modeling approach, which is based on *ISE* and *MSE*. Close loop and open loop investigations were conducted in two cases.

- The third part presents the thermal and electrical behavior for the testing experimental work of cooling and controlling organizations.

## 5.1. ANALYTICAL MODELLING RESULTS

The findings of *NAR*, *NARX*, and nonlinear input/output time series *ANN* analytical modeling are presented in this section. The input data for the three techniques were the ambient temperature, current, voltage, and solar irradiance. Note that because they were regarded as constants, humidity and wind speed were not considered. The output

data, however, was the surface temperature of the PV panel. Data on output and input were taken between Sep 15 and Oct 30, 2022, between 7 *AM* and 2 *PM* in clear weather. The work was carried out in the Iraqi province of Baghdad. There were 214 input data sets and an equal number of output data sets. The reading time between one data set and the next was roughly 2.5 minutes. The input/output data was changed for all techniques so that 50% of them were used as training range, 25% as validation range, and 25% as testing range. As a consequence, with regard to the validation, training, and testing ranges, the 214 input/output data were transformed into 53 data sets, 107 data sets, and 53 data sets, respectively.

Figure 5.1-Figure 5.4 manifest the temperature of the solar panel (output), and the inputs (the panel temperture, ambient temperature, solar radiation and voltage) respectively.
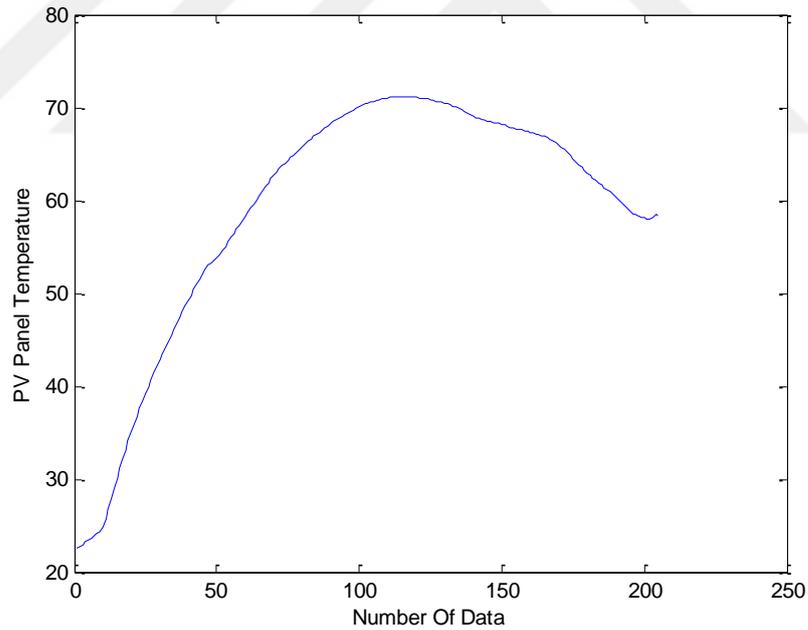


Figure 0.1. The *PV* Panel Temperature (*°C*).
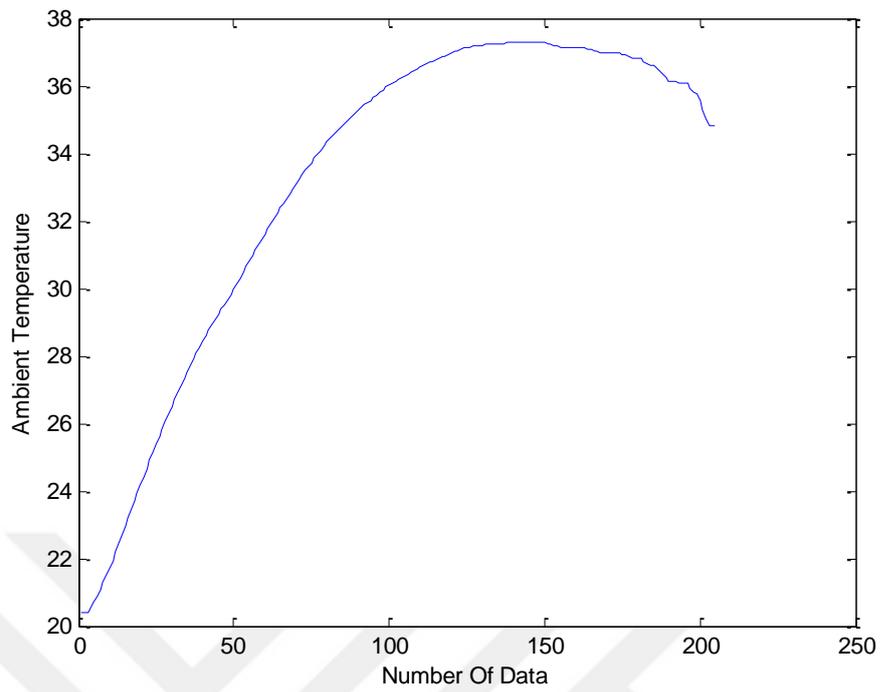
Figure 0.2. The *PV* Ambient Temperature (${}^{o}C$).
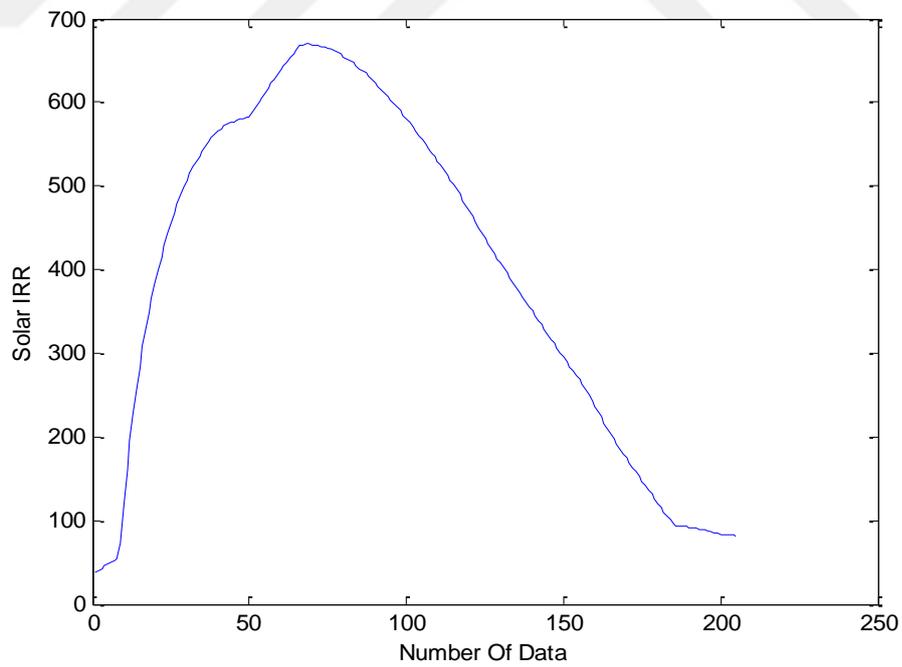


Figure 0.3. The Solar *IRR*.
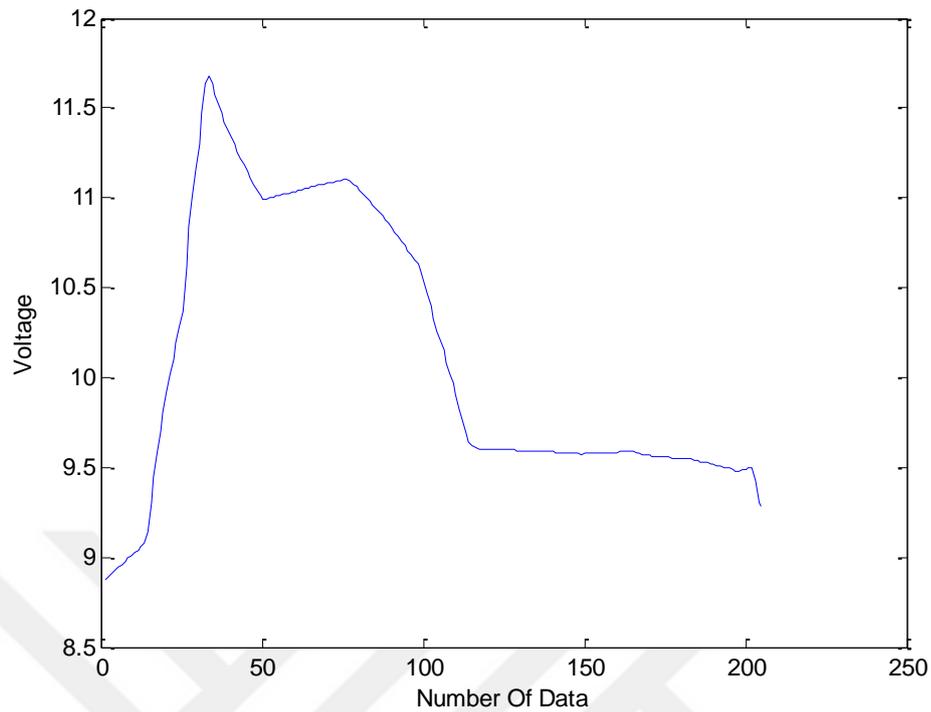
Figure 0.4. The Voltage (*Volt*).

All modeling techniques follow the same stages for solving the problem. In the initial phase, Nn is fixed at 10, and *Nd* is varied between 2 and 12. The following step is to alter *Nn* number starting at 2 and finishing at 12, setting *Nd* number to the lowest *MSE* value.

## 5.2. ANALYTICAL MODELLING RESULTS WITHOUT COOLING

### 5.2.1. *NARX* Modelling Technique

According to Figure 5.5, the predicted output temperature in *NARX* is derived from 2 input series, input data, and external input series that are represented by actual photo-voltaic panel surface temperatures.
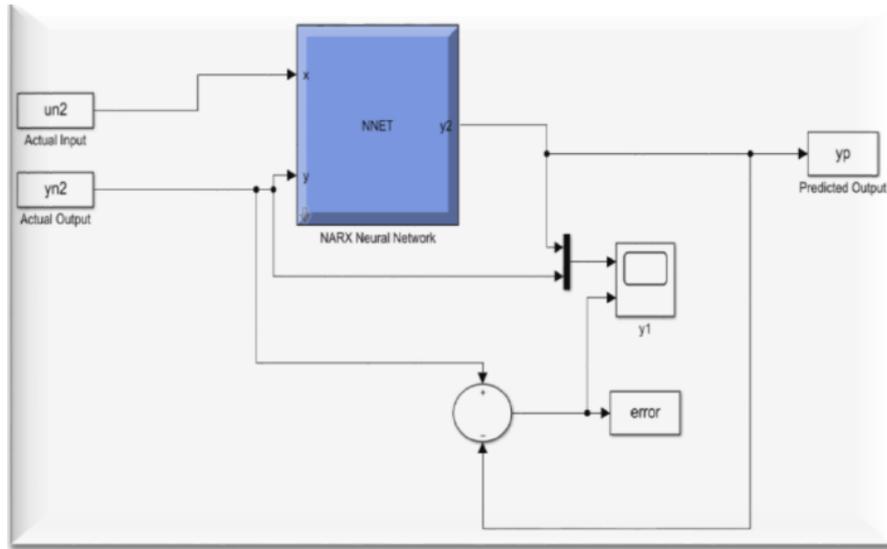
Figure 0.5.The block diagram of modelling technique *NARX*.

The lowest *MSE* occurs in the case,that equals to 2.09 when *Nn* number is equal to 10 and *Nd* number is equal to 4, as shown in Table 5.1, The following stage involves setting *Nd* number on 4 and adjusting *Nn* number from 2 and 12. when *Nn* number is fixed at the value of 10 and the *Nd* number is varied between 2 and 12. The optimal *MSE* for this modeling method is 0.84 at *Nn* number is equal to 7 and *Nd* number is equal to 4, as illustrated in Table 5.2. The actual and predicted *PV* panel surface temperatures are shown in Figure 5.5 and Figure 5.6, respectively, while the prediction error for the *NARX* modelling approach is shown in Figure 5.7.

Table 0.1. The First Step of Narx Modelling Method MSE.

| Sets Number | Training *MSE* Error | Validation *MSE* Error | Testing *MSE* Error | Overall *MSE* | Epoch |
|---|---|---|---|---|---|
| 10-2 | $1.66*10^{-1}$ | $8.28*10^{-1}$ | 1.25 | 2.244 | 11 |
| 10-3 | $5.77*10^{-1}$ | 1.75 | 1.07 | 3.397 | 12 |
| 10-4 | $1.55*10^{-1}$ | $5.55*10^{-1}$ | 1.38 | 2.09 | 14 |
| 10-5 | $7.14*10^{-2}$ | 1.85 | 2.27 | 4.191 | 13 |
| 10-6 | $1.11*10^{-3}$ | 1.51 | 1.51 | 3.02 | 14 |
| 10-7 | $1.08*10^{-1}$ | 4.13 | 10.46 | 14.69 | 15 |
| 10-8 | 1.13 | 3.42 | 2.85 | 7.4 | 11 |
| 10-9 | $6.59*10^{-2}$ | 2.08 | 2.23 | 4.37 | 8 |
| 10-10 | 1.03 | 3.67 | 4.06 | 8.76 | 10 |
| 10-11 | $4.76*10^{-9}$ | 1.44 | 3.26 | 4.7 | 7 |
| 10-12 | $8.93*10^{-22}$ | 3.64 | 6.43 | 10.07 | 7 |

Table 0.2. The Second Step of NARX Modelling Method MSE.

| Sets Number | Training *MSE* Error | Validating *MSE* Error | Testing *MSE* Error | Overall *MSE* | Epoch |
|---|---|---|---|---|---|
| **2-4** | 0.28 | 0.807 | 0.18 | 1.267 | 299 |
| **3-4** | 0.49 | 0.33 | 0.27 | 1.09 | 23 |
| **4-4** | 0.29 | 0.33 | 0.74 | 1.36 | 11 |
| **5-4** | 0.39 | 0.23 | 0.43 | 1.05 | 13 |
| **6-4** | 0.28 | 0.27 | 0.78 | 1.33 | 45 |
| **7-4** | 0.24 | 0.31 | 0.29 | 0.84 | 125 |
| **8-4** | 0.25 | 0.55 | 0.38 | 1.18 | 51 |
| **9-4** | 0.33 | 0.74 | 0.53 | 1.6 | 38 |
| **10-4** | 0.32 | 0.61 | 0.4 | 13.3 | 11 |
| **11-4** | 1.06 | 0.77 | 0.63 | 2.46 | 14 |
| **12-4** | 0.22 | 0.45 | 0.96 | 1.63 | 111 |
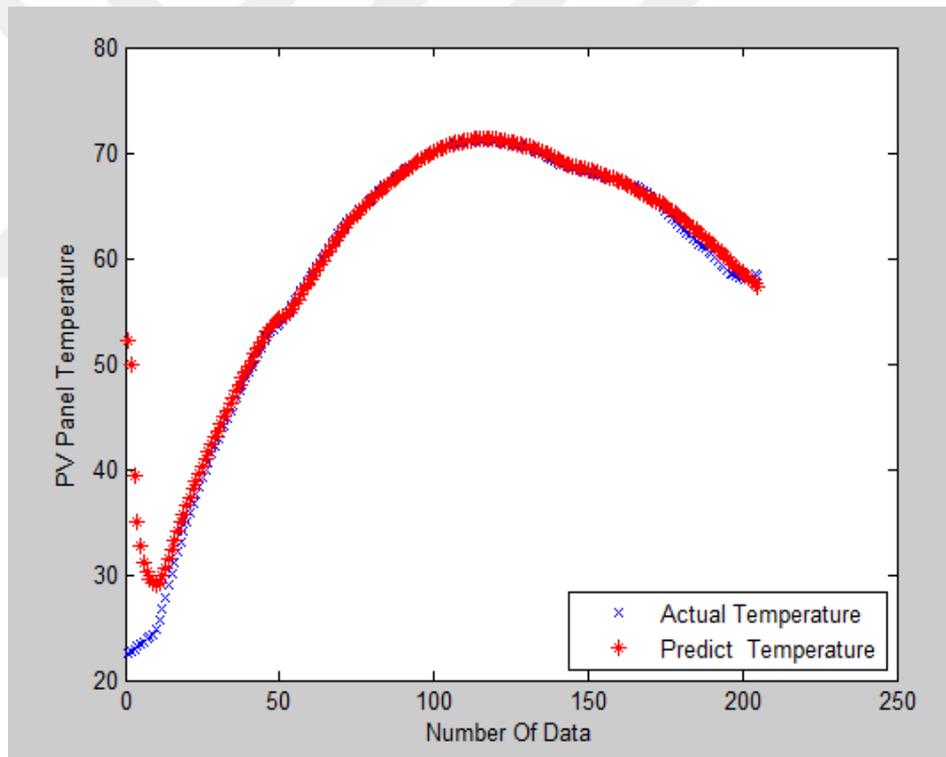


Figure 0.6. The predicted and actual *PV* panel surface temperatures of *NARX* modelling method.
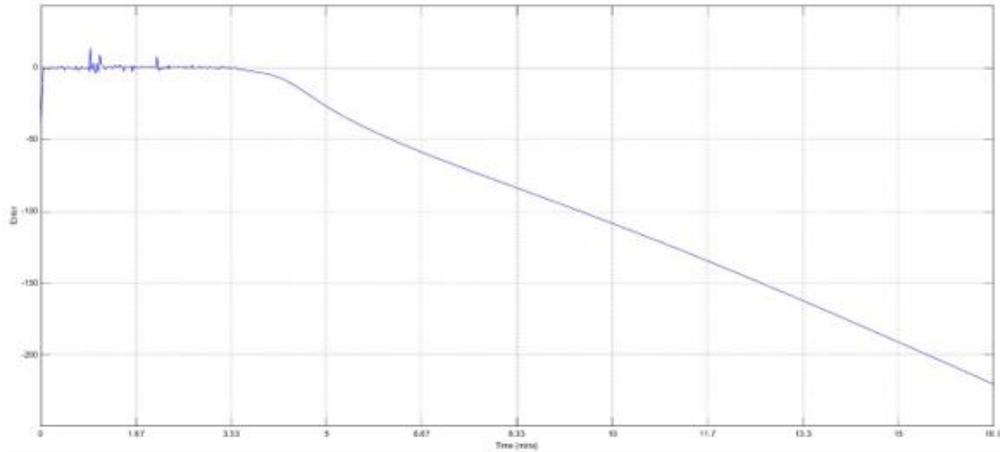
Figure 0.7. The *NARX* modelling method prediction error.

## 5.2.2. NAR Modelling Technique

According to Figure 5.8, the predicted output temperature in the *NAR* is derived from a single input series represented by the output temperature predicted in a previous stage based on actual output data.
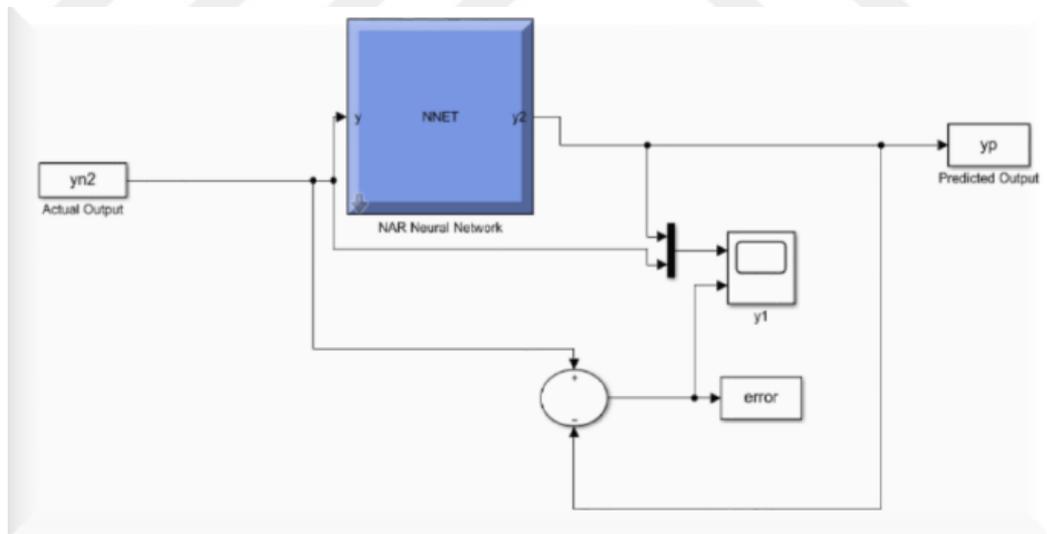


Figure 0.8. The block diagram of *NAR* modelling method.

The minimal *MSE* was 1.065 at *Nn* equal to 10 and *Nd* equal to 10, as shown in Table 5.3, which is followed by fixing *Nd* number to 10 and altering *Nn* number from 2 to 12. when *Nn* number is fixed at 10 and the *Nd* number is varied between 2 and 12. The optimal *MSE* for this modeling method was 1.049 at *Nn* number is equal to 10 and *Nd*

number is equal to 3, as it is listed in Table 5.4, *NAR* modeling method's actual and predicted *PV* panel surface temperatures are shown in Figure 5.10, whereas the prediction error is shown in Figure 5.6.

Table 0.3. The First step of NAR modelling method MSE.

| Sets Number | Training *MSE* Error | Validation *MSE* Error | Testing *MSE* Error | Overall *MSE* | Epoch |
|---|---|---|---|---|---|
| **10-2** | $1.98*10^{-1}$ | $3.3*10^{-1}$ | $5.9*10^{-1}$ | 1.118 | 45 |
| **10-3** | $2.31*10^{-1}$ | $3.56*10^{-1}$ | $9.45*10^{-1}$ | 1.532 | 14 |
| **10-4** | $2.09*10^{-1}$ | $6.46*10^{-1}$ | $5.23*10^{-1}$ | 1.378 | 13 |
| **10-5** | $3.35*10^{-1}$ | $8.22*10^{-1}$ | $6.42*10^{-1}$ | 1.799 | 11 |
| **10-6** | $2.38*10^{-1}$ | $3.88*10^{-1}$ | $7.99*10^{-1}$ | 1.425 | 14 |
| **10-7** | $2.22*10^{-1}$ | $3.92*10^{-1}$ | $5.8*10^{-1}$ | 1.194 | 11 |
| **10-8** | $2.14*10^{-1}$ | $4.02*10^{-1}$ | $6.22*10^{-1}$ | 1.238 | 109 |
| **10-9** | $1.08*10^{-1}$ | $4.5*10^{-1}$ | 1.15 | 1.708 | 15 |
| **10-10** | $1.77*10^{-1}$ | $5.41*10^{-1}$ | $3.47*10^{-1}$ | 1.065 | 13 |
| **10-11** | $3.87*10^{-1}$ | $3.71*10^{-1}$ | $3.32*10^{-1}$ | 1.09 | 14 |
| **10-12** | $2.08*10^{-1}$ | $8.7*10^{-1}$ | 1.96 | 3.038 | 15 |

Table 0.4. The Second step of the NAR modeling approach MSE

| Sets Number | Training *MSE* Error | Validation *MSE* Error | Testing *MSE* Error | Overall *MSE* | Epoch |
|---|---|---|---|---|---|
| **2-10** | $4.48*10^{-1}$ | $2.6*10^{-1}$ | $4.45*10^{-1}$ | 1.153 | 45 |
| **3-10** | $3.54*10^{-1}$ | $2.19*10^{-1}$ | $4.76*10^{-1}$ | 1.049 | 41 |
| **4-10** | $3.39*10^{-1}$ | $6.31*10^{-1}$ | $7.37*10^{-1}$ | 1.707 | 15 |
| **5-10** | $2.1*10^{-1}$ | $5.5*10^{-1}$ | $8.6*10^{-1}$ | 1.62 | 15 |
| **6-10** | $2.06*10^{-1}$ | $8.22*10^{-1}$ | $3.64*10^{-1}$ | 1.392 | 16 |
| **7-10** | $7.25*10^{-1}$ | $6.28*10^{-1}$ | 6.1 | 13.105 | 23 |
| **8-10** | 1.24 | 2.97 | 2.004 | 6.214 | 14 |
| **9-10** | $5.02*10^{-2}$ | $4.81*10^{-1}$ | 1.57 | 2.1 | 31 |
| **10-10** | $5.87*10^{-2}$ | 1.55 | 2.66 | 4.26 | 12 |
| **11-10** | $7.11*10^{-2}$ | $9.88*10^{-1}$ | $7.99*10^{-1}$ | 1.85 | 14 |
| **12-10** | $1.57*10^{-1}$ | 3.32 | 6.21 | 9.68 | 17 |
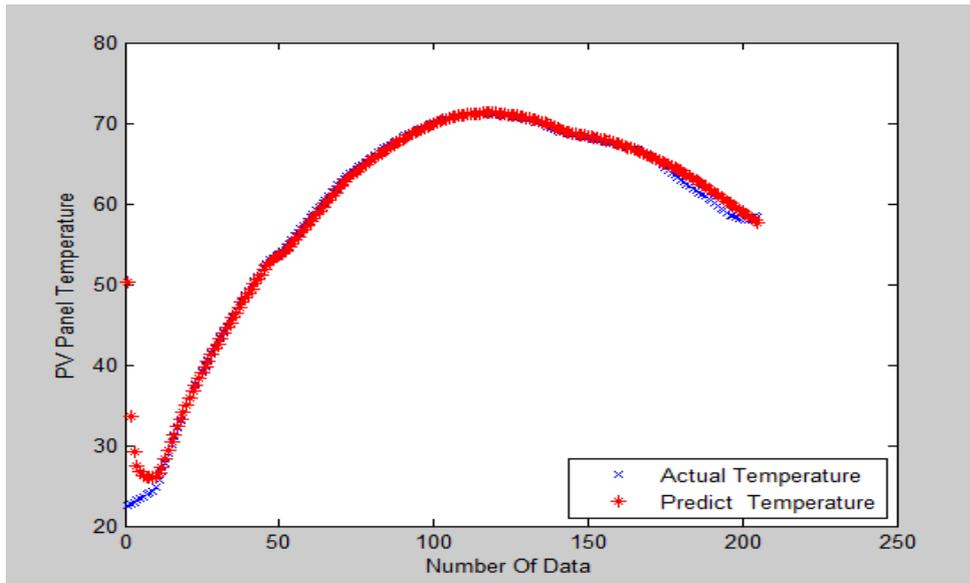
Figure 0.9. The predicted and actual *PV* panel surface temperatures of *NAR* modelling method.
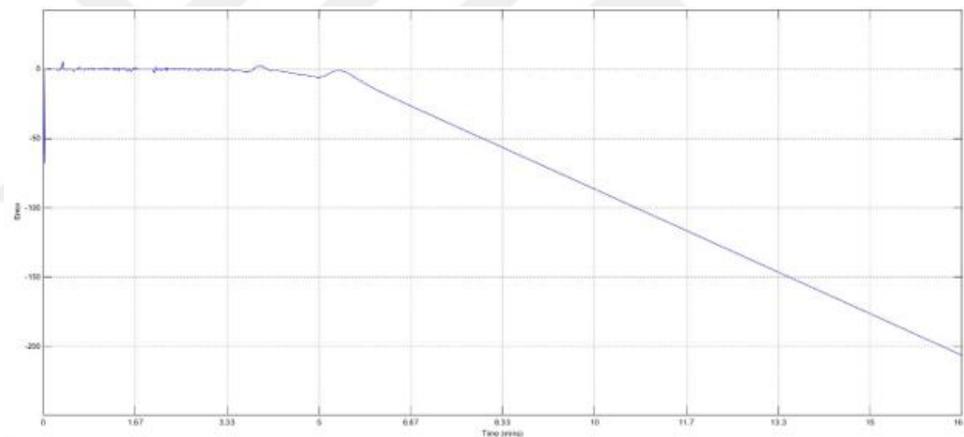


Figure 0.10. The *NAR* modeling method prediction error.

### 5.2.3. Non-Linear Input/ Output Modelling Approach

The predicted temperature of the output in the nonlinear input/output is derived from a single input series that are signified by input datasets, and only in this case it is compared to real output datasets that have been made, as can be seen from Figure 5.11.

65
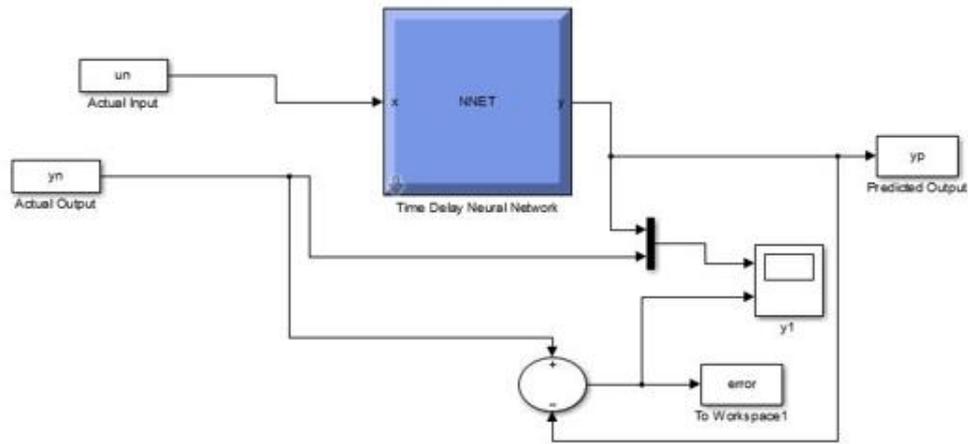
Figure 0.11. The diagram of Non-linear Input/Output modeling approach.

The lowest *MSE* occurs in the case, that equals to 8.62 when the *Nd* number is equal to 3 and *Nn* number is equal to 10, as it is shown in Table 5.5, when *Nn* number is fixed at 3 and *Nd* number is varied between 2 and 12. The following phase involves setting *Nd* number to 3 and adjusting the *Nn* number from 2 to 12. The optimal *MSE* for this modeling method was 11.77 the *Nd* number equal to 3 and when *Nn* number equal to 6, as shown in Table 5.6. The nonlinear input/output modeling method's predicted and actual *PV* panel surface temperatures are displayed in Figure 5.12. Figure 5.13 also shows the nonlinear input/output modeling technique's prediction error.

Table 0.5. The First Step of Non-Linear Modelling Method.

| Sets Number | Training *MSE* Error | Validation *MSE* Error | Testing *MSE* Error | Overall *MSE* | Epoch |
|---|---|---|---|---|---|
| **10-2** | 1.53 | 3.47 | 4.52 | 9.52 | 17 |
| **10-3** | 1.83 | 3.13 | 3.66 | 8.62 | 27 |
| **10-4** | 1.88 | 11.13 | 9.07 | 22.08 | 11 |
| **10-5** | 1.88 | 5.39 | 3.52 | 10.79 | 12 |
| **10-6** | 1.3 | 9.03 | 13.26 | 23.59 | 20 |
| **10-7** | 2.75 | 9.96 | 10.17 | 23.42 | 12 |
| **10-8** | 8.33 | 6.9 | 12.9 | 28.13 | 11 |
| **10-9** | 0.42 | 8.7 | 15.5 | 24.62 | 25 |
| **10-10** | 1.14 | 5.24 | 3.42 | 9.8 | 14 |
| **10-11** | 1.96 | 16.22 | 9.87 | 27.96 | 11 |
| **10-12** | 0.04 | 5.53 | 7.78 | 13.35 | 21 |

Table 0.6. The Second Step of Non -Linear Modelling Method.

| Sets Number | Training *MSE* Error | Validation *MSE* Error | Testing *MSE* Error | Overall *MSE* | Epoch |
|---|---|---|---|---|---|
| **2-3** | 7.42 | 10.92 | 12.79 | 31.13 | 14 |
| **3-3** | 2.77 | 4.6 | 8.3 | 15.67 | 17 |
| **4-3** | 4.3 | 6.76 | 16.22 | 27.28 | 27 |
| **5-3** | 2.76 | 6.69 | 3.6 | 13.06 | 13 |
| **6-3** | 1.39 | 4.72 | 5.66 | 11.77 | 15 |
| **7-3** | 3.21 | 9.32 | 12.11 | 24.64 | 14 |
| **8-3** | 6.94 | 16.7 | 11.21 | 34.85 | 16 |
| **9-3** | 1.83 | 7.31 | 5.82 | 14.96 | 11 |
| **10-3** | 0.97 | 7.04 | 6.04 | 14.05 | 15 |
| **11-3** | 2.33 | 5.3 | 6.97 | 14.6 | 11 |
| **12-3** | 2.61 | 20.3 | 35.7 | 58.61 | 14 |
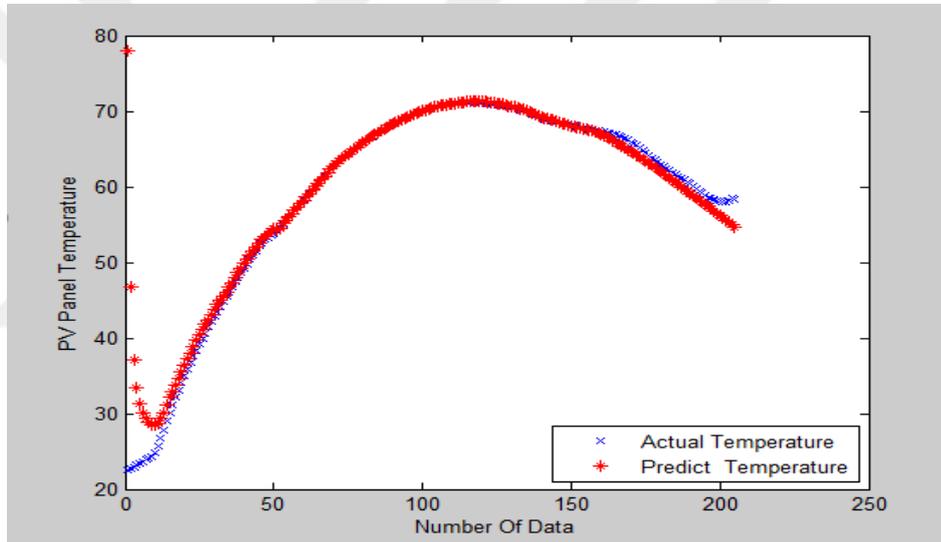


Figure 0.12. The predicted and actual *PV* panel surface temperatures of nonlinear input/output modelling technique.
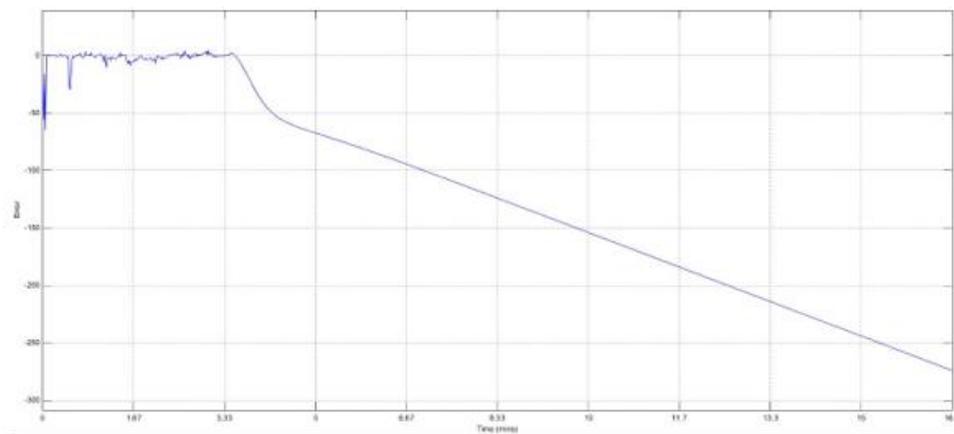


Figure 0.13. Prediction error for Non-linear Input/Output modeling approach.

## 5.3. RESULTS OF SIMULATION CONTROL

*NARX* is the most effective modeling approach for this system. Therefore, the normal *PID* controller is converted into an intelligent one using the *PSO* intelligent approach. Depending on the findings of the *NARX* modeling method, *KI*, *KP*, and *KD* were accustomed to utilize Integral Absolute Error (*IAE*), *MSE*, and Integral Square Error (*ISE*) to find the optimal approach for regulating the PV panel temperature of the system. The *PID-Practical* Swarm Search Intelligent Controller Block Diagram is shown in Figure 5.14.
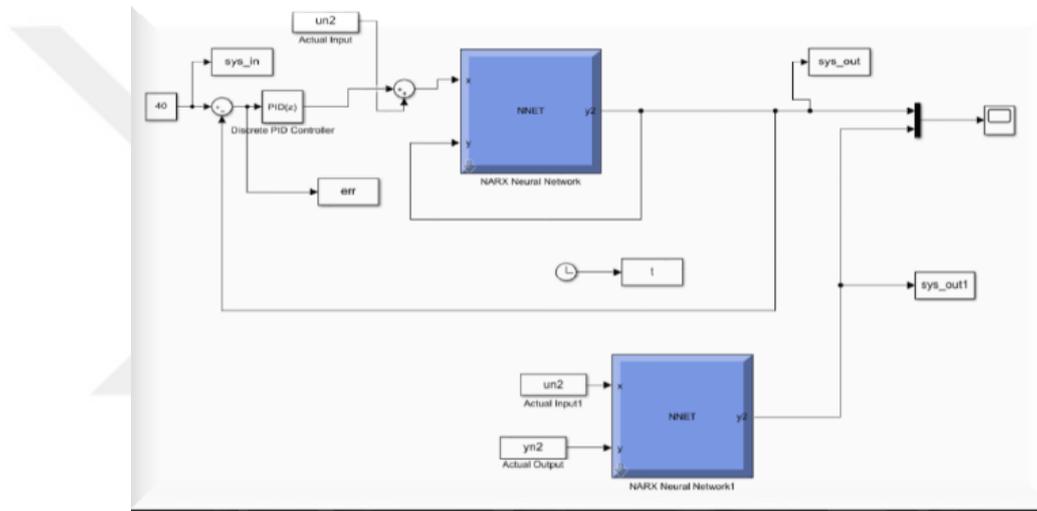


Figure 0.14. The block diagram of *PID- PSO* search intelligent controller.

The three methods are efficient and controlled the system temperature successfully. The best method is the one that based on the *MSE* because it is more effective than other two methods, also all *PID* parameters have no null values. The *MSE* is 2.578 as given in Table 5.7.

Table 0.7. The *PID–PSO* search intelligent controlling.

| *PID* Parameters | | | Error | | |
|---|---|---|---|---|---|
| *KP* | *KI* | *KD* | *MSE* | *ISE* | *IAE* |
| 80 | 88.05 | 11.1 | 2.57 | - | - |
| 24 | 23.5 | 0 | - | 4.703e+03 | - |
| 100 | 90 | 0 | - | - | 2.975e+03 |

### 5.3.1. *PID- PSO* Search Based on *MSE*

In this method, the error is 2.57, while *KP*, *KI and KD* values are 80, 88.05 and 11.1 respectively. Figure 5.15 and Figure 5.16 elucidate the (*KP*, *KI and KD*) factors convergence and the *MSE* convergence, respectively.
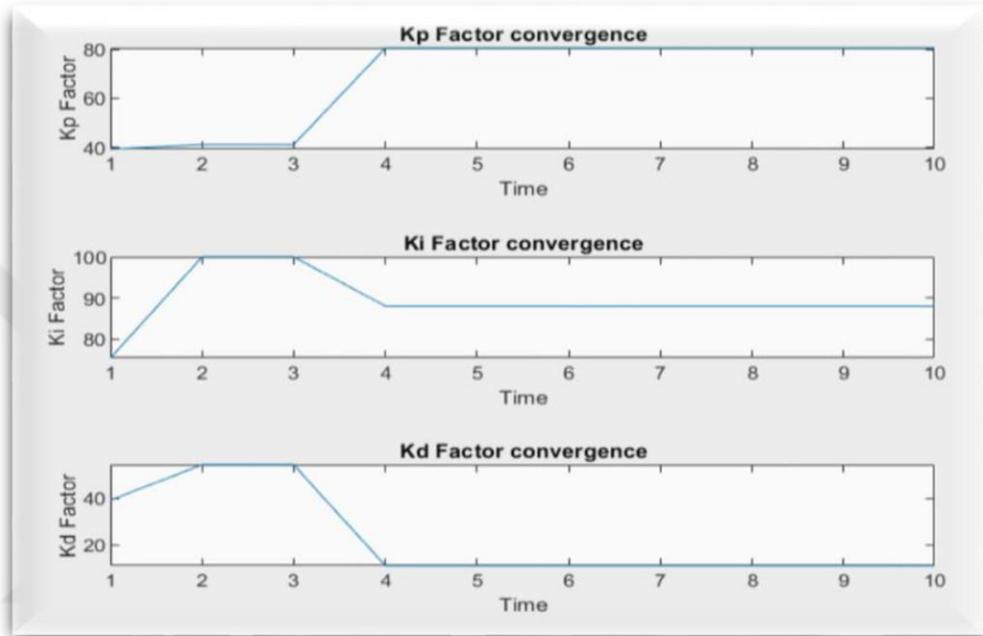


Figure 0.15. The *KP*, *KI and KD* factors convergence.
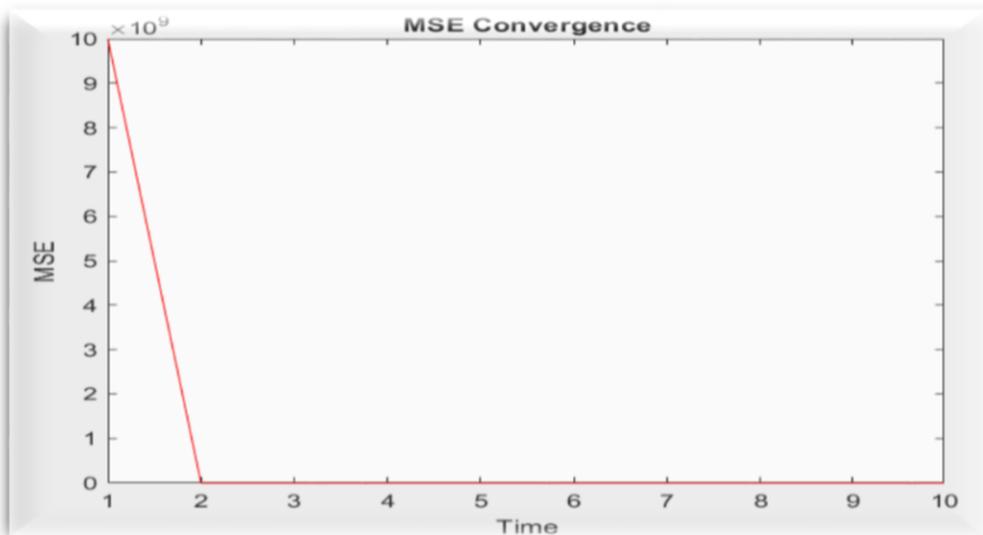


Figure 0.16. The *MSE* convergence

### 5.3.2. *PID- PSO* **Search Based on** *ISE*

In this method, the error is 4.703e-03, while *KP*, *KI and KD* values are 24, 23.5 and Zero, respectively. Figure 5.17 and Figure 5.18 display the (*KP, KI and KD*) factors convergence and *ISE* convergence, respectively.
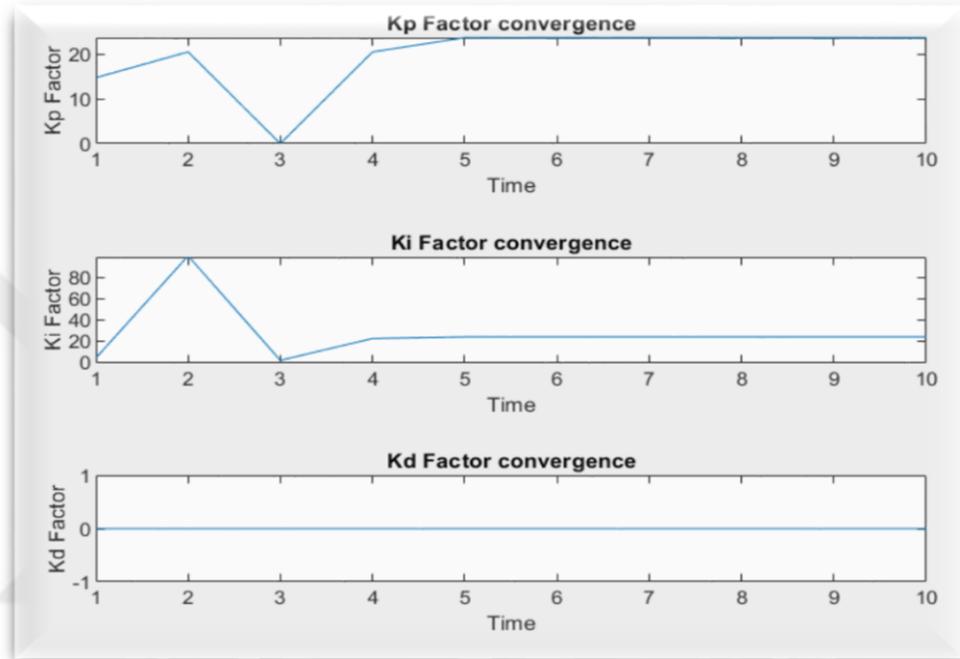


Figure 0.17. The (*KP,KI and KD*) factors convergence.
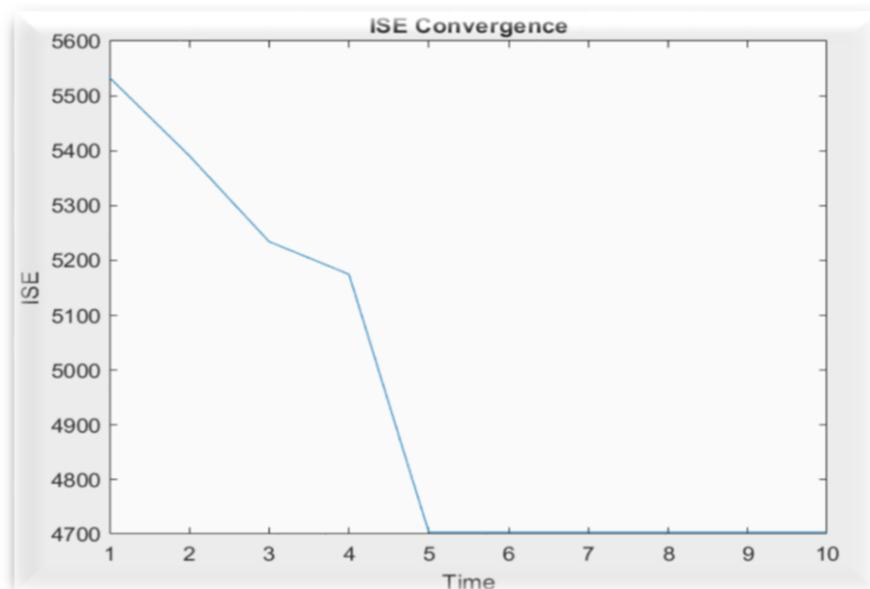


Figure 0.18. The *ISE* convergence.

### 5.3.3. *PID-PSO* Search Based on *IAE*

In this method, the error is 2.975e-03, while *KP*, *KI and KD* values are 100, 90 and Zero, respectively. Figure 5.19 and Figure 5.20 show the (*KP*, *KI and KD*) factors convergence and *MSE* convergence, respectively.
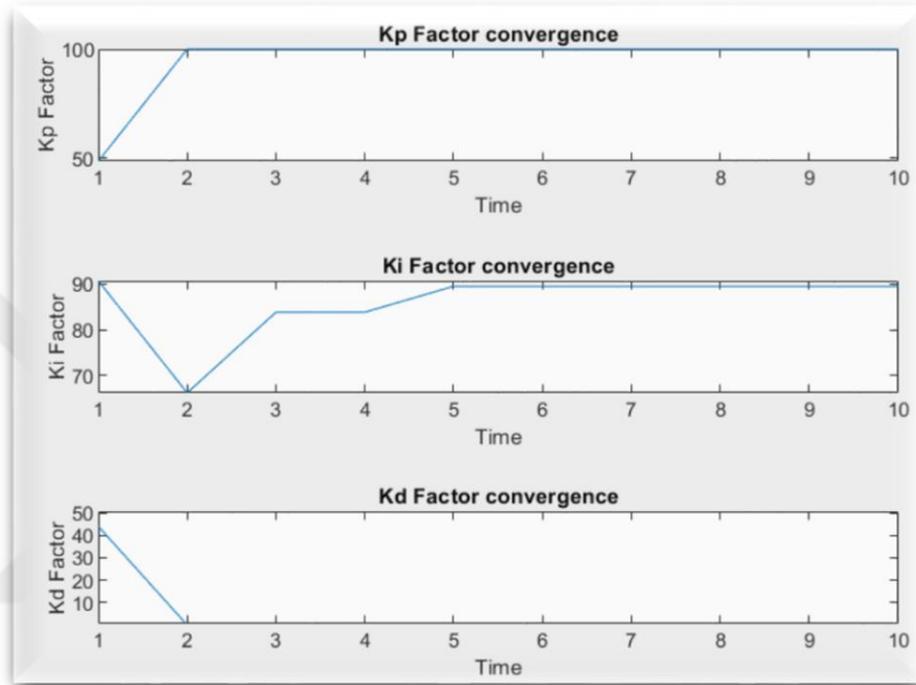


Figure 0.19. The *Kp*, *Ki and Kd* factors convergence.
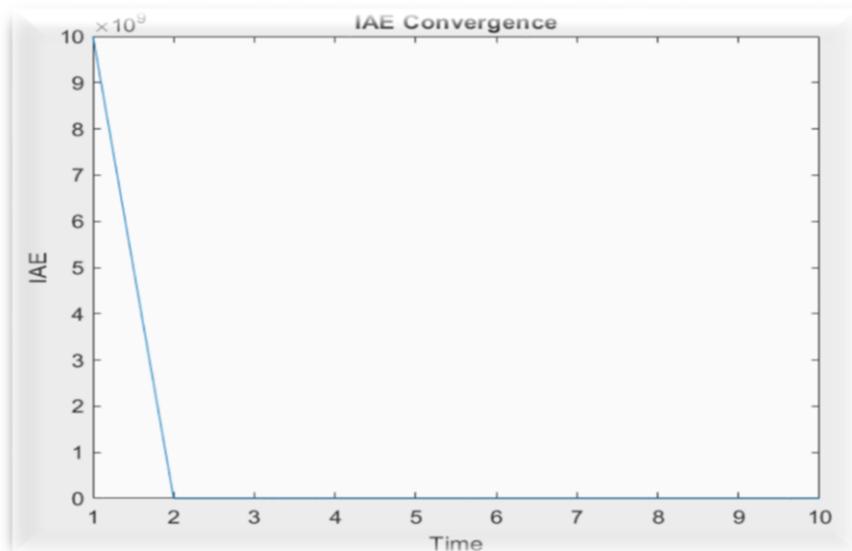


Figure 0.20.The *IAE* convergence.

## 5.4. EXPERIMENTAL VALIDATION

The experimental results are divided into two parts, including system experimental results without controller and system experimental outcomes with controller.

### 5.4.1. Porosity Calculations

The porous media consists of 25 parts with the same dimensions. The first step is determining the volume of each of the porous media parts by water displacement technique. A (500 $mL$) measuring cylinder was used with a known water volume in it, and then the porous media part was put in it to read the total volume of both water and porous media part. The porous media volume can be determined by subtracting the nano-fluid volume from the total volume. The volume of each part of porous media is equal to 5 $mL$.

The second step is determining the total porous media parts volume ($Vp$) using Eq. (3.2). By multiplying 25 parts by 5 mL, Vp is equal to 125 $cm^3$. The next step is calculating the total volume ($Vt$), which is denoted by the Perspex container that the porous media inserted into the volume. With the knowledge of the length, width and thickness of the container, the total volume can be calculated by multiplying theses dimensions using Eq. (3.1). $Vt$ is equal 3528 $cm^3$.

The final step is calculating the porosity using Eq. (3.3). By subtracting $Vp$ from $Vt$, and then dividing the result on $Vt$, the porosity is 0.965 (96.5%).

### 5.4.2. System experimental Results without controller

The experiment was carried out by utilizing tilt angles of 30 degrees, which are the best angles all year round [56]. The photovoltaic panels were all oriented southward. After inspecting this system, checking its effectiveness, the accuracy of hardware connection, and obtaining the test readings of this system for confirmation, readings have started at 2.5-minute intervals.

The experimental results were obtained between September 15 and October 30, 2022, in clear climate between 7 *AM* and 2 *PM* and depending in this study on the data for one day only from above results. The study was conducted in the Baghdad region, Iraq and the input data was ambient temperature, voltage, current, and solar irradiance. Note that the wind speed and humidity were not taken into account, as they were considered constant. On the other hand, the *PV* panel surface temperature was the output data.

### 5.4.3. Experimental Performance of *PV* Module with and without *Nano-fluid* Cooling

The experimental comparison regarding the *PV* and *PV/T* temperature variations throughout the operating hours portrayed in Figure (5.21) It is discovered that in the case when $AL_2O_3$ concentration is 2% *wt*, the output temperature lowers and, consequently, the temperature difference reduces. The *PV* panel temperature, which was measured at 70 $^{\circ}C$, was the highest one the device has ever reached without cooling. The *PV* panel's temperature was 45 $^{\circ}C$ with a 2 *wt*% nano-fluid. The performance of the solar panel is impacted by a number of elements. Those elements include solar radiation, the direction and angle of inclination, and the surrounding temperature. In comparison to base fluid, the value of thermos physical properties, particularly heat conduction, is raised by increasing the volume fraction of solid $AL_2O_3$. The temperature distribution in the cooling fluid becomes uniform and the amount of temperature gradients, particularly in areas adjacent to the wall, is lowered by boosting the coolant fluid's heat conduction. When put in comparison with base fluid, the heat transfer for nano-fluid is higher.

This demonstrates that the presence of $Al_2O_3$ nanoparticles can increase heat transfer efficiency, and that this improvement can be shown even at low concentrations as compared to water. There are two explanations for this: Increased efficient thermal conductivity and increased heat transfer caused by the combination of successful particle migration.

Furthermore, although the thermal efficiency was highest for the 2 *wt.% nano-fluid*, the increase in thermal power was not proportional to the concentration of Nano-fluid. This is since the decreased momentum transfer caused by higher viscosity reduces the enhancement of heat transfer efficiency caused by increased thermal conductivity.
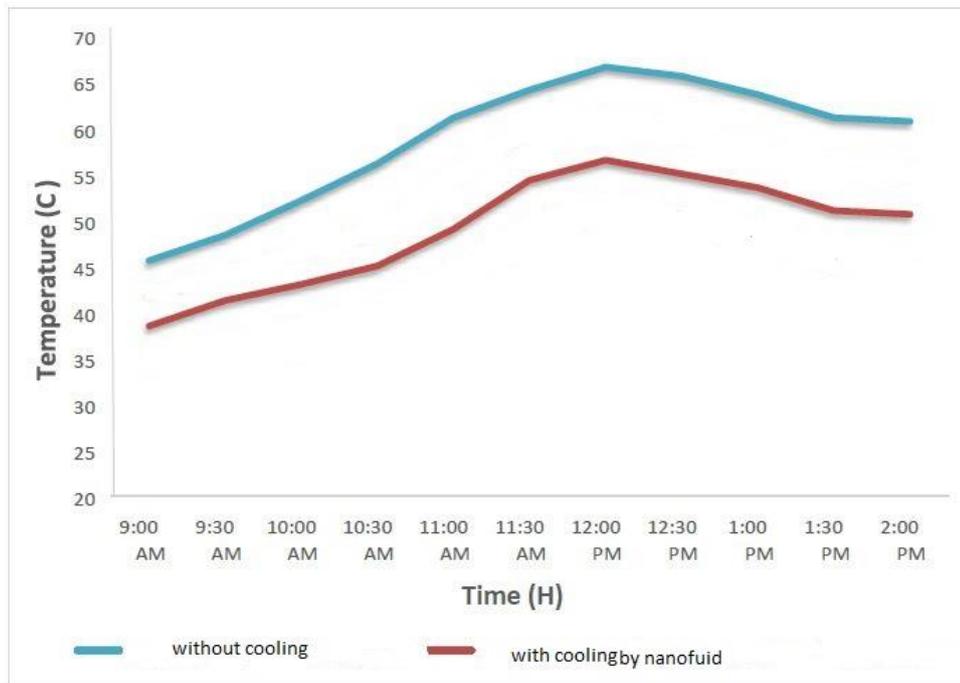


Figure 0.21. The temperatures of cell without cooling and with cooling by *nano-fluid*.

### 5.4.3.1. Electrical Performance

The cooling of solar cells affects the electrical efficiency of *PV* module, causing electrical productivity presented by voltage to increase. The solar cells consume around 15% of the solar radiation and turn the remainder into heat, allowing the cell temperature to increase. Therefore, as the $Al_2O_3$ concentration increases, the voltage increases, as the nano-fluid flow removes the heat from the PV module. It is obvious that the electrical power is also increasing with increasing solar intensity, as more electrons are emitted from solar cells and more current is generated. In addition, the change in concentration of $Al_2O_3$ affects the electrical power that decreases as the water flow decreases due to the drop in cell temperature and the maximum power. The electrical efficiency is dependent on solar radiation and cell temperature, but it depends in particular on the cell temperature, which takes into account the increase in electrical

output. Therefore, the electrical output is decreased in spite of the rise in electrical power due to the cell temperature rising. Furthermore, the increase of the concentration of $Al_2O_3$ occurs in electrical efficiency by removing the heat from *PV* cells and rising the cell temperature. According to this reason, Figures 5.22 and Figure 5.23 display the load current and load voltage both without and with nano-fluid cooling. The key influencing factors will be ambient temperature and solar radiation, on which PV depends for electricity generation, as the direction is fixed to south and the tilted angle is fixed at 30. The limitation of the module temperature is significantly influenced by the ambient temperature. Due to the materials used in solar modules' high heat capacity, it is well known that their temperature rises to a level that is close to 1.75 degrees higher than the surrounding air in a case without cooling. The irradiance (*Gs*), another component, has a direct impact on the temperatures of the modules. In both scenarios of cooling and no cooling, the peak solar radiation intensity was seen between 12:00 pm and 1:00 pm, which caused PV panels to reach their highest temperatures. In comparison to the non-cooling case, the cooling system was able to produce an average temperature drop of 5 $^{\circ}C$. The power and electrical efficiency as well as overall efficiency with cooling and without cooling by nano-fluid are evinced in Figure 5.24-Figure 5.26.
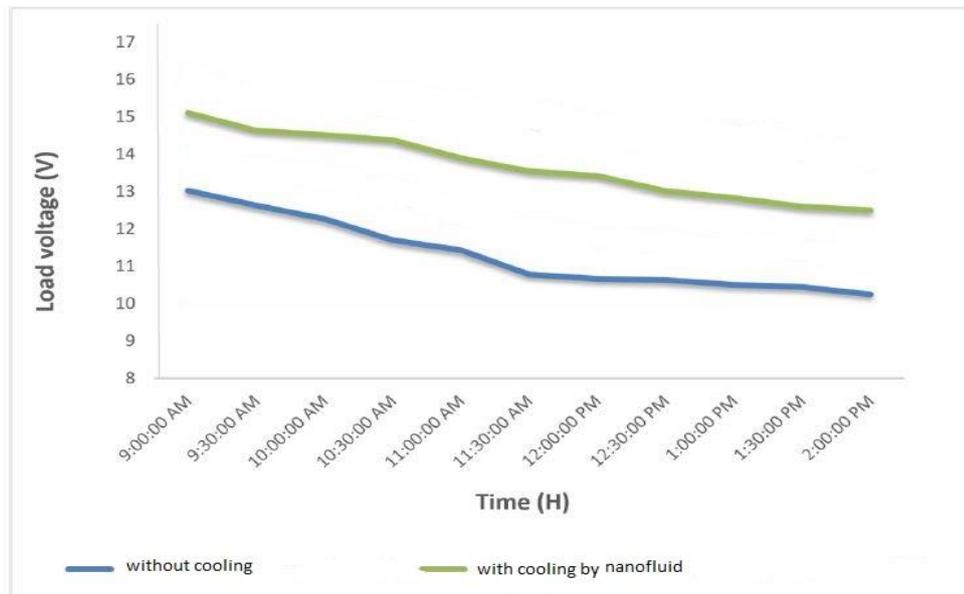


Figure 0.22. The system voltage for with and without cooling.
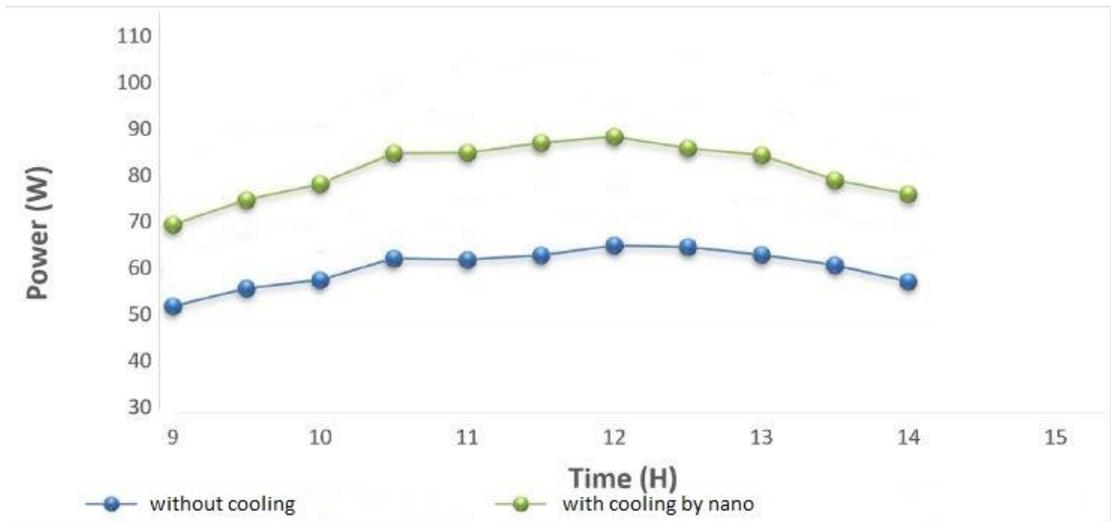
Figure 5.23. The system current for with and without cooling.
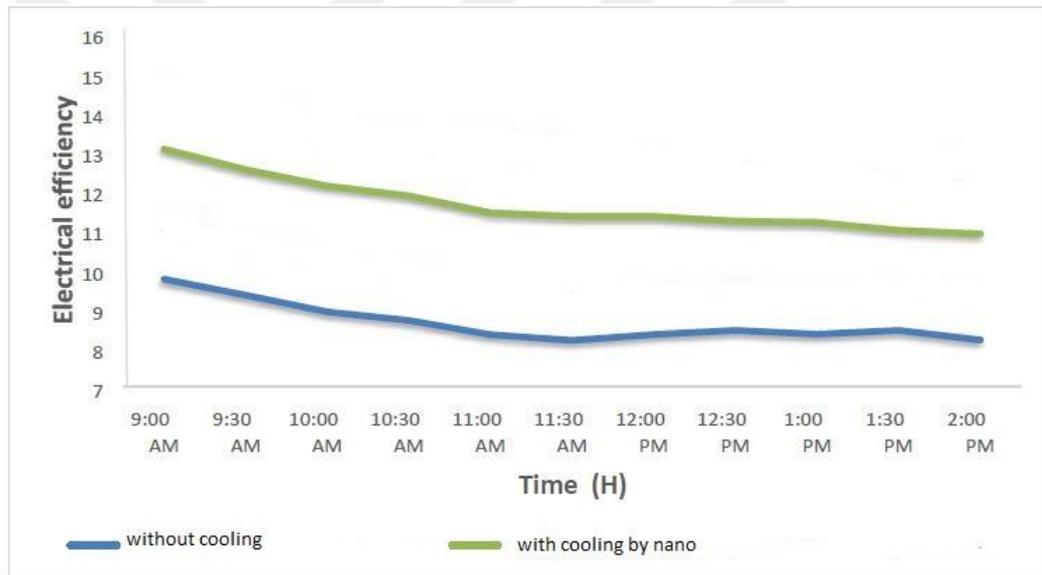


Figure 0.24. The experimental comparison between the *PV* and *PV/T* for electrical efficiency.
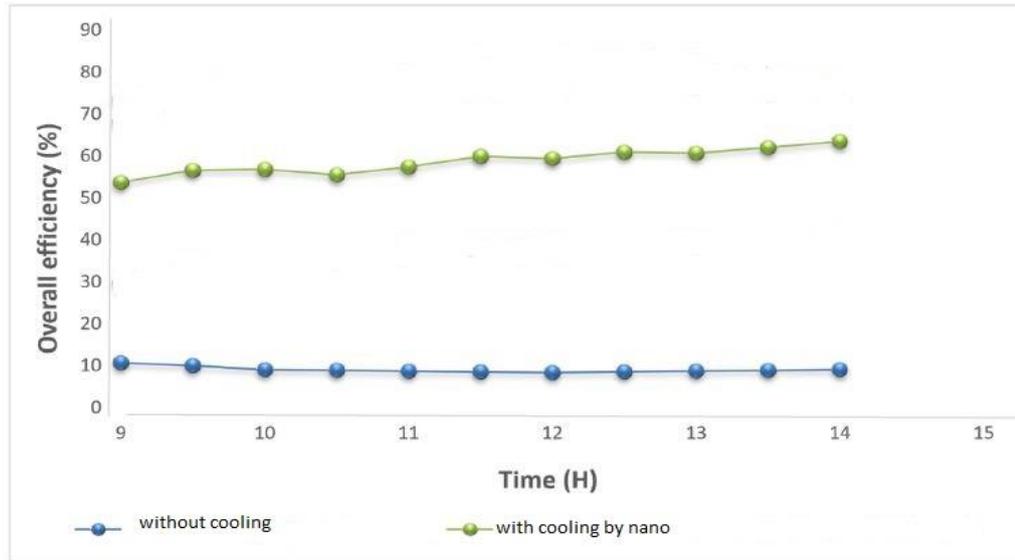
Figure 0.25. The experimental comparison between the *PV* and *PV/T* for overall efficiency.

Table 0.8. The comparison in the case of no cooling and the case of cooling using nano-fluid technology at a concentration of 2%.

| Cases | Temperature reduction (˚C) (%) | Electrical efficiency enhancement (%) | Overall efficiency enhancement (%) |
|---|---|---|---|
| without cooling | - | 15 | 40 |
| with cooling by nano-fluid 2 *wt*% | 15.04 | 55 | 111 |

## 5.4.3.2. The Comparison between Overall Efficiency and Electrical Efficiency in the *PV* and *PV/T*

The key difference between electrical efficiency and overall efficiency in *PV* panels lies in the aspects of these efficiencies measure. The electrical efficiency is a measurement of how effectively a *PV* panel converts the sunlight (incident solar radiation) into electrical energy, expressed as a percentage of the input sunlight energy. In this case, the electrical efficiency enhancement is equal to 55%, which means that the *PV* panel's ability to convert the sunlight into electricity has improved by 55%. The overall efficiency, on the other hand, considers not only how effectively a *PV* panel turns the sunlight into electric energy but also how efficiently the overall system

operates under the real-world conditions, using different factors, like temperature, dust, and other variables that can impact the performance continuing from the previous paragraphs. The higher overall efficiency of the *PV* or *PV/T* system indicates the effective utilization of both electrical and thermal energy outputs. It's important to note that an overall efficiency of more than 100% may seem counterintuitive; however, in the context of combined *PV/T* systems, it represents an effective harnessing of both electricity and heat generated from the same source. This demonstrates the potential for these systems to maximize the energy production and increase the overall efficiency, making them a valuable solution in the renewable energy applications. Additionally, the integration of thermal energy generation adds an extra benefit, allowing for the utilization of the excess heat in various applications, such as space heating or water heating, further enhancing the overall energy efficiency of the system. In summary, the electrical efficiency focuses solely on the sunlight-to-electricity conversion, while the overall efficiency accounts for a more comprehensive assessment of the entire *PV* system performance under the real-world operating conditions.

# PART 6

## CONCLUSSIONS AND RECOMMENDATION

There are two sections in this chapter. The first discusses the conclusions, whereas the second provides some recommendations for further research.

### 6.1. CONCLUSIONS

The application of nano-fluids and porous media in solar panel technology has emerged as a promising intelligent control technique. By integrating these advanced materials, we are able to significantly enhance the efficiency of solar panels while simultaneously addressing key issues related to heat transfer and energy management. This innovative approach offers a multitude of benefits, such as improved performance in varying environmental conditions, increased durability, and enhanced overall system reliability. Additionally, the utilization of nano-fluids and porous media provides the opportunity to optimize the utilization of solar energy and minimize wastage, resulting in a more sustainable and cost-effective solution for harnessing solar power. The most critical findings of the study can be described as follows:

- The electrical power produced by the *PV* panel depends mainly on the radiation. The rising cell temperature is inversely proportional to the *PV-modulated* power generation. As temperature rose from $25^{\circ}C$ to $75\ ^{\circ}C$ the power fell from 90 *W* to 75 W at constant solar radiation (*700 W/m$^2$*).

- Unless the solar panels are cooled due to its high temperature, it is not possible to obtain the best power and in the presence of solar radiation. The highest power can be obtained at the highest solar radiation, and this is at 12 *pm* when it has a value of *700 W/m$^2$*.

- The method for controlling the temperature of solar panels in this study included the coordinate effect on the performance improvements, since the temperature of the panels was checked at *40°C.*

- When *Nd* equals 4 and Nn equals 7, *NARX* has the lowest *MSE* (0.84), making it the best *ANN* modeling method.

- The simulation that was based on *MSE* produced the best results for the *PID-PSO* intelligent controller. The *KI, KP*, and *KD* values were, respectively, 80, 88.05, and 11.1. The error, however, was 2.57.

- The addition of the cooling system to the module reduced *PV* panel's surface temperature.

- *PV* panels performed better as a result of the cooling system's control since the set point of (*40 °C*) was successfully reached.

- In the case when a cooling system was added to the module, the existence of $Al_2O_3$ Nps increased the thermal efficiency, produced power, and electrical efficiency. Also, the overall efficiency increased with the use of *Nps*, in which the 2 *wt* % achieved approximately 111% and he electrical efficiency achieved approximately 55%.

## 6.2. RECOMMENDATIONS

In this section, some suggestions for future work are listed as follows:

- Rather than the *PID-PSO* utilized in this study, employing adaptive neuro-fuzzy inference system or *ANFIS*.

- Using different types of nano-fluid or hybrid nano-fluid to study the influence of those fluids on the performance of the solar panels.

- Utilizing tracking system to maximize the time that the solar panel observe the sun.

- Using different porosities of aluminum porous media and comparing between the cooling results of them.

- Using a trucking system to truck the solar radiation.

- Trucking the optimum power using *MPPT* and conducting a comparison between the two methods.

- Using solar panels with a larger capacity and larger size as well asstudying their effect on the electrical efficiency and electrical performance of the panels.

# REFERENCES

1. Buitrago, J. and Asfour, S., "Short-Term Forecasting of Electric Loads Using Nonlinear Autoregressive Artificial Neural Networks with Exogenous Vector Inputs", *Energies*, 10 (1): 40 (2017).

2. Connor, J. T., Martin, R. D., and Atlas, L. E., "Recurrent neural networks and robust time series prediction", *IEEE Transactions On Neural Networks*, 5 (2): 240–254 (1994).

3. Benmouiza, K. and Cheknane, A., "Small-scale solar radiation forecasting using ARMA and nonlinear autoregressive neural network models", *Theoretical And Applied Climatology*, 124 (3): 945–958 (2016).

4. Yong, C. Y., Hajibeigy, M. T., Vaithilingam, C. A., and Walvekar, R. G., "Characteristics Study of Photovoltaic Thermal System with Emphasis on Energy Efficiency", (2018).

5. Menzies, T., Chen, Z., Hihn, J., and Lum, K., "Selecting Best Practices for Effort Estimation", *Software Engineering, IEEE Transactions On*, 32: 883–895 (2006).

6. Zhou, Y. T., Nie, J. B., Han, N., Chen, C., and Yue, Z. F., "Study on PID Parameters Tuning Based on Particle Swarm Optimization", *Advanced Materials Research*, 823: 432–438 (2013).

7. Yang, X.-S. and Deb, S., "Cuckoo Search via Lévy flights", *2009 World Congress on Nature & Biologically Inspired Computing (NaBIC)*, (2009).

8. Yang, X.-S. and Deb, S., "Engineering optimisation by cuckoo search", *International Journal Of Mathematical Modelling And Numerical Optimisation*, 1 (4): 330–343 (2010).

9. Mat Darus, I. Z. and Al-Khafaji, A. A. M., "Bio-inspired Algorithms for Modeling and Control of Underwater Flexible Single-Link Manipulator", Singapore, (2021).

10. Maid, I., Hilal, K., and Hassun, J., "EXPERIMENTAL STUDY OF HEAT TRANSFER ENHANCEMENT IN HEAT EXCHANGER USING POROUS MEDIA", (2019).

11. El-seesy, I., Khalil, T., and Ahmed, M., "Experimental investigations and developing of photovoltaic/thermal system", 19: 1342–1347 (2012).

12. Irwan, Y. M., Leow, W. Z., Irwanto, M., Fareq.M, Amelia, A. R., Gomesh, N., and Safwati, I., "Indoor Test Performance of PV Panel through Water Cooling Method", *Energy Procedia*, 79: 604–611 (2015).

13. Nouri, A., "Design and Implementation of Solar Tracking System and Water Flow Double Glazing Based on PLC", *University of Technology*, Baghdad, (2017).

14. Schiro, F., Benato, A., Stoppato, A., and Destro, N., "Improving photovoltaics efficiency by water cooling: Modelling and experimental approach", *Energy*, 137: 798–810 (2017).

15. AHMED, D., "Cooling Enhancement of PV Panel Using Heat Sink and Wood Wool Pad with Temperature Prediction by Particals Swarm Optimization", *University of Technology*, Baghdad, (2018).

16. Masoud Parsa, S., Yazdani, A., Aberoumand, H., Farhadi, Y., Ansari, A., Aberoumand, S., Karimi, N., Afrand, M., Cheraghian, G., and Muhammad Ali, H., "A critical analysis on the energy and exergy performance of photovoltaic/thermal (PV/T) system: The role of nanofluids stability and synthesizing method", *Sustainable Energy Technologies And Assessments*, 51: 101887 (2022).

17. Hamrouni, N., Jraidi, M., Dhouib, A., and Adnen, C., "Design of a command scheme for grid connected PV systems using classical controllers", *Electric Power Systems Research*, 143: 503–512 (2017).

18. Mosaad Ali, O. A., El-Zoghby, H. M., and Ghany, A. G. M. A., "Maximum Power Point Tracking for Hybrid Wind-Solar Energy System Using Optimum Controllers Techniques", *2018 Twentieth International Middle East Power Systems Conference (MEPCON)*, (2018).

19. Borni, A., Abdelkrim, T., Zaghba, L., Bouchakour, A., Lakhdari, A., and Zarour, L., "Fuzzy logic, PSO based fuzzy logic algorithm and current controls comparative for grid-connected hybrid system", *TECHNOLOGIES AND MATERIALS FOR RENEWABLE ENERGY, ENVIRONMENT AND SUSTAINABILITY: TMREES16-Cnam*, Paris, France, (2017).

20. Pannase, V. R. and Nanavala, H. B., "A review of PV technology power generation, PV material, performance and its applications", *2017 International Conference On Inventive Systems And Control (ICISC)*, 1–5 (2017).

21. Hammed, M., "Improvement of shell and tube heat exchanger performance by using porous media.", *Middle Technical University, Engineering Technical College*, Baghdad, (2018).

22. Daradji, N. and Bouaziz, M. N., "Modelling a Spiral Porous Fin with Temperature Dependent and Independent Thermal Conductivity", (2018).

23. Rydalina, N., Antonova, E., Akhmetova, I., Ilyashenko, S., Afanaseva, O., Bianco, V., and Fedyukhin, A., "Analysis of the Efficiency of Using Heat

Exchangers with Porous Inserts in Heat and Gas Supply Systems", *Energies*, 13 (22): 5854 (2020).

24. Boussaada, Z., Curea, O., Remaci, A., Camblong, H., and Mrabet Bellaaj, N., "A Nonlinear Autoregressive Exogenous (NARX) Neural Network Model for the Prediction of the Daily Direct Solar Radiation", *Energies*, 11 (3): 620 (2018).

25. Hasan, I. A., Mohammed, M. J., and Lafta, F. A., "Intelligent Nero modelling methods for PV panel system", *IOP Conference Series: Materials Science And Engineering*, 765 (1): 012044 (2020).

26. Lafta, F., Ahmed, I., and Mohammed, M., "PID-PSO CONTROLLER FOR PV PANEL SYSTEM IDENTIFICATION MODELS ON ANFIS AND NN-NARX SYSTEM", *Journal Of Engineering Science And Technology*, 16: 4505–4517 (2021).

27. Samara, S. and Natsheh, E., "Intelligent PV Panels Fault Diagnosis Method Based on NARX Network and Linguistic Fuzzy Rule-Based Systems", *Sustainability*, 12 (5): 2011 (2020).

28. Lee, J. H., Hwang, S. G., and Lee, G. H., "Efficiency Improvement of a Photovoltaic Thermal (PVT) System Using Nanofluids", *Energies*, 12 (16): 1–16 (2019).

29. Ahmed, A., Baig, H., Sundaram, S., and Mallick, T. K., "Use of Nanofluids in Solar PV/Thermal Systems", *International Journal Of Photoenergy*, 2019: e8039129 (2019).

30. Connor, J. T., Martin, R. D., and Atlas, L. E., "Recurrent neural networks and robust time series prediction", *IEEE Transactions On Neural Networks*, 5 (2): 240–254 (1994).

31. Mah, C.-Y., Lim, B.-H., Wong, C.-W., Tan, M.-H., Chong, K.-K., and Lai, A.-C., "Investigating the Performance Improvement of a Photovoltaic System in a Tropical Climate using Water Cooling Method", *Energy Procedia*, 159: 78–83 (2019).

32. Diwania, S., Agrawal, S., Siddiqui, A. S., and Singh, S., "Photovoltaic–thermal (PV/T) technology: a comprehensive review on applications and its advancement", *International Journal Of Energy And Environmental Engineering*, 11 (1): 33–54 (2020).

33. Rajput, U. J. and Yang, J., "Comparison of heat sink and water type PV/T collector for polycrystalline photovoltaic panel cooling", *Renewable Energy*, 116: 479–491 (2018).

34. Solihin, M. I., Tack, L. F., and Kean, M. L., "Tuning of PID Controller Using Particle Swarm Optimization (PSO)", *International Journal On Advanced Science, Engineering And Information Technology*, 1 (4): 458 (2011).

35. He, H., Zhou, J.-Z., Lei, H., Li, C.-S., and Yang, L., "Research on fuzzy-PID excitation controller of synchronous generator based on improved PSO algorithm", *2009 International Conference on Machine Learning and Cybernetics*, (2009).

36. Ahmed, I., Mohammed, M., and Abbas, B., "Characteristics Performance Prediction of PV Panel Using Cuckoo Search Algorithm Characteristics Performance Prediction of PV Panel Using Cuckoo Search Algorithm", *IOP Conference Series: Materials Science and Engineering*, (2019).

37. Raptodimos, Y. and Lazakis, I., "Application of NARX neural network for predicting marine engine performance parameters", *Ships And Offshore Structures*, 15 (4): 443–452 (2020).

38. Zhou, Y. T., Nie, J. B., Han, N., Chen, C., and Yue, Z. F., "Study on PID Parameters Tuning Based on Particle Swarm Optimization", *Advanced Materials Research*, 823: 432–438 (2013).

39. Clerc, M., "The swarm and the queen: towards a deterministic and adaptive particle swarm optimization", *Proceedings of the 1999 Congress on Evolutionary Computation-CEC99 (Cat. No. 99TH8406)*, (1999).

40. Yang, X.-S. and Deb, S., "Engineering optimisation by cuckoo search", *International Journal Of Mathematical Modelling And Numerical Optimisation*, 1 (4): 330–343 (2010).

41. Yang, X.-S. and Deb, S., "Engineering optimisation by cuckoo search", *International Journal Of Mathematical Modelling And Numerical Optimisation*, 1 (4): 330–343 (2010).

42. Mat Darus, I. Z. and Al-Khafaji, A. A. M., "Bio-inspired Algorithms for Modeling and Control of Underwater Flexible Single-Link Manipulator", Singapore, (2021).

43. Maid, I., Hilal, K., and Hassun, J., "EXPERIMENTAL STUDY OF HEAT TRANSFER ENHANCEMENT IN HEAT EXCHANGER USING POROUS MEDIA", (2019).

44. Khadim, I. J., Mahdi, E. J., and Ubaid, A. H., "Determining Tilt Angle for Fixed Solar Panel Tosites of Iraq's Provinces by Using the Programs on NASA and Google Earth Websites", *Engineering And Technology Journal*, (2014).

45. El-seesy, I., Khalil, T., and Ahmed, M., "Experimental investigations and developing of photovoltaic/thermal system", 19: 1342–1347 (2012).

46. Mat Darus, I. Z. and Al-Khafaji, A. A. M., "Bio-inspired Algorithms for Modeling and Control of Underwater Flexible Single-Link Manipulator", Singapore, (2021).

47. Safari, A. and Mohammadi, M., "ASSESSING LINEAR AND NONLINEAR MODELS TO FORECAST OPEC OIL PRICES", (2017).

48. Yong, C. Y., Hajibeigy, M. T., Vaithilingam, C. A., and Walvekar, R. G., "Characteristics Study of Photovoltaic Thermal System with Emphasis on Energy Efficiency", (2018).

49. Clerc, M., "The swarm and the queen: towards a deterministic and adaptive particle swarm optimization", *Proceedings of the 1999 Congress on Evolutionary Computation-CEC99 (Cat. No. 99TH8406)*, (1999).

50. Solihin, M., Tack, L., and Moey, L. K., "Tuning of PID Controller Using Particle Swarm Optimization (PSO)", *Proceeding Of The International Conference On Advanced Science, Engineering And Information Technology*, 1: (2011).

51. He, H., Zhou, J.-Z., Lei, H., Li, C.-S., and Yang, L., "Research on fuzzy-PID excitation controller of synchronous generator based on improved PSO algorithm", *2009 International Conference on Machine Learning and Cybernetics*, (2009).

52. Ahmed, I., Mohammed, M., and Abbas, B., "Characteristics Performance Prediction of PV Panel Using Cuckoo Search Algorithm Characteristics Performance Prediction of PV Panel Using Cuckoo Search Algorithm", *IOP Conference Series: Materials Science and Engineering*, (2019).

53. Raptodimos, Y. and Lazakis, I., "Application of NARX neural network for predicting marine engine performance parameters", *Ships And Offshore Structures*, 15: 1–10 (2019).

54. Khadim, I., Mahdi, E., and Ubaid, A., "Determining Tilt Angle for Fixed Solar Panel Tosites of Iraq's Provinces by Using the Programs on NASA and Google Earth Websites", *Engineering And Technology Journal*, 32: 498–506 (2014).

55. Ahmed, I. and J. Mohammed, M., "Analysis And Intelligent Control Of The Cooling Photovoltaic Thermal Cell Using Nanofluid", .

56. Masoud Parsa, S., Yazdani, A., Aberoumand, H., Farhadi, Y., Ansari, A., Aberoumand, S., Karimi, N., Afrand, M., Cheraghian, G., and Muhammad Ali, H., "A critical analysis on the energy and exergy performance of photovoltaic/thermal (PV/T) system: The role of nanofluids stability and synthesizing method", *Sustainable Energy Technologies And Assessments*, 51: 101887 (2022).

57. Ebaid, Munzer. S. Y., Ghrair, Ayoup. M., and Al-Busoul, M., "Experimental investigation of cooling photovoltaic (PV) panels using (TiO 2 ) nanofluid in water -polyethylene glycol mixture and (Al 2 O 3 ) nanofluid in water-cetyltrimethylammonium bromide mixture", *Energy Conversion And Management*, 155: 324–343 (2018).

58. Al-Najideen, M. I. and Alrwashdeh, S. S., "Design of a solar photovoltaic system to cover the electricity demand for the faculty of Engineering- Mu'tah University in Jordan", *Resource-Efficient Technologies*, 3 (4): 440–445 (2017).

59. "Shenzhen Jing Handa Electronics Co. LTD - LCD Module, LCD Display, LCM", **https://jhdlcd.en.ecplaza.net/** (2023).

60. "HUMI-01 OSEPP Electronics | Mouser", **https://eu.mouser.com/ProductDetail/375-HUMI-01** (2023).

61. "Allegro MicroSystems | Innovation with Purpose", **https://www.allegromicro.com/en/** (2023).

62. "Software", **https://www.arduino.cc/en/software** (2023).

63. "Mixed-Signal and Digital Signal Processing ICs | Analog Devices", **https://www.analog.com/en/index.html** (2023).

64. "Digital Servo, Micro Servo, Servo Motor, Servo Rc - Desheng", **https://www.dspowerservo.com/** (2023).
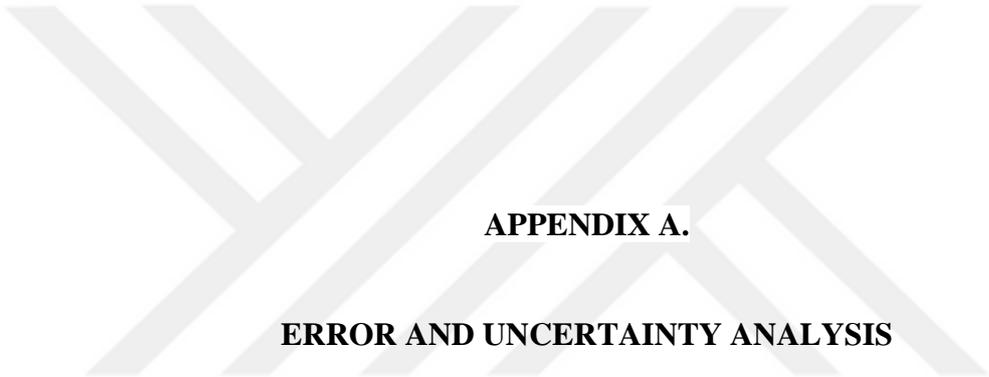
**APPENDIX A.**

**ERROR AND UNCERTAINTY ANALYSIS**

**Temperature Measurement Accuracy:**

The uncertainty of the data logger is systematic uncertainty.

$$U_{data\ logger} = U_{sys} = \pm 0.5\ \%$$

Total uncertainty of thermocouple temperature measurement is the sum of the thermocouple temperature random uncertainty and data logger systematic uncertainty.

The total temperature measurementment accuracy can be written as:

$$T = 0.5\% + 0.15\% = \pm 0.67$$

The temperature maximum range of $K^-$ thermocouple is *1372 °C*.

$$\frac{0.67}{100} \times 1372 = 8.91\ ^\circ C$$

The Maximum measured temperature in the system during the experimental work was *75 °C*.

The maximum possible error of experimental work for the temperature is:

$$\frac{0.67}{100} \times 75 = 0.502\ ^\circ C$$

**Solar Intensity Accuracy:**

*Accuracy* $= \pm\ \mathbf{5}\ \%$

*The maximum solar intensity is 1150 W/m²*

The maximum possible error of the experimental work for the solar intensity is:

$$\frac{5}{100} \times 1150 = 57.5 W/m^2$$

the mean maximum solar intensity reading which captured during the measurement was 765 W/m² and according to this the maximum solar intensity error will be:

$$\frac{5}{100} \times 765 = 38.25 \ W/m^2$$

**Mass Flow Rate Accuracy:**

Mass flow rate is the sum of the density and Velocity errors.

$\dot{m}_{error} = \pm \ 0.645 + \ \pm 3.1 = \ \pm 3.7745 \ \%$

$$\dot{m} = \rho.A.V$$

$$\dot{m}_{max} = 1.085 \times 0.00193 \times (1.95 - 0.013) = 0.00405 \ Kg/ \ s$$

The mass flow rate mean error is:

$$\frac{0.00405 - 0.00403}{0.00405} \times 100 = 0.493\%$$

The max flow rate accuracy is:

$$0.00405 - 0.00403 = 0.00002 \ Kg/ \ s$$

**Voltage Measurement Accuracy:**

The voltage uncertainty is the sum of voltage random uncertainty and the data logger systematic uncertainty as followers:

$$V_{error} = \pm 0.8\% + \ \pm 5$$

the maximum measured voltage in the system during the experimental work was 18.6 volt.

The maximum possible error of the experimental work for the voltage is :

$$\frac{0.8}{100} \times 18.6 + 0.05 = 0.1988 \ volt.$$

**DC current Measurement Accuracy:**

90

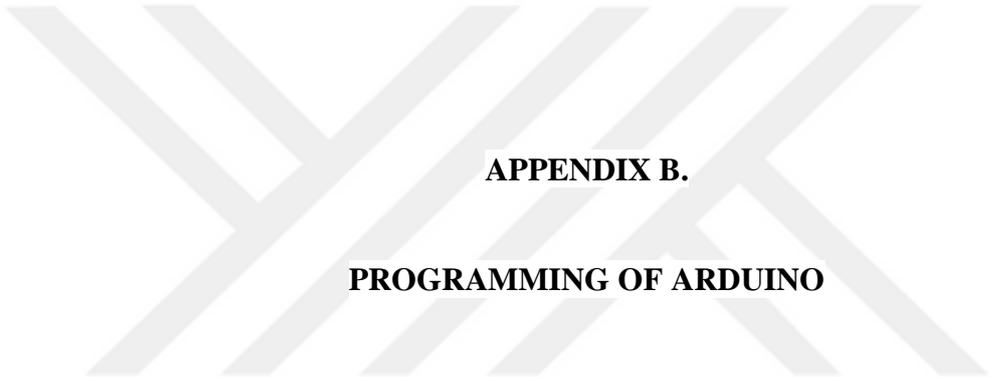The DC current uncertainty is the sum of voltage random uncertainty and the data logger systematic uncertainty as followers:

$$V_{error} = \pm(0.5\ \% +\ 2)$$

the maximum measured *DC* current in the system during the experimental work was 3.44 *A*.

the maximum possible error of the experimental work for the *DC* current is:

$$\frac{0.5}{100} \times 3.44 + 0.02 = 0.0372$$

**APPENDIX B.**

**PROGRAMMING OF ARDUINO**

```
include <Wire.h>
#include <BH1750.h>
#include "max6675.h"
#include<LiquidCrystal_I2C_Hangul.h>

LiquidCrystal_I2C_Hangul lcd(0x27,20,4); //LCD 클래스 초기화

BH1750 lightMeter;
#define ANALOG_IN_PIN A0
 int thermoDO1 = 2;// 1
int thermoCS1 = 3;//1
int thermoCLK1 = 4;//1
MAX6675 thermocouple1(thermoCLK1, thermoCS1, thermoDO1);

// Floats for ADC voltage & Input voltage
float adc_voltage = 0.0;
float in_voltage = 0.0;

// Floats for resistor values in divider (in ohms)
float R1 = 30000.0;
float R2 = 7500.0;

// Float for Reference Voltage
float ref_voltage = 5.0;

// Integer for ADC value
int adc_value = 0;

void setup()
{
 lcd.init();                // initialize the lcd
  // Print a message to the LCD.
  lcd.backlight();
```

```arduino
    Wire.begin();
  // On esp8266 you can select SCL and SDA pins using Wire.begin(D4, D3);
  // For Wemos / Lolin D1 Mini Pro and the Ambient Light shield use Wire.begin(D2,
D1);
  lightMeter.begin();
   // Setup Serial Monitor


   Serial.begin(9600);
Serial.println("CLEARSHEET"); //clears up any data left from previous projects
Serial.println("LABEL, Date, Time, Temperature, Voltage, Current, IRR"); //always
write LABEL, to indicate it as first line


}

void loop(){

  float lux = lightMeter.readLightLevel();
  float irr = (lux*0.0079);
  //Serial.print("irradiance: ");
  //Serial.println(" W/m2");
   // Read the Analog Input
   unsigned int x=0;
float AcsValue=0.0,Samples=0.0,AvgAcs=0.0,AcsValueF=0.0;
for (int x = 0; x < 150; x++){ //Get 150 samples
  AcsValue = analogRead(A1);    //Read current sensor values
  Samples = Samples + AcsValue;  //Add samples together
  delay (5); // let ADC settle before next sample 3ms
  }
  AvgAcs=Samples/150.0;//Taking Average of Samples


//((AvgAcs * (5.0 / 1024.0)) is converitng the read voltage in 0-5 volts
//2.5 is offset(I assumed that arduino is working on 5v so the viout at no current
comes
```

94

```
//out to be 2.5 which is out offset. If your arduino is working on different voltage
than
//you must change the offset according to the input voltage)
//0.185v(185mV) is rise in output voltage when 1A current flows at input
AcsValueF = (2.5 - (AvgAcs * (5.0 / 1024.0)) )/0.185;

 // Serial.print("Input current = ");

  delay(50);

  adc_value = analogRead(ANALOG_IN_PIN);

  // Determine voltage at ADC input
  adc_voltage  = (adc_value * ref_voltage) / 1024.0;

  // Calculate voltage at divider input
  in_voltage = adc_voltage / (R2/(R1+R2)) ;

  // Print results to Serial Monitor to 2 decimal places
 // Serial.print("Input Voltage = ");

 // Short delay
 delay(2000);

 lcd.setCursor(0,0);
 lcd.print("Temperature = ");
   lcd.print(thermocouple1.readCelsius());
lcd.setCursor(0,1);
 lcd.print("Voltage = ");
   lcd.print(in_voltage, 2);
 lcd.setCursor(0,2);
 lcd.print("Current = ");
   lcd.print(AcsValueF, 2);
```

```arduino
    lcd.setCursor(0,3);
  lcd.print("IRR W/m2 = ");
    lcd.print(irr);


//   Serial.println(  (String)  "DATA," + thermocouple1.readCelsius() + "," +
in_voltage, 2 + "," + AcsValueF, 2 + "," + irr + ",SCROLLDATA_20");


Serial.print("DATA" );
 Serial.print(","); //Move to next column using a ","
 Serial.print("DATE" );
 Serial.print(","); //Move to next column using a ","
  Serial.print("TIME" );
 Serial.print(","); //Move to next column using a ","
Serial.print(thermocouple1.readCelsius());
 Serial.print(","); //Move to next column using a ","


Serial.print(in_voltage, 2);
 Serial.print(","); //Move to next column using a ","


Serial.print(AcsValueF, 2);//Print the read current on Serial monitor
 Serial.print(","); //Move to next column using a ","
Serial.print(irr);
 Serial.print(","); //Move to next column using a ","
Serial.println("SCROLLDATA_20");


}
```

## RESUME

Alyaa Jaafar Abdulhasan AL-DAAEWE she graduated primary, elementary, and high school from Baghdad's school. After that, she completed her bachelor's degree at the University of Technology, Department of Mechanical Engineering in Baghdad in 2001-2002. Then in 2021, she started studing at Karabük University Mechanical Engineering Department to complete her M.Sc. Education.